UNI OF M TY GAN
APR 1958
ENGINEERING LIBRARY

JOURNAL OF FLUID MECHANICS

VOLUME 3 PART 6

MARCH 1958

Published by

CAMBRIDGE UNIVERSITY PRESS

BENTLEY HOUSE, 200 EUSTON ROAD, LONDON, N.W.1
AMERICAN BRANCH: 32 EAST 57th STREET, NEW YORK 22, N.Y.

Price 20*s*. (*U.S.A.* $3.25)

The JOURNAL OF FLUID MECHANICS exists for the publication of theoretical and experimental investigations of all aspects of the mechanics of fluids, and is issued in six parts per volume.

Editor

Dr. G. K. BATCHELOR, Cavendish Laboratory, University of Cambridge, Cambridge, England.

Assistant Editors

Dr. T. B. BENJAMIN, Dr. I. PROUDMAN, Dr. P. G. SAFFMAN.

Associate Editors

Prof. G. F. CARRIER, Pierce Hall, Harvard University, Cambridge 38, Massachusetts, U.S.A.

Dr. W. C. GRIFFITH, Research and Development Laboratory, Missile Systems Division, Lockheed Aircraft Corporation, Palo Alto, California, U.S.A.

Prof. M. J. LIGHTHILL, Department of Mathematics, The University, Manchester, England.

Authors wishing to have papers published in the JOURNAL should communicate them to any one of the persons named above, choosing one in their own country where possible.

Authors are urged to ensure that their papers are written clearly and attractively, in order that their work will be readily accessible to readers.

Manuscripts should be typed in double spacing on one side of the paper only, with references listed at the end in alphabetical order of authors. Drawings should be done on a large scale in Indian ink on tracing cloth or drawing paper, with the list of captions typed at the end of the manuscript. Proofs of papers from overseas will usually be despatched to authors by airmail. Authors are entitled to receive 50 offprints of a paper in the JOURNAL free of charge, and additional offprints can be purchased if ordered in advance.

SUBSCRIPTIONS

The subscription price for a volume of six parts is £5 10*s*. net, post free, payable in advance; separate parts 20*s*. net, plus postage. Subscriptions may be sent to any bookseller, or to the Cambridge University Press, Bentley House, 200 Euston Road, London, N.W.1.

Subscribers in the United States should send their orders to the Cambridge University Press, American Branch, 32 East 57th Street, New York 22. Subscription price per volume $18.50 post free, payable in advance; separate parts $3.25, plus postage.

The flow of a compressible fluid with weak entropy changes

By ROY GUNDERSEN
Department of Mathematics, Illinois Institute of Technology

(*Received* 7 *August* 1957 *and in revised form* 27 *November* 1957)

SUMMARY

Perturbations of a given flow are considered, and the equations which govern the one-dimensional, non-steady flow of an inviscid, ideal compressible gas are linearized in the neighbourhood of this known solution, assumed isentropic, by a formal perturbation expansion. The perturbed flow is not assumed isentropic. Explicit solutions are obtained for a basic flow which is uniform or a centred simple wave and for an arbitrary simple wave if the perturbed flow is isentropic.

The perturbation of a uniform shock and perturbations in a shock tube lead to functional equations of a particular type, and a discussion of their solution is given.

A similar analysis is used to discuss the flow in a tube of slowly varying cross-section.

1. INTRODUCTION

The one-dimensional, non-steady flow of an inviscid compressible gas which, furthermore, is assumed to be ideal and polytropic with constant specific heats is governed by a system of non-linear, first-order partial differential equations which is always hyperbolic. Given an isentropic flow, a solution of the governing equations, this paper will discuss 'perturbations' of this basic flow; i.e. this flow is disturbed by some means, and it is desired to find the resultant flow.

To linearize in the neighbourhood of this known solution, the dependent variables are formally expanded as functions of a small parameter δ, viz.

$$u(x,t) = u_0(x,t) + \delta u_1(x,t) + \delta^2 u_2(x,t) + \ldots,$$
$$c(x,t) = c_0(x,t) + \delta c_1(x,t) + \delta^2 c_2(x,t) + \ldots,$$
$$s(x,t) = s_0 + \delta s_1(x,t) + \delta^2 s_2(x,t) + \ldots,$$

where u, c and s are respectively the particle velocity, the local speed of sound and the specific entropy, and the zero subscript denotes the basic (known) flow. When these expansions are substituted into the governing equations and grouped with respect to increasing powers of δ, the terms free of δ are satisfied identically, so that the resulting equations may be divided through by δ and, taking the limit as $\delta \to 0$, the equations governing the first approximation to the behaviour of the disturbed flow are obtained.

These equations are linear with the same characteristic surfaces as the original system and form a system of non-homogeneous first-order partial differential equations. It is convenient to attack the problem by first considering the associated homogeneous system, which has the physical significance that, to the order of terms retained (i.e. to the order of δ), the perturbed flow is still isentropic. The problem is consequently reduced to the determination of a particular solution of the non-homogeneous equations. Since the equations for the perturbations are linear, superposition of flows is possible.

Explicit solutions are obtained for a basic flow which is uniform or a centred simple wave, and for an arbitrary simple wave if the perturbed flow is isentropic. The application of these results to the perturbation of a uniform shock and perturbations in a shock tube lead to functional equations of a particular type, and a discussion of their solution is given in Appendices I and II. The flow in a long tube whose cross-section is made to undergo a small variation with x is treated by a similar analysis in part III.

Many authors have discussed the application of perturbation techniques to gas-dynamical problems, but, in general, have linearized in the neighbourhood of a constant state, with the result that the characteristics are rectilinear and parallel. For many flows, these characteristics are inadequate, and a more exact treatment of the characteristics is necessary. In the present paper, the question of correcting characteristics is not met, for the exact characteristics of the initial flow are always employed. A summary of §2, §3 and §5 has already been given by Germain & Gundersen (1955).

PART I. GENERAL THEORY

2. The basic equations and solution for an originally uniform flow

The equation of state is

$$P = \exp\left[\frac{s - s^*}{c_v}\right]\rho^{\gamma},$$

and the equations which characterize the one-dimensional non-steady flow are

$$c_t + uc_x + \tfrac{1}{2}(\gamma - 1)cu_x = 0,$$

$$u_t + uu_x + 2cc_x/(\gamma - 1) - c^2 s_x/c_v\gamma(\gamma - 1) = 0,$$

$$s_t + us_x = 0,$$

where P is the pressure, ρ the density, s^* the specific entropy at some reference state, γ the ratio of the specific heats at constant pressure c_p and at constant volume c_v, and the subscripts denote partial derivatives.

Throughout, it is assumed that an isentropic solution is known, namely, $u_0(x, t)$, $c_0(x, t)$, s_0 = constant. A formal linearization in the neighbourhood

of this known solution gives the following equations which govern the first approximation to the behaviour of the disturbed flow:

$$c_{1t}+u_0 c_{1x}+\tfrac{1}{2}(\gamma-1)c_0 u_{1x}+u_1 c_{0x}+\tfrac{1}{2}(\gamma-1)u_{0x}c_1=0, \tag{2.1}$$

$$\tfrac{1}{2}(\gamma-1)u_{1t}+\tfrac{1}{2}(\gamma-1)u_0 u_{1x}+c_0 c_{1x}+\tfrac{1}{2}(\gamma-1)u_{0x}u_1+c_1 c_{0x}=c_0^2 s_{1x}/2c_v\gamma, \tag{2.2}$$

$$s_{1t}+u_0 s_{1x}=0. \tag{2.3}$$

These equations are linear with the same characteristic surfaces as the original system.

According to (2.3), s_1 remains constant along the particle paths of the given flow, i.e. along $dx/dt=u_0$. Also, $\rho_0(dx-u_0\,dt)$ is the exact differential of a function ψ_0 which, when equated to a constant, defines the particle paths. Consequently, the solution of (2.3) is

$$s_1=\omega(\psi_0), \tag{2.4}$$

with ω an arbitrary function. It is convenient to define a new function $H_0(x,t)$ by

$$c_0^2 s_{1x}=\rho_0 c_0^2\,\omega'(\psi_0)=\gamma(\gamma-1)c_v H_0. \tag{2.5}$$

Therefore, the two equations which serve to determine u_1, c_1 are

$$c_{1t}+u_0 c_{1x}+\tfrac{1}{2}(\gamma-1)c_0 u_{1x}+u_1 c_{0x}+\tfrac{1}{2}(\gamma-1)u_{0x}c_1=0, \tag{2.6}$$

$$u_{1t}+u_0 u_{1x}+2(\gamma-1)^{-1}c_0 c_{1x}+u_{0x}u_1+2(\gamma-1)^{-1}c_{0x}c_1=H_0. \tag{2.7}$$

It is convenient to introduce the characteristic parameters of the basic flow

$$\tfrac{1}{2}u_0+c_0/(\gamma-1)=\alpha, \qquad -\tfrac{1}{2}u_0+c_0/(\gamma-1)=\beta,$$

and the functions

$$\tfrac{1}{2}u_1+c_1/(\gamma-1)=A, \qquad -\tfrac{1}{2}u_1+c_1/(\gamma-1)=B.$$

The combinations $(2.6)/(\gamma-1)\pm\tfrac{1}{2}(2.7)$ give

$$A_t+(u_0+c_0)A_x+\tfrac{1}{2}[A(\gamma+1)+(\gamma-3)B]\alpha_x=\tfrac{1}{2}H_0, \tag{2.8}$$

$$B_t+(u_0-c_0)B_x+\tfrac{1}{2}[A(3-\gamma)-(\gamma+1)B]\beta_x=-\tfrac{1}{2}H_0. \tag{2.9}$$

A perturbation in which the perturbed flow is still isentropic corresponds to a solution of the homogeneous ($H_0=0$) system associated with the linear system (2.8) and (2.9).

For the case of an initially uniform flow, u_0 and c_0 are constants, and therefore $\alpha_x=\beta_x=0$. The homogeneous system then admits the following general solution, in terms of two arbitrary functions F and G of one argument

$$A=F[x-(u_0+c_0)t], \qquad B=G[x-(u_0-c_0)t]. \tag{2.10}$$

In the non-isentropic case, from (2.4) and (2.5), H_0 is a function of $x-u_0 t$, and

$$H_0=2\chi'(x-u_0 t), \qquad c_0 A=c_0 B=\chi(x-u_0 t), \tag{2.11}$$

where χ is an arbitrary function, is a particular solution for which $u_1=0$; i.e. the addition of an entropy perturbation affects $c_1(x,t)$ but not $u_1(x,t)$.

3. Perturbation of a simple wave: general theory

For the case of the simple wave, one of the characteristic parameters of the basic flow remains constant, e.g. $\beta = \beta_0$. B is then determined from (2.9) and A from (2.8). The solution for the perturbation of an arbitrary simple wave will be given but, first, the centred simple wave will be discussed in some detail.

The wave is assumed to be centred at the origin and characterized by $\beta = \beta_0$. From the definition of the characteristic parameters,

$$u_0 = \alpha - \beta_0, \qquad c_0 = \tfrac{1}{2}(\gamma-1)(\alpha+\beta_0);$$

therefore

$$u_0 + c_0 = \tfrac{1}{2}(\gamma+1)\alpha + \tfrac{1}{2}(\gamma-3)\beta_0 = x/t,$$

$$\alpha = \frac{2}{\gamma+1}\left[\frac{x}{t} - \frac{\gamma-3}{2}\,\beta_0\right].$$

Substituting these results into (2.8) and (2.9) specialized to the case of an isentropic perturbed flow, the following equations are obtained:

$$tA_t + xA_x + \left[A + \frac{\gamma-3}{\gamma+1}B\right] = 0, \tag{3.1}$$

$$tB_t + \left[\frac{3-\gamma}{\gamma+1}\,x - 4\frac{\gamma-1}{\gamma+1}\,\beta_0\, t\right]B_x = 0. \tag{3.2}$$

B will be determined first by solving (3.2), and, after this result has been substituted into (3.1), A may easily be determined. The characteristics of (3.2) may be written as

$$\frac{dt}{t} = \frac{(\gamma+1)dx}{(3-\gamma)x - 4(\gamma-1)\beta_0 t} = \left(\frac{\gamma+1}{3-\gamma}\right)\frac{d(x+2\beta_0 t)}{x+2\beta_0 t}, \tag{3.3}$$

and $dB = 0$. It follows from (3.3) that

$$t = K_1(x+2\beta_0 t)^{(\gamma+1)/(3-\gamma)}$$

with K_1 a constant; and since

$$c_0 = \frac{\gamma-1}{\gamma+1}\left[\frac{x+2\beta_0 t}{t}\right],$$

the representation of the curvilinear characteristics of the simple wave is

$$t = K_2(c_0 t)^{(\gamma+1)/(3-\gamma)}$$

with K_2 a constant, or

$$\rho_0 c_0 t^2 = \text{const.} \tag{3.4}$$

This form is not classical, but will be seen to be a very convenient one.

If F is an arbitrary differentiable function, it is convenient to write the solution of (3.2) as

$$B = 2(\rho_0 c_0)^{1/2} t\, F'(\rho_0 c_0 t^2). \tag{3.5}$$

Consequently, the solution of (3.1) is

$$At = \frac{3-\gamma}{\gamma+1}\,\frac{1}{(\rho_0 c_0)^{1/2}}\,F(\rho_0 c_0 t^2) + G(x/t), \tag{3.6}$$

where G is an arbitrary function.

The particle paths are given by $\rho_0 c_0 t = \text{const.}$, or

$$y \equiv c_0^2 t^{2(\gamma-1)/(\gamma+1)} = \text{const.}$$

For the non-isentropic case, it is convenient to write

$$\tfrac{1}{2}H_0 = (2c_0/t)\omega_1'(y).$$

The following particular integral (to be added to the previous solution) is easily obtained:

$$A = B = \frac{\gamma+1}{2(\gamma-1)}\frac{c_0}{y}\omega_1(y),$$

i.e.

$$u_1 = 0, \qquad c_1 = \tfrac{1}{4}(\gamma+1)(c_0/y)\omega_1(y),$$

with ω_1 an arbitrary function and, as in the perturbation of a constant state, the addition of the entropy perturbation affects $c_1(x,t)$ but not $u_1(x,t)$. This question will be taken up in detail after the arbitrary simple wave has been discussed.

For the arbitrary simple wave (isentropic perturbed flow), let $x_0(z)$, $t_0(z)$ be the parametric representation of a curvilinear characteristic of the given flow. The wave may be represented by

$$x = x_0(z) + [u_0(z) + c_0(z)]\tau, \qquad t = t_0(z) + \tau, \tag{3.7}$$

$$-\tfrac{1}{2}u_0(z) + c_0(z)/(\gamma-1) = \beta_0. \tag{3.8}$$

Equation (2.9) reduces to

$$B_t + (u_0 - c_0)B_x = 0, \tag{3.9}$$

i.e. B is constant along any curvilinear characteristic. The characteristics of (3.9) are $dB = 0$ and $dx = (u_0 - c_0)\,dt$, or, from (3.7),

$$\frac{dx_0}{dz} + \tau\frac{d}{dz}(u_0 + c_0) + \frac{d\tau}{dz}2c_0 = (u_0 - c_0)\frac{dt_0}{dz};$$

hence, as (x_0, t_0) is a curvilinear characteristic, the following differential equation is obtained for $\tau(z)$:

$$2c_0\frac{d\tau}{dz} + \tau\frac{d}{dz}(u_0 + c_0) = 0,$$

or, utilizing (3.8),

$$\frac{1}{\tau}\frac{d\tau}{dz} = -\frac{1}{2}\frac{\gamma+1}{\gamma-1}\frac{1}{c_0}\frac{dc_0}{dz}.$$

This has the solution

$$\rho_0 c_0 \tau^2 = \text{const.}, \quad \text{or } \rho_0 c_0 (t - t_0)^2 = \text{const.}$$

This result for the representation of the curvilinear characteristics of the simple wave could have been written down immediately by analogy with (3.4). The solution for B is

$$B = 2(\rho_0 c_0)^{1/2}(t - t_0)F'[\rho_0 c_0 (t - t_0)^2] \tag{3.10}$$

in terms of an arbitrary, differentiable function F. The characteristics of (2.8) may be written as

$$dt = \frac{dx}{u_0 + c_0} = \frac{2\,dA}{[(3-\gamma)B - (\gamma+1)A]x_x}. \tag{3.11}$$

The integral of the first equation of (3.11) has the first family of characteristics (rectilinear characteristics) for level curves. Let this first integral be

$$z(x,t) = \text{const.} \tag{3.12}$$

This function is given implicitly by

$$x - x_0(z) = [u_0(z) + c_0(z)][t - t_0(z)].$$

From the definition of the characteristic parameters, it follows that

$$\alpha = 2(\gamma+1)^{-1}[u_0 + c_0 - \tfrac{1}{2}(\gamma-3)]\beta_0.$$

Substitution in (3.11) yields the following differential equation for A:

$$\left[t - t_0 - \frac{2c_0(dt_0/dz)}{(dc_0/dz)}\frac{\gamma-1}{\gamma+1}\right]\frac{dA}{dt} + A = \frac{3-\gamma}{\gamma+1}B.$$

To integrate this equation, B is substituted from (3.10) and the first integral (3.12) is employed, i.e. z may be considered as constant. This yields another first integral, and the solution for $A(t,z)$ is

$$\left[t - t_0 - \frac{2c_0(dt_0/dz)}{(dc_0/dz)}\frac{\gamma-1}{\gamma+1}\right]A = G(z) + \\ + \frac{3-\gamma}{\gamma+1}\frac{1}{(\rho_0 c_0)^{1/2}}F[\rho_0 c_0(t-t_0)^2] \tag{3.13}$$

in terms of the arbitrary functions F and G. In the non-isentropic case, the problem is reduced to two ordinary differential equations, but it does not seem possible to solve these two equations explicitly in the general case. The question of actually determining these arbitrary functions in a specific problem will be discussed later.

4. Criterion for the existence of a particular solution $u_1 = 0$ in the non-isentropic case

In the non-isentropic perturbation of a constant state and of a centred simple wave, the addition of the entropy perturbation just affects the sound speed, whereas the particle velocity is the same for isentropic and non-isentropic perturbed flows, i.e. there exists a particular solution $u_1 = 0$. Unfortunately, such a nice result does not obtain for the arbitrary simple wave. It is of interest to determine under what conditions such a result is to be expected, for the answer is not at all obvious.

It is equivalent to look for a solution of (2.6) and (2.7) with $u_1 = 0$, viz.

$$c_{1t} + u_0 c_{1x} + \tfrac{1}{2}(\gamma-1)u_{0x}c_1 = 0, \tag{4.1}$$

$$(c_1 c_0)_x = (\rho_0 c_0^2/2c_0\gamma)\omega'(\psi_0), \tag{4.2}$$

$$d\psi_0 = \rho_0(dx - u_0\,dt).$$

Thus, it is clear that the problem consists of expressing the compatibility of equations (4.1) and (4.2), and the corresponding identities will determine which functions $u_0(x,t)$, $c_0(x,t)$ allow this compatibility.

The characteristics of (4.1) are

$$dt = \frac{dx}{u_0} = -\frac{2dc_1}{(\gamma-1)u_{0x}c_1}.$$

From the first two ratios, a first integral is

$$dx - u_0\,dt = 0, \qquad \text{or } \psi_0 = \text{const.}$$

A second one will be found easily since $c_0(x,t)$ is a particular solution of (4.1). This first integral is $c_1/c_0 = \text{const}$. Hence, the solution of (4.1) is

$$c_0 c_1 = c_0^2 f(\psi_0) \tag{4.3}$$

where f is an arbitrary function. Substitution of (4.3) into (4.2) gives

$$\frac{c_{0x}}{\rho_0 c_0} = \frac{1}{2f}\left\{\frac{\omega'(\psi_0)}{2c_v\gamma} - f'\right\}.$$

Hence, the necessary and sufficient conditions for the existence of a particular solution $u_1 = 0$ is

$$\frac{c_{0x}}{\rho_0 c_0} = c^{-(\gamma+1)(\gamma-1)}c_{0x} = \text{a function of } \psi_0.$$

By taking the material derivative, this condition becomes

$$u_{0xx} = 0.$$

Consequently, in order to have a particular solution with $u_1 = 0$, it is necessary and sufficient that $u_0(x,t)$ is a linear function of x. Then $c_1 = c_0 f(\psi_0)$ with a convenient function f. It is necessary to investigate all solutions of this form, i.e. $u_0 = a(t)x + b(t)$. This has been carried out but will not be included here.

5. An approximation for flows which differ only slightly from a uniform state

In general, it does not seem possible to solve (2.8) and (2.9) explicitly for an arbitrary initial flow. However, the preceding techniques may be utilized if the given flow does not differ greatly from a uniform state or a simple wave.

For example, consider the problem of a flow, which is nearly a uniform flow (u_0, c_0). Denote by u_1, c_1, s_1 and u_2, c_2, s_2 the terms of first and second order obtained by a formal perturbation method. Let

$$\bar{u}_0 = u_0 + u_1, \quad \bar{c} = c_0 + c_1 + c_2, \quad \bar{c}_0 = c_0 + c_1, \quad \bar{u} = u_0 + u_1 + u_2, \quad \bar{s} = s_1 + s_2.$$

By termwise addition of the equations determining u_1, c_1, s_1 and u_2, c_2, s_2 and neglecting terms of third order (e.g. $u_1 c_2$, $u_2 c_1$), the following equations are obtained:

$$\left.\begin{aligned} \bar{c}_t + \bar{u}_0\bar{c}_x + \tfrac{1}{2}(\gamma-1)\bar{c}_0\bar{u}_x &= 0, \\ \bar{u}_t + \bar{u}_0\bar{u}_x + 2(\gamma-1)^{-1}\bar{c}_0\bar{c}_x &= \bar{c}_0^2\bar{s}_x/\gamma(\gamma-1)c_v, \\ \bar{s}_t + \bar{u}_0\bar{s}_x &= 0. \end{aligned}\right\} \tag{5.1}$$

Formally, this system of equations is identical to (2.1), (2.2) and (2.3) if the terms u_{0x} and c_{0x} are neglected. Consequently, the following principle has been established. *If $\bar{u}_0$ and $\bar{c}_0$ define the flow to the second order, $\bar{u}$ and $\bar{c}$ define the flow to the third order.*

The solution of the system (5.1) is immediate. With the introduction of the quantities A, B, α and β, the system may be written as

$$A_\beta = \tfrac{1}{2}H_0 t_\beta, \qquad B_\alpha = -\tfrac{1}{2}H_0 t_\alpha,$$

and may be solved by quadratures. In the isentropic case, $A = F(\alpha)$, $B = G(\beta)$ where F and G are two arbitrary functions. Thus, it is clear that the analysis is exactly that which is met in the classical theory (the Euler–Poisson equation).

Note that the neglect of the terms u_{0x} and c_{0x} does not affect the principal part of each differential equation, so that the characteristics remain unchanged.

6. Isentropic perturbation of an arbitrary simple wave: determination of arbitrary functions

In §3, the perturbation of a simple wave was solved in terms of two arbitrary functions. The present and subsequent section are devoted to the question of the determination of these arbitrary functions. It will be shown that, at least theoretically, no difficulties are met.

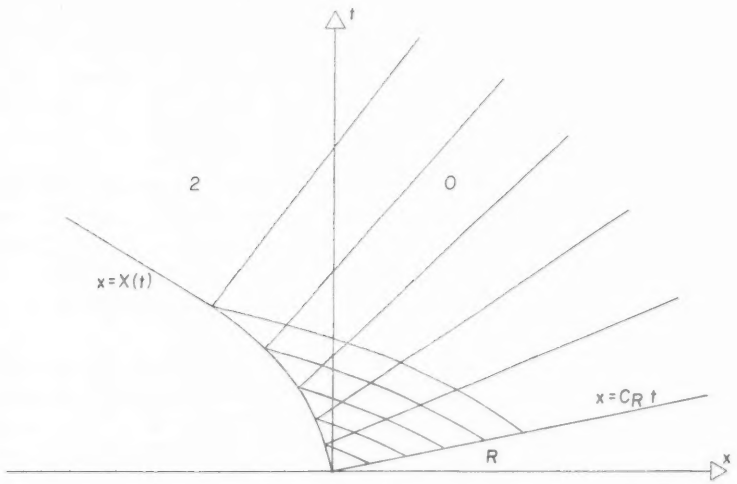

Figure 1.

Consider a tube of gas, initially at rest with constant sound speed c_R and constant density ρ_R, from which a piston, originally at rest, is withdrawn with increasing speed until a constant final velocity is attained. A simple wave, which advances with the speed c_R into the gas at rest, is generated. The (x, t)-representation of the flow is shown in figure 1. The region $x > c_R t$, denoted in figure 1 by the symbol R, is a constant state with $(u, c) = (0, c_R)$. The flow due to the receding motion of the piston is restricted to the region $x \leqslant c_R t$, and the region denoted by O is a simple wave. As the piston attains its final velocity, the flow becomes a constant state, denoted by the symbol 2, with particle velocity equal to the piston velocity. This is a classical problem, and the solution is well known.

It is now assumed that a small perturbation takes place and that the resultant flow is still isentropic. This problem was solved in § 3 in terms of two arbitrary functions. The discussion of this section will be in rather general terms without concern for computational details, for it is the basic principles, and not the details, which are important here; they will provide the basis for the solution of the perturbation of the centred simple wave.

Let the following initial conditions be given for $t = 0$:

$$u = \delta g(x), \qquad c = c_R + \delta h(x),$$

where g and h are known functions.

From the perturbation of a constant state (§ 2), the solution for $x \geqslant c_R t$ is

$$\bar{u}_R = \eta(x - c_R t) - \xi(x + c_R t), \qquad 2(\gamma - 1)^{-1}\bar{c}_R = \eta(x - c_R t) + \xi(x + c_R t),$$

where

$$\eta(x) = \tfrac{1}{2}g(x) + h(x)/(\gamma - 1), \qquad \xi(x) = -\tfrac{1}{2}g(x) + h(x)/(\gamma - 1),$$

and perturbations are denoted by a bar. Also, let the piston velocity be

$$u = \dot{x} = \dot{X}(t) + \delta\bar{\dot{X}}(t).$$

The rectilinear characteristics of the simple wave are given by $z = \text{const.}$, and the curvilinear cross-characteristics by

$$\rho_0 c_0 (t - t_0)^2 = a,$$

where a is a constant. Recall that $[x_0(z), t_0(z)]$ is the parametric representation of a non-linear characteristic of the given simple wave.

The function z was defined implicitly, and it is assumed that this relation has been inverted to give $z(x, t)$. This value is substituted into $\rho_0(z)$, etc., which gives functions which will be denoted by $\rho_{01}(x, t)$, etc. These are substituted into (3.10) and (3.13), and the resultant functions are called $B = B_1(x, t)$, $A = A_1(x, t)$, $G(z) = G_1(x, t)$ and F_1.

The perturbations introduced at $t = 0$ travel along the characteristics in region R to the first characteristic of the simple wave, viz. $x = c_R t$. At a point $(x_1, t_1) = (c_R t_1, t_1)$ of this characteristic, the perturbations are

$$A_1(x_1, t_1) = \eta(0), \qquad B_1(x_1, t_1) = \xi(2c_R t_1). \tag{6.1}$$

This perturbation $(\bar{u}_R^1, \bar{c}_R^1)$ travels along the non-linear characteristic through the point (x_1, t_1) to the piston curve. Let the equation of this non-linear characteristic be

$$\rho_{01} c_{01} (t - t_{01})^2 = a_1, \tag{6.2}$$

and let the intersection of (6.2) with the piston path, $x = X(t)$, be (x_1^1, t_1^1). The conditions (6.1) on $x = c_R t$ allow the determination of F_1 from

$$2(\rho_{01} c_{01})^{1/2}(t - t_{01})F_1'[\rho_{01} c_{01}(t - t_{01})^2] = \xi(2c_R t_1). \tag{6.3}$$

Thus F_1, and therefore B_1, is known throughout the simple wave region.

In general, $\bar{u}_0 = A_1 - B_1$; therefore, at the point (x_1^1, t_1^1) of the piston curve, we have

$$\bar{\dot{X}}_1(t_1^1) = A_1(x_1^1, t_1^1) - B_1(x_1^1, t_1^1). \tag{6.4}$$

Now let

$$D_1^1 = \left[t - t_0 - 2c_0 \frac{\gamma-1}{\gamma+1} \frac{(dt_0/dz)}{(dc_0/dz)} \right]_{(x_1^1, t_1^1)}.$$

As the first and last terms in (6.4) are known, this gives a condition for the determination of $G_1(x_1^1, t_1^1)$:

$$G_1(x_1^1, t_1^1) = D_1^1[\tilde{X}_1(t_1^1) + B_1(x_1^1, t_1^1)] + \\ + \frac{\gamma-3}{\gamma+1} \frac{1}{(\rho_{01}^1 c_{01}^1)^{1/2}} F_1[\rho_{01}^1 c_{01}^1 (t - t_{01}^1)^2]. \quad (6.5)$$

Clearly, this analysis applies at each point of the first characteristic of the simple wave, i.e. at each point the perturbation travels along the non-linear characteristic through the point to the piston curve. Consequently, (6.5) holds, with appropriate changes in the arguments, all along the portion of the piston curve in the simple wave region and allows the determination of $G_1(x, t)$. From classical theory, this is a well-set problem (in Picard's terminology, a third problem) as the value of B_1 is known along the characteristic $x = c_R t$ and the value of A_1 is known along the piston curve which has time-like orientation.

The function G_1 determines the perturbations which travel along the rectilinear characteristics of the simple wave. The perturbed flow in region 2 is determined by data along the last characteristic of the simple wave and on the rectilinear portion of the piston curve.

7. Isentropic perturbation of a centred simple wave

Consider the same original situation as in §6, but suppose now that the acceleration of the piston from rest to a constant terminal velocity $u_1 = -V$ $(V > 0)$ takes place instantaneously. The rectilinear characteristics of the rarefaction wave, generated by this piston motion, all pass through the origin as depicted in figure 2.

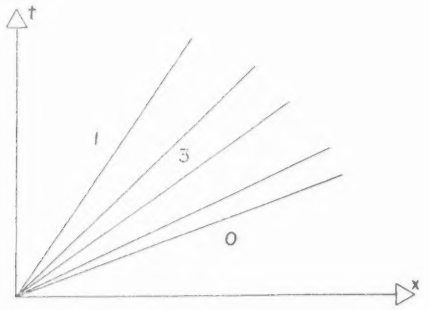

Figure 2.

On this known initial flow, the following initial conditions for the perturbed flow are superposed: $\tilde{u}_0 = 0$, $t = 0$; $\tilde{c}_0 = (\gamma-1)f(x)$, $x > 0$; $\tilde{u}_0(0, 0) = 0$; $\tilde{c}_0(0, 0) = (\gamma-1)f(0)$. The analysis of §6 will be used to

determine the solution of the present problem. The subsequent analysis will also give information about the value of $\bar{c}_0(0,0)$.

The utilization of the solution for the perturbation of a constant state and initial conditions gives

$$A = f(x - c_R t), \qquad B = f(x + c_R t). \tag{7.1}$$

The application of (7.1) on $x = c_R t$ and substitution in (3.5) and (3.6) gives

$$G(c_R) = f(0)t + \frac{\gamma - 3}{\gamma + 1} \frac{1}{(\rho_R c_R)^{1/2}} F(\rho_R c_R t^2),$$
$$f(2c_R t) = 2(\rho_R c_R)^{1/2} t\, F'(\rho_R c_R t^2).$$

In the limit as $t \to 0$,

$$\left.\begin{aligned} G(c_R) &= \frac{\gamma - 3}{\gamma + 1} \frac{1}{(\rho_R c_R)^{1/2}} F(0), \\ f(0) &= 0, \end{aligned}\right\} \tag{7.2}$$

where it is assumed that f is continuous and that F' is bounded near $t = 0$. This last statement implies that the perturbations are bounded near $t = 0$.

Equation (7.2) says that, for the present problem, it is necessary that $\bar{c}_0(0,0) = 0$, i.e. both perturbation velocities must vanish at the origin where the basic flow is discontinuous.

The present problem is clearly a limiting case of the problem of § 6. The G-function, a function of x/t, determines the perturbations which travel along the rectilinear characteristics of the simple wave. It is determined by the perturbations carried to the piston curve along the curvilinear cross-characteristics of the simple wave. In the limit as the rectilinear characteristics form a pencil of lines through the origin, the G-function will be determined by the perturbations at the origin only. As the perturbations are zero at the origin, it is clear that G is at most a constant, and this constant will be chosen as zero for convenience.

It is easily found that

$$F(\rho_3 c_3 t^2) = (\rho_R c_R)^{1/2} \int_0^{(\rho_3 c_3/\rho_R c_R)^{1/2} t} f(2c_R y)\, dy.$$

The solution in the simple wave is now known, and the perturbed flow in region 1 is determined by conditions along the last characteristic of the simple wave and along the piston.

PART II. APPLICATIONS

As a first application, the perturbation of a shock produced by a uniform compressive motion of a piston will be considered. A piston, initially at rest, is at $t = 0$ suddenly pushed with constant velocity into a gas which is also initially at rest. A uniform shock is produced, which moves with constant velocity into the gas, and the gas behind the shock is in a steady

state with gas velocity equal to the piston velocity. The state of rest in front of the shock is denoted by R, and the constant state behind the shock is denoted by 0. The shock velocity is given by

$$W_0 = \tfrac{1}{4}(\gamma+1)u_0 + [c_R^2 + \{(\gamma+1)u_0/4\}^2]^{1/2}.$$

Suppose that the piston is given a small prescribed perturbation for $t \geqslant t_1$. This will perturb the shock locus, and, as this is the perturbation of a strong shock, the flow behind the shock will no longer be isentropic; thus the entropy perturbations must be considered. It is convenient to solve this problem in two steps. First, the inverse problem of the determination of the perturbed piston path when the shock is given a small perturbation is solved, and, second, this solution is used to solve the direct problem.

8. The inverse problem

Suppose that, from some particular time t_2, the shock is given a small prescribed perturbation; i.e. let the shock velocity be $W = W_0$ for $t < t_2$ and $W = W_0 + \epsilon(t)$ for $t \geqslant t_2$, where $\epsilon(t)$ is a known function sufficiently small so that terms of higher order than the first may be neglected. This perturbation will cause a corresponding perturbation of the particle velocity; let the new particle velocity near the shock be $u = u_0 + \eta(t)$, where $\eta(t)$ is also small and must be a function of $\epsilon(t)$ as will be shown.

The perturbations of u_0, c_0 and s_0, which will be denoted by $\bar{u}_0$, $\bar{c}_0$ and $\bar{s}_0$, will be found in terms of $\epsilon(t)$ along the shock. With these boundary conditions, the solution for the non-isentropic perturbation of a constant state may be utilized to find the perturbed flow behind the shock. Then, $\bar{u}_0(u_0 t, t)$ gives the perturbation of the piston velocity.

It is convenient to tabulate many of the standard relations between the flow parameters in perturbation form. Appendix III contains some of the more important relations.

By the use of the Prandtl relation in perturbation form (Appendix III, relation VIII), it follows that

$$\bar{u}_0 = 2K_1\epsilon(t), \qquad \bar{c}_0 = (\gamma-1)K_2\epsilon(t),$$

where

$$K_1 = \tfrac{1}{2}[2(1-\theta-u_0/W_0], \qquad K_2 = 2(\gamma+1)^{-1}(W_0-u_0)/c_0 + u_0^2/2W_0c_0,$$
$$\theta = (\gamma-1)/(\gamma+1).$$

Consequently,

$$A = (K_1+K_2)\epsilon(t) = K_3\epsilon(t), \qquad B = (K_2-K_1)\epsilon(t) \quad K_1\epsilon(t) \tag{8.1}$$

on the shock.

From relation V of Appendix III,

$$\frac{\bar{\rho}_0}{\rho_0} = \left[\frac{u_0-(1-\theta)W_0}{W_0(u_0-W_0)}\right]\epsilon(t);$$

and from relation I of Appendix III,

$$\bar{s}_0 = \left\{\frac{2c_v}{c_0}(\gamma-1)K_2 - \frac{(\gamma-1)}{W_0}c_v\frac{[u_0-(1-\theta)W_0]}{(u_0-W_0)}\right\}\epsilon(t) = K_5\epsilon(t). \tag{8.2}$$

In general, from (2.11) and (2.5),

$$\bar{s}_0 = 2c_v\gamma(\gamma-1)c_0^{-2}\chi(x-u_0t)$$

which implies, from (8.2), that

$$\chi(x-u_0t) = \frac{K_5c_0^2}{2c_v\gamma(\gamma-1)}\epsilon\left[\frac{x-u_0t}{W_0-u_0}\right] \tag{8.3}$$

throughout region O.

By the use of the general solution for the perturbation of a constant state and the conditions (8.1) and (8.3), and applying the boundary conditions on the unperturbed shock locus*, the following solution is obtained:

$$A = \frac{c_0K_5}{2c_v\gamma(\gamma-1)}\epsilon\left[\frac{x-u_0t}{W_0-u_0}\right]+\left[K_3-\frac{c_0K_5}{2c_v\gamma(\gamma-1)}\right]\epsilon\left[\frac{x-(u_0+c_0)t}{W_0-u_0-c_0}\right],$$

$$B = \frac{c_0K_5}{2c_v\gamma(\gamma-1)}\epsilon\left[\frac{x-u_0t}{W_0-u_0}\right]+\left[K_4-\frac{c_0K_5}{2c_v\gamma(\gamma-1)}\right]\epsilon\left[\frac{x-(u_0-c_0)t}{W_0-u_0+c_0}\right].$$

Hence

$$\tilde{u}_0 = \left[K_3-\frac{c_0K_5}{2c_v\gamma(\gamma-1)}\right]\epsilon\left[\frac{x-(u_0+c_0)t}{W_0-u_0-c_0}\right]+$$
$$+\left[\frac{c_0K_5}{2c_v\gamma(\gamma-1)}-K_4\right]\epsilon\left[\frac{x-(u_0-c_0)t}{W_0-u_0+c_0}\right] \tag{8.4}$$

is the particle velocity perturbation throughout region O, and, in particular its value on the piston path is obtained by setting $x = u_0t$ in (8.4). The perturbed piston and shock paths are obtained by simple integration.

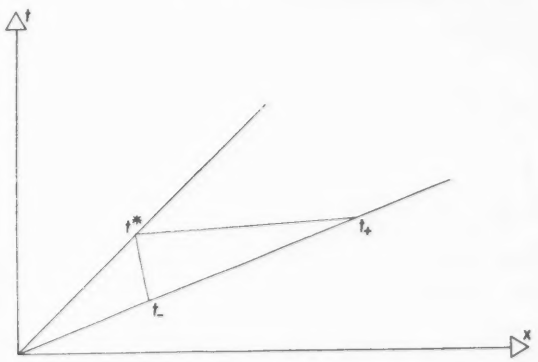

Figure 3.

It is not immediately obvious how the characteristics should be oriented. However, in figure 3, consider an arbitrary point on the piston curve

* The error thus introduced is of the order of the neglected terms and therefore neglible, viz. if the original shock locus is $x = W_0t$, the new shock locus is $x = W_0t+\int_{t_2}^{t}\epsilon(y)\,dy$, and

$$\eta\left[W_0t+\int_{t_2}^{t}\epsilon(y)\,dy\right] = \eta(W_0t)+\eta'(W_0t)\int_{t_2}^{t}\epsilon(y)\,dy+\ldots.$$

(e.g. t^*), and let t_- be the intersection of the shock locus and the characteristic with slope $u_0 - c_0$ through this point. The characteristic with slope $u_0 + c_0$ through t^* intersects the shock locus in a point which will be denoted by t_+. These points are given by

$$t_+ = c_0 t^*/(u_0 + c_0 - W_0), \qquad t_- = c_0 t^*/(c_0 - u_0 + W_0).$$

Consequently, from (8.4) with $x = u_0 t$, it is seen that a perturbation at a particular point of the piston curve is determined by the perturbation at two points of the shock curve with the depicted orientation. Hence, the (x, t)-representation is as in figure 4. The region in which the flow is perturbed is cross-hatched. The relation between t_1 and t_2 is

$$t_2 = c_0 t_1/(u_0 + c_0 - W_0).$$

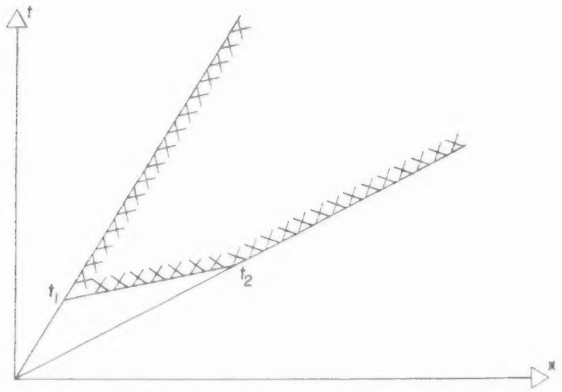

Figure 4.

9. Direct problem

From the solution of the inverse problem, the solution of the direct problem is easily obtained, and the solution is given by a uniformly convergent infinite series. Let $\eta(t)$ be the prescribed perturbation of the piston velocity, and $\epsilon(t)$ the perturbation of the shock velocity. From (8.4), we get

$$\begin{aligned}\eta(t) &= \left[K_3 - \frac{c_0 K_5}{2c_v\gamma(\gamma-1)}\right]\epsilon\left[\frac{c_0 t}{c_0 + u_0 - W_0}\right] + \\ &\quad + \left[\frac{c_0 K_5}{2c_v\gamma(\gamma-1)} - K_4\right]\epsilon\left[\frac{c_0 t}{W_0 - u_0 + c_0}\right] \\ &= R_1\epsilon\left[\frac{c_0 t}{c_0 - u_0 + W_0}\right] + R_2\epsilon\left[\frac{c_0 t}{u_0 + c_0 - W_0}\right]. \qquad (9.1)\end{aligned}$$

Figure 5 illustrates the scheme to be utilized. The lines drawn between the piston and shock paths are the characteristics, the odd-numbered lines having slope $(u_0 + c_0)$ and the even-numbered lines having slope $(u_0 - c_0)$.

Now, η evaluated at the point 1 is given in terms of multiples of ϵ evaluated at the points 1′ and 2′. $\eta(2)$ is given in terms of multiples of $\epsilon(2')$ and $\epsilon(3')$, etc. $\epsilon(1')$ will be determined. Symbolically, take the first-mentioned relation (1, 1′, 2′), equation (9.2), and for 2′ substitute its equivalent from equation (9.3). This gives a relation (1, 3, 1′, 4′). By continuing this process, a relation of the form (1, 3, 5, 7, ..., n, 1′, $[n+1]'$) for n odd is obtained. By indefinite continuation of this process, a series representation is obtained for ϵ in terms of multiples of η evaluated at the points K, where $K = 1, 3, 5, \ldots$. The general term of this series is determined and proved by induction, and the convergence is established.

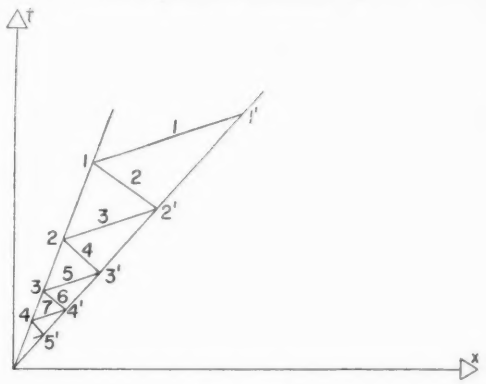

Figure 5.

The coordinates of the point 1′ are chosen to be $(x, t) = (W_0 t^*, t^*)$, and the following notation will be employed:

$$u_0 + c_0 - W_0 \equiv r, \qquad W - u_0 + c_0 \equiv q, \qquad c_0 t^* \equiv t_1.$$

By induction,

$$\eta(1) = R_1 \epsilon(rt_1/q^2) + R_2 \epsilon(t_1/r) \tag{9.2}$$

$$\eta(2) = R_1 \epsilon(r^2 t_1/q^3) + R_2 \epsilon(t_1/q)$$

$$\eta(3) = R_1 \epsilon(r^3 t_1/q^4) + R_2 \epsilon(rt_1/q^2) \tag{9.3}$$

. . . . . .

$$\eta(n) = R_1 \epsilon(r^n t_1/q^{n+1}) + R_2 \epsilon(r^{n-2} t_1/q^{n-1}). \tag{9.4}$$

From (9.2),

$$\epsilon(t_1/r) = \eta(1)/R_2 - (R_1/R_2)\epsilon(rt_1/q^2).$$

The last term is replaced by its equivalent from (9.3), with the result

$$\epsilon(t_1/r) = \eta(1)/R_2 - (R_1/R_2^2)\eta(3) + (R_1/R_2)^2 \epsilon(r^3 t_1/q^4).$$

For the first n terms, the series is

$$\epsilon(t_1/r) = \sum_{K=1}^{n} (-1)^{K+1} R_1^{K-1} R_2^{-K} \eta(2K-1) + (-1)^n (R_1/R_2)^n \epsilon(r^{2n-1} t_1/q^{2n}). \tag{9.5}$$

Mathematical induction is used to prove this assertion, which is certainly true for $K = 1$. Assume it is true for $K = n$. From (9.4), it follows that

$$\epsilon(r^{2n-1} t_1/q^{2n}) = \eta(2n+1)/R_2 - (R_1/R_2)\epsilon(r^{2n+1} t_1/q^{2n+2}). \tag{9.6}$$

Substitution of (9.6) into (9.5) gives

$$\epsilon(t_1/r) = \sum_{K=1}^{n+1} \eta(2K-1)(-1)^{K+1} R_1^{K-1} R_2^{\ K} + (-1)^{n+1}(R_1/R_2)^{n+1}\epsilon(r^{2n+1}t_1/q^{2n+2}). \tag{9.7}$$

Therefore, the assumption that (9.5) is true for n implies it is true for $n+1$. Hence, (9.5) is true for all n.

Since it is assumed that all perturbations are small, the assumption is made that ϵ and η are uniformly bounded. With this reasonable assumption and the easily-seen fact that $R_1/R_2 < 1$, it is readily established that, as $n \to \infty$, the series is uniformly convergent. Hence

$$\epsilon(t_1/r) = \sum_{K=1}^{\infty} (-1)^{K+1} R_1^{K-1} R_2^{\ K} \eta(2K-1).$$

Functional equations of the type (9.1) are treated from a general point of view in Appendix I.

10. Perturbations in a shock tube

The orthodox shock tube consists of a tube divided by a membrane (say at $x = 0$) which separates two fluids, not necessarily the same, originally at rest but not at the same pressure. This is one frequently used device for generating constant shocks in a long tube. It will be assumed that the fluid in the region $x > 0$ is at the higher pressure. If, at $t = 0$, the membrane is removed instantaneously, the fluid in the region $x > 0$ will expand, while the fluid in the region $x < 0$ will be compressed. Under these assumptions, the expansion takes place through a centred rarefaction wave, and the compression across a uniform shock. In general, there will be a contact discontinuity which separates the two portions of fluid as depicted in figure 6.

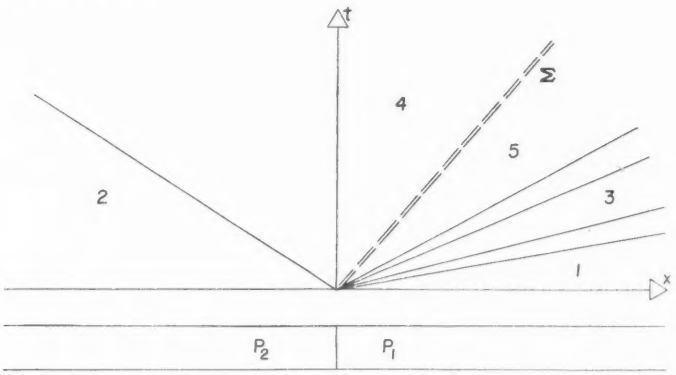

Figure 6.

On this basic flow, which is assumed to be completely known, a perturbation is imposed. The perturbation conditions are not assumed to be the same for the two portions of the fluid. In particular, the isentropic

character of the initial flow will not be retained for the region $x > 0$. Let these conditions be: for $t = 0$ and $x > 0$, $u = \delta g(x)$, $c = c_1 + \delta h(x)$, $s = s_0 + \delta f(x)$; for $t = 0$ and $x < 0$, $u = \delta n(x)$, $c = c_2 + \delta m(x)$, $s = s_0$. Here c_1, c_2 and s_0 are constants, and g, h, f, m and n are known functions. For continuity at $x = 0$, it is assumed that $g(0) = n(0)$, $h(0) = m(0)$ and $f(0) = 0$. The contact discontinuity is given by $x = Kt$.

It is not possible to solve independently for the perturbed flows on the two sides of the contact discontinuity. For the region $x > 0$, no difficulty is encountered in regions 1 and 3. The solution in 3 gives conditions on the last characteristic of the simple wave, but these are insufficient to determine the flow in region 5. However, if on the contact discontinuity $\bar{u}_5$ is specified as $\xi_1(t)$, which is not known, the flow in region 5 can be easily determined in terms of $\xi_1(t)$. For the region $x < 0$, the flow will be non-isentropic since the shock is perturbed. By expressing $\bar{u}_4$, $\bar{c}_4$ and $\bar{s}_4$ in terms of the shock velocity perturbation $\bar{W}$, the flow in region 4 can be determined in terms of $\bar{W}$, which is not known.

Across the contact discontinuity, there is continuity of pressure and particle velocity, and it is easy to see that this implies continuity of the corresponding perturbations. This continuity condition yields two equations in $\xi_1(t)$ and $\bar{W}(t)$. By elimination of $\xi_1(t)$, a functional equation, treated in detail in Appendix II, is obtained for $\bar{W}$ and, once $\bar{W}$ has been determined, the solution of the problem is easily completed.

In terms of $\eta(x)$ and $\xi(x)$, as defined in § 6, the solution in region 1 is

$$\bar{u}_1 = \eta(x - c_1 t) - \xi(x + c_1 t) - \tfrac{1}{2}\rho_1 c_1 f'(x - c_1 t) + \tfrac{1}{2}\rho_1 c_1 f'(x + c_1 t),$$

$$2(\gamma - 1)^{-1}\bar{c}_1 = \eta(x - c_1 t) + \xi(x + c_1 t) - \tfrac{1}{2}\rho_1 c_1 f'(x - c_1 t) - \\ - \tfrac{1}{2}\rho_1 c_1 f'(x + c_1 t) + \rho_1 c_1 f'(x),$$

$$\bar{s}_1 = \gamma(\gamma - 1) c_v \rho_1 f(x).$$

These perturbations travel along the characteristics in region 1 to the first characteristic of the centred simple wave, where they supply boundary conditions for determining the perturbed flow in region 3. On $x = c_1 t$, the first characteristic of the simple wave is

$$B = \xi(2c_1 t) - \tfrac{1}{2}\rho_1 c_1 f'(2c_1 t) + \tfrac{1}{2}\rho_1 c_1 f'(c_1 t),$$

$$\bar{s}_{1,x} = \gamma(\gamma - 1) c_v \rho_1 f'(c_1 t).$$

Application of these conditions and the solution for the non-isentropic perturbation of a centred simple wave gives

$$\omega_1(c_3^2 t^{2\theta}) = \theta c_1^3 \rho_1 \int_0^{(c_3/c_1)^{1/\theta}} y^{2\theta} f'(c_1 y)\, dy,$$

$$F(\rho_3 c_3 t^2)/(\rho_1 c_1)^{1/2} = \int_0^{(\rho_3 c_3/\rho_1 c_1)^{1/2} t} \{\xi(2c_1 z) - \tfrac{1}{2}\rho_1 c_1 f'(2c_1 z) + \tfrac{1}{2}\rho_1 c_1 f'(c_1 z)\}\, dz - \\ - \rho_1 c_1^3 \int_{z=0}^{t} z^{-2\theta} \int_{y=0}^{z} y^{2\theta} f'(c_1 y)\, dy dz.$$

Consequently, A, B and $\bar{s}_3$ are known throughout the simple wave. As the expressions are very complicated, let the values on the last characteristic of the simple wave be

$$A = \zeta_1(t), \qquad B = \zeta_2(t), \qquad \bar{s}_{3x} = \zeta_3(t),$$

where ζ_1, ζ_2 and ζ_3 are known functions. However, these conditions are not sufficient to determine the perturbed flow in region 5. This is clear, for it cannot be expected that data along one characteristic, but nothing on another curve, would yield a well-set problem. It is convenient to let $\bar{u}_5 = \xi_1(t)$ on $x = Kt$, the contact discontinuity, where, of course, $\xi_1(t)$ is not known at the present time. The perturbed flow in region 5 can now be easily found. Simple reasoning shows that $\bar{c}_5$ is a constant multiple of $\xi_1(t)$ plus and a known function and, therefore,

$$\bar{P}_5 = \nu \xi_1(t) + \Gamma(t)$$

where ν is a constant and Γ is a known function.

As the pressure and velocity are continuous across the contact discontinuity, the perturbations of these quantities are also continuous across this surface, so that

$$\bar{u}_4 = \xi_1(t), \qquad \bar{P}_4 = \nu \xi_1(t) + \Gamma(t)$$

on $x = Kt$.

For region 2, the solution is easily found. This gives $\bar{u}_2$ and $\bar{c}_2$ and, from Appendix III, all perturbed quantities in region 2 are easily determined.

From Appendix III, the values of the perturbed quantities in region 4 may be found just behind the shock in terms of $\bar{W}$. The analysis is simple though tedious, and simple reasoning shows that they have the following form:

$$\left.\begin{aligned} \bar{P}_4 = R_5 + R_6 \bar{W}, \qquad \bar{\rho}_4 = R_7 + R_8 \bar{W}, \qquad \bar{c}_4 = R_9 + R_{10} \bar{W}, \\ \bar{s}_4 = R_{11} + R_{12} \bar{W}, \qquad \bar{u}_4 = R_{13} + R_{14} \bar{W}, \\ A = R_{15} + R_{16} \bar{W}, \qquad B = R_{17} + R_{18} \bar{W}, \end{aligned}\right\} \tag{10.1}$$

where all the R's are known, and odd-numbered subscripts denote functions of t while even-numbered subscripts denote constants.

Utilization of the solution for the non-isentropic perturbation of a constant state and the boundary conditions (10.1) gives

$$\begin{aligned} A = R_{19}\left[\frac{x - u_4 t}{W - u_4}\right] + R_{21}\left[\frac{x - (u_4 + c_4)t}{W - u_4 - c_4}\right] + \\ + R_{22} \bar{W}\left[\frac{x - (u_4 + c_4)t}{W - u_4 - c_4}\right] + R_{20} \bar{W}\left[\frac{x - u_4 t}{W - u_4}\right], \end{aligned}$$

$$\begin{aligned} B = R_{19}\left[\frac{x - u_4 t}{W - u_4}\right] + R_{23}\left[\frac{x - (u_4 - c_4)t}{W - u_4 + c_4}\right] + \\ + R_{24} \bar{W}\left[\frac{x - (u_4 - c_4)t}{W - u_4 + c_4}\right] + R_{20} \bar{W}\left[\frac{x - u_4 t}{W - u_4}\right], \end{aligned}$$

where all the R's are known.

Throughout the region 4, we have

$$\bar{P}_4 = \frac{2\gamma\rho_4}{c_4(\gamma-1)}\bar{c}_4 - \frac{P_4}{(\gamma-1)c_v}\bar{s}_4.$$

The continuity of $\bar{P}$ across the contact discontinuity gives an equation of the form

$$\xi_1(t) = R_{25}(t) + R_{22}\bar{W}\left[\left(\frac{K-u_4-c_4}{\bar{W}-u_4-c_4}\right)t\right] + \\ + R_{24}\bar{W}\left[\left(\frac{K-u_4+c_4}{\bar{W}-u_4+c_4}\right)t\right] + R_{26}\bar{W}\left[\left(\frac{K-u_4}{\bar{W}-u_4}\right)t\right], \quad (10.2)$$

and the continuity of $\bar{u}$ across the contact discontinuity gives

$$\xi_1(t) = R_{27}(t) + R_{28}\bar{W}\left[\left(\frac{K-u_4-c_4}{\bar{W}-u_4-c_4}\right)t\right] + R_{30}\bar{W}\left[\left(\frac{K-u_4+c_4}{\bar{W}-u_4+c_4}\right)t\right]. \quad (10.3)$$

Division of (10.2) by (10.3) serves to eliminate $\xi_1(t)$, with the result

$$R_{32}\bar{W}\left[\left(\frac{K-u_4+c_4}{\bar{W}-u_4+c_4}\right)t\right] + R_{34}\bar{W}\left[\left(\frac{K-u_4-c_4}{\bar{W}-u_4-c_4}\right)t\right] + \\ + R_{36}\bar{W}\left[\left(\frac{K-u_4}{\bar{W}-u_4}\right)t\right] = R_{31}(t),$$

where all the R's are known. Once $\bar{W}$ has been found, $\xi_1(t)$ is given immediately, and the solution is easily completed. This functional equation is discussed in Appendix II.

PART III. TUBE OF SLOWLY VARYING CROSS-SECTION

The flow in a long tube whose cross-section is made to undergo a small variation with x can be treated by a similar analysis. It is convenient to express the cross-section of the tube in the form $E(x) = E_0 + \delta E_1(x)$, where E_0 is the original uniform cross-sectional area and δ is a small parameter.

It will be assumed that the tube consists of two parts, one of uniform cross-section, and one of perturbed cross-section. A uniform shock, introduced in the tube where the cross-section is uniform, will travel along the tube and remain uniform until it reaches the transition section. The gas in front of the shock is assumed to be at rest, and the small effects due to the discontinuity in the slope of the tube at the transition section will be neglected. After the shock passes the transition section, it will be perturbed, and the flow behind the shock will necessarily be non-isentropic. The problem is to describe the flow behind the shock and to find the perturbed shock locus. The results are applied to several problems, and some comparisons are made with work by a previous author.

11. Derivation of equations which govern the flow

Clearly, the Euler and energy equations are not affected by the cross-sectional perturbation, but the continuity equation contains an additional

term. The mass, contained in an arbitrary volume τ, may be written as

$$M = \int_{\tau} \rho \, d\tau = \int_{x} \rho \, E(x) \, dx.$$

The continuity equation, $DM/Dt = 0$, implies that

$$(\rho E)_t + (\rho E u)_x = 0.$$

Consequently, the basic equations are

$$u_t + u u_x + 2c_x/(\gamma - 1) = s_x c^2/c_v \gamma(\gamma - 1),$$
$$2Ec_t/(\gamma - 1) + 2Euc_x/(\gamma - 1) + cEu_x + cE_t + ucE_x = 0,$$
$$s_t + us_x = 0.$$

A formal linearization in the neighbourhood of an originally isentropic flow gives

$$u_0 u_{1x} + u_{1t} + 2c_0 c_{1x}/(\gamma - 1) + u_1 u_{0x} + 2c_{0x} c_1/(\gamma - 1) = c_0^2 s_{1x}/c_v \gamma(\gamma - 1), \quad (11.1)$$

$$2c_{1t}/(\gamma - 1) + c_0 u_{1x} + 2u_0 c_{1x}/(\gamma - 1) + c_1 u_{0x} + 2u_1 c_{0x}/(\gamma - 1) + u_0 c_0 E_{1x}/E_0 + 2c_{0t} E_1/E_0(\gamma - 1) + c_0 u_{0x} E_1/E_0 + 2u_0 c_{0x} E_1/E_0(\gamma - 1) = 0, \quad (11.2)$$

$$s_{1t} + u_0 s_{1x} = 0. \quad (11.3)$$

It is thus clear that the cross-sectional perturbation merely introduces a non-homogeneous term into the basic perturbation equations which were previously derived, so that the mathematical results of the previous sections may be utilized, and the problem is reduced to the determination of a particular integral of (11.1), (11.2) and (11.3).

For the case of an initially uniform flow, (11.3) may be solved independently, and, utilizing the same procedure as employed in §2, the following equations are obtained:

$$A_t + (u_0 + c_0)A_x = -\tfrac{1}{2}u_0 c_0 E_{1x}/E_0 + \tfrac{1}{2}H_0,$$
$$B_t + (u_0 - c_0)B_x = -\tfrac{1}{2}u_0 c_0 E_{1x}/E_0 - \tfrac{1}{2}H_0.$$

The general solution in terms of three arbitrary functions is

$$H_0 = 2\chi'(x - u_0 t),$$
$$A = F[x - (u_0 + c_0)t] + c_0^{-1}\chi(x - u_0 t) - \tfrac{1}{2}u_0 c_0 E_1/E_0(u_0 + c_0), \quad (11.4)$$
$$B = G[x - (u_0 - c_0)t] + c_0^{-1}\chi(x - u_0 t) - \tfrac{1}{2}u_0 c_0 E_1/E_0(u_0 - c_0). \quad (11.5)$$

Consequently, there is a perturbation, due to the entropy variations, which travels along the particle paths, and this is measured by χ; the perturbations measured by F travel along one family of characteristics with sonic velocity relative to the fluid, and the perturbations measured by G travel along the other family of characteristics with sonic velocity relative to the fluid.

Chester (1953) has considered the disturbance produced behind a plane shock of arbitrary strength travelling down a two-dimensional channel of non-uniform width, and the problem was linearized on the basis of small variations of the width of the channel. The variations in width were assumed

to take place within a finite length of the channel, and this region of transition separates two uniform portions each of infinite length but not necessarily equal widths. The pressure field behind the shock was built up from the known solution of the diffraction of a shock wave travelling along a wall with a corner (Lighthill 1948). In a later paper, Chester (1954) considered essentially the same problem, but a different approach was used and applied to a tube of arbitrary cross-section.

Let the flow in front of the shock be given by $u_0 = 0$, c_0, P_0, ρ_0, the flow behind by u_2, c_2, P_2, ρ_2, and the shock velocity by w. Let $v_2 = u_2 - w$ and $M_0 = w/c_0$. The following relations are easily obtained:

$$u_2 = 2w(1 - M_0^{-2})/(\gamma+1),$$

$$|v_2| = |u_2 - w| = w(\gamma - 1 + 2M_0^{-2})/(\gamma+1),$$

$$(\gamma+1)P_2 = 2\rho_0[w^2 + (1-\gamma)c_0^2/2\gamma] = P_0[2\gamma M_0^2 - \gamma + 1],$$

$$M_1 = |v_2|/c_2 = [(\gamma - 1 + 2M_0^{-2})/(2\gamma - (\gamma-1)M_0^{-2})]^{1/2},$$

$$m = u_2/c_2 = 2(1 - M_1^2)/M_1(\gamma+1).$$

Chester restricted his treatment to the investigation of the average pressure and, for the case where the tube consists of two cylinders connected by a transition section, the following result was obtained:

$$\bar{P}_2 = -K^*(P_2 - P_0)E_1/E_0,$$

$$K^* = 2(1+m)^{-1}(1 + M_0^{-2} + 2M_1)^{-1}.$$

The parameter K^* decreases monotonically with the shock strength, and $0{\cdot}5 \geqslant K^* > 0{\cdot}394$. Actually, it is clear that the disturbance depends only on the variations in the area of the tube and not on the actual shape of the cross-section, as will be seen shortly.

It will now be shown that, using the purely one-dimensional analysis of this section, Chester's result can be obtained quite simply. Consider the general solution (11.4) and (11.5). The term in E_1 is due directly to the changes in cross-section, and this disturbance is reflected at the shock and gives rise to the term involving G. From the way Chester has formulated the problem (i.e. with the shock coming from infinity, so to speak), the contribution given by F is not included, for there is no mechanism (e.g. a piston curve) for reflection upstream of the shock which could give rise to such a term. In other words, Chester's result should be obtainable from (11.4) and (11.5) by putting $F = 0$. The details are sketched below. If $F = 0$, it follows from (11.4) that

$$\frac{\bar{u}_2}{2c_2} + \frac{\bar{c}_2}{c_2(\gamma-1)} - \frac{\bar{s}_2}{2c_p\gamma(\gamma-1)} = -\frac{m(1+m)^{-1}E_1}{2E_0}.$$

From the shock perturbation tables given in Appendix III, it is easily determined that

$$\bar{c}_2/c_2(\gamma-1) - \tfrac{1}{2}\bar{s}_2/c_p\gamma(\gamma-1) = \tfrac{1}{2}\bar{P}_2/\gamma P_2.$$

Hence

$$\bar{u}_2/c_2 = -\bar{P}_2/\gamma P_2 - mE_1/(1+m)E_0. \tag{11.6}$$

As

$$u_2/c_0 = 2(M_0 - M_0^{-1})/(\gamma+1), \qquad (\gamma+1)\bar{u}_2/c_0 = 2(1+M_0^{-2})\bar{M}_0,$$

and, from relation IX of Appendix III,

$$\bar{P}_2/P_2 = 4\gamma \bar{M}_0 M_0/(2\gamma M_0^2 - \gamma + 1),$$

then

$$\frac{\bar{u}_2}{c_0} = \frac{(1+M_0^2)(2\gamma M_0^2 - \gamma + 1)\bar{P}_2}{2\gamma(\gamma+1)M_0^2 P_2},$$

$$\frac{c_2^2}{c_0^2} = \frac{P_2\rho_0}{P_0\rho_2} = \frac{(2\gamma M_0^2 - \gamma + 1)[2+(\gamma-1)M_0^2]}{M_0^2(\gamma+1)^2}.$$

Hence

$$c_0\,\bar{u}_2/c_2\,c_0 = \bar{u}_2/c_2 = (1+M_0^2)\bar{P}_2/2\gamma M_0^2 M_1 P_2.$$

Also, from (11.6),

$$\bar{P}_2(1+M_0^2+2M_0^2M_1)/2P_2M_0^2 = -\gamma M_1 m E_1/(1+m)E_0.$$

Finally, since

$$P_2 = \{2\gamma M_0^2 - (\gamma-1)\}(P_2 - P_0)/2\gamma(M_0^2-1),$$

then

$$\bar{P}_2 = -(P_2-P_0)E_1E_0^{-1}(1+m)^{-1}(1+2M_1+M_0^{-2})^{-1}\left\{\frac{mM_1(2\gamma M_0^2-\gamma+1)}{M_0^2-1}\right\}.$$

It is easily shown that the term in braces is equal to 2. Hence, the result is the same as that obtained by Chester.

The analysis of the present paper is useful because it can be applied to a variety of problems. In the next section, a problem where the perturbations are reflected on a piston curve is treated. The analysis could be applied to a problem where the tube is open at one end. In such a problem, reflection at a surface of constant pressure would be encountered.

12. Slowly converging or diverging cross-section

For this problem, $E_1(x) = Kx$, where $K > 0$ for a diverging cross-section and $K < 0$ for a converging cross-section. By a uniform compressive motion, a uniform shock is introduced at $x = 0$. It is assumed that the

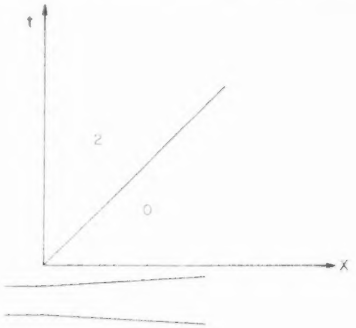

Figure 7.

piston is pushed continuously with velocity V, and the original shock velocity is w. Figure 7 is the (x,t)-representation of the flow. Region O is a rest state, and the perturbed flow behind the shock is denoted by 2.

The problem will be solved by expressing the perturbations $\bar{u}_2$, $\bar{c}_2$ and $\bar{s}_2$ in terms of $\bar{w}$, at present unknown, and using the general solution (§ 11) to find A and B throughout region 2 in terms of $\bar{w}$. From the assumptions of the problem, $\bar{u}_2 = 0$ on the piston path; this gives a functional equation from which $\bar{w}$ can be easily determined.

The Prandtl relation, in perturbation form, gives

$$\bar{u}_2 = 2K_1\bar{w}, \qquad \bar{c}_2 = K_2(\gamma-1)\bar{w}$$

on the shock, with

$$2K_1 = 2(1-\theta) - u_2/w = 2(\gamma+1)^{-1}(1+M_0^{-2}),$$

$$K_2 = \frac{2(w-u_2)}{c_2(\gamma+1)} + \frac{u_2^2}{2wc_2} = \frac{2}{\gamma+1}M_1 + \frac{m}{\gamma+1}(1-M_0^{-2}).$$

Consequently

$$A = (K_1+K_2)\bar{w} = K_3\bar{w}, \qquad B = (K_2-K_1)\bar{w} = K_4\bar{w}$$

on the shock.

By the same analysis as in part II,

$$\bar{s}_2 = \left\{\frac{2c_v K_2(\gamma-1)}{c_2} - \frac{(\gamma-1)c_v[u_2-(1-\theta)w]}{w(u_2-w)}\right\}\bar{w}(t)$$

$$= \frac{c_v(\gamma-1)}{w}\left\{\frac{4}{\gamma+1}\frac{(1-M_1^2)}{(1-M_0^{-2})} + m^2 - 1 + \frac{\gamma-1}{\gamma-1+2M_0^{-2}}\right\} \equiv K_5\bar{w}(t),$$

on the shock. Throughout region 2,

$$\bar{s}_2 = 2c_v\gamma(\gamma-1)c_2^{-2}\chi(x-u_2t),$$

so that

$$2c_v\gamma(\gamma-1)\chi(x-u_2t) = K_5c_2^2\bar{w}[(x-u_2t)/(w-u_2)].$$

By the use of the general solution and the boundary conditions, the solution for region 2 is

$$A = -\frac{u_2c_2Kx}{2E_0(u_2+c_2)} + c_2K_5[2c_v\gamma(\gamma-1)]^{-1}\bar{w}\left[\frac{x-u_2t}{w-u_2}\right] +$$
$$+\left\{K_3 - \frac{c_2K_5}{2c_v\gamma(\gamma-1)}\right\}\bar{w}\left[\frac{x-(u_2+c_2)t}{w-u_2-c_2}\right] +$$
$$+u_2c_2Kw\frac{[x-(u_2+c_2)t]}{[2E_0(u_2+c_2)][w-u_2-c_2]},$$

$$B = -\frac{u_2c_2Kx}{2E_0(u_2-c_2)} + \frac{c_2K_5}{2c_v\gamma(\gamma-1)}\bar{w}\left[\frac{x-u_2t}{w-u_2}\right] +$$
$$+\left[K_4 - \frac{c_2K_5}{2c_v\gamma(\gamma-1)}\right]\bar{w}\left[\frac{x-(u_2-c_2)t}{w-u_2+c_2}\right] +$$
$$+\left[\frac{x-(u_2-c_2)t}{w-u_2+c_2}\right]\frac{u_2c_2Kw}{2E_0(u_2-c_2)}.$$

As $u_2 = 0$ on $x = Vt$, the following equation is obtained for the determination of $\bar{w}$:

$$\left[K_3 - \frac{c_2K_5}{2c_v\gamma(\gamma-1)}\right]\bar{w}\left[\frac{-c_2t}{w-u_2-c_2}\right] + \bar{w}\left[\frac{c_2t}{w-u_2+c_2}\right]\left[\frac{c_2K_5}{2c_v\gamma(\gamma-1)} - K_4\right]$$
$$= u_2c_2^2K(w-u_2)[(w-u_2)^2-c_2^2]^{-1}E_0^{-1}t.$$

It is easily seen that a linear function of t satisfies this equation, and the solution is

$$\left[\frac{K_5 M_1 c_2}{2c_v \gamma(\gamma-1)} - K_1 - K_2 M_1\right] 2E_0 \bar{v}(t) = u_2 K(w-u_2)t.$$

The pressure perturbation behind the shock is, in terms of the parameters M_0, M_1 and m,

$$\bar{P}_2 = -K_6(P_2 - P_0)E_1 E_0^{-1},$$

$$(\gamma+1)K_6 = 2(\gamma-1+2M_0^{-2})\left[2M_1^2 + mM_1(1-M_0^{-2}) + (1+M_0^{-2}) - \right.$$

$$\left. - \frac{(\gamma-1+2M_0^{-2})}{2\gamma}\left\{\frac{4(1-M_1^2)}{(\gamma+1)(1-M_0^{-2})} + m^2 - 1 + \frac{\gamma-1}{(\gamma-1+2M^{-2})}\right\}\right]^{-1}.$$

Here K_6 is a monotonically decreasing function of the shock strength; and, for $\gamma = 7/5$, $0{\cdot}259 < K_6 \leqslant 0{\cdot}608$. A graph of this function is given in figure 8.

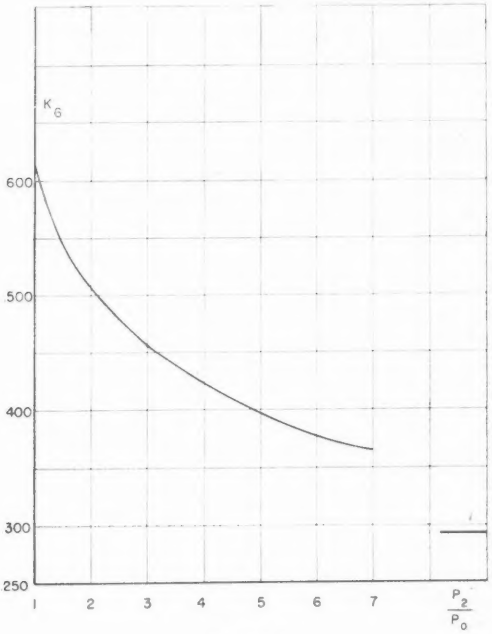

Figure 8.

13. Conclusions

In this work, several problems of flows with weak entropy changes have been considered and solved explicitly. Without going further into the details of the problems treated, we may note the type of functional equations to which the solutions of these problems lead. That is, the values of the function to be found appeared in the same relation for different values of the independent variable.

It is clear that in cases where an analytic solution cannot be found, the general equations are suitable for a numerical calculation developed step by step along the characteristics. This procedure would be necessary for the perturbation of a flow with a shock of constant intensity.

It is also clear that the problems treated here are among the most simple non-isentropic flows that can be considered. Undoubtedly, an analogous theory could be developed for steady flow in two dimensions. However, it is not at all sure that analytic results as complete as the present ones could be obtained. Perturbations can also be considered which introduce a new coordinate, but the problem is then even more complex. Several particular cases where the perturbed flow is uniform have already been considered, but much important work remains to be done.

The following problem, which has already been solved (Gundersen 1954), may be noted. By the use of the method of characteristic coordinates, an analytic solution was obtained for the interaction, in an inviscid ideal gas with a constant ratio of specific heats of 5/3, of a centred rarefaction wave and a non-uniform shock of constant intensity, i.e. the entropy jump is constant all along the shock with the result that the flow is isentropic on both sides of the shock. This work shows that the analysis of this paper need not be restricted to the perturbation of uniform shocks.

These studies are important because flows with shock waves play an increasingly important role in numerous technical problems, and, except for certain exceptional cases, such flows are not isentropic.

The problem discussed in this paper was suggested by Professor Paul Germain and the research directed by him. The author wishes to express his sincere appreciation to Professor Germain for his valuable advice and his continuous and stimulating interest in the project.

Appendix I

The functional equation

$$Af(at)+Bf(bt)=g(t) \tag{A 1}$$

will be considered, where A, B, a and b are constants. Assume

$$|B|>|A|, \qquad |b|>|a|, \tag{A 2}$$

and put

$$\left.\begin{aligned} a/b=\xi, \quad A/B=K, \quad \tau=bt, \quad f(bt)=F(\tau), \quad g(\tau/b)=BG(\tau), \\ f(at)=f(bta/b)=F(\xi\tau). \end{aligned}\right\} \tag{A 3}$$

Consequently, (A 1) may be written as

$$KF(\xi\tau)+F(\tau)=G(\tau), \qquad |\xi|<1, \quad |K|<1. \tag{A 4}$$

Conversely, if $G(\tau)$ is known, and if $F(\tau)$ satisfies (A 4), i.e. if (A 4) can be solved, (A 1) can also be solved.

Theorem: If $G(\tau)$ is continuous in an interval I $(-N\leqslant\tau\leqslant N)$, which implies that $G(\tau)$ is also bounded in I, and if $F(\tau)$ is uniformly bounded

in a neighbourhood of $\tau = 0$, there exists one and only one solution of (A 4) defined in I. $F(\tau)$ is a continuous function in I. If $G(\tau)$ is continuously differentiable in I, $F(\tau)$ is also continuously differentiable in I.

Proof: If $\tau \in I$, $\xi^n \tau \in I$ because $|\xi| < 1$. Then

$$F(\tau) + K F(\xi\tau) = G(\tau),$$
$$F(\xi\tau) + K F(\xi^2\tau) = G(\xi\tau),$$
$$\cdots\cdots\cdots,$$
$$F(\xi^n\tau) + K F(\xi^{n+1}\tau) = G(\xi^n\tau).$$

Consequently,

$$F(\tau) + (-1)^n K^{n+1} F(\xi^{n+1}\tau) = G(\tau) + \sum_{p=1}^{n} (-1)^p K^p G(\xi^p\tau) = g_n(\tau).$$

Hence

$$|F(\tau) - g_n(\tau)| = |K^{n+1}||F(\xi^{n+1}\tau)|.$$

As $F(\tau)$ is to be uniformly bounded in a neighbourhood of $\tau = 0$, it is possible to find n large enough so that $|F(\xi^{n+1}\tau)|$ is bounded. Call this bound C. Thus

$$|F(\tau) - g_n(\tau)| \leqslant C|K^{n+1}|. \tag{A 5}$$

Since $|K| < 1$, if such a solution $F(\tau)$ exists, it must be the uniform limit of the sequence $g_n(\tau)$ in I (uniform convergence). Conversely, if $g_n(\tau)$ is a uniform sequence of functions in I, the limit is the unique solution of (A 4). However, it is obvious that the series

$$\sum_{p=0}^{\infty} (-1)^p K^p G(\xi^p\tau)$$

is uniformly convergent in I. Hence the solution of (A 4) is

$$F(\tau) = \sum_{p=0}^{\infty} (-1)^p A^p B^{-p-1} g(a^p\tau/b^{p+1}).$$

Remarks: 1. If $G(\tau) = \tau^n$, $F(\tau) = \tau^n/(1 + K\xi^n)$, $n \geqslant 0$. Thus, if $G(\tau)$ may be approximated by $\sum_{p=1}^{n} d_p \tau^p$, $F(\tau)$ may be approximated by

$$\sum_{p=1}^{n} d_p \tau^p/(1 + K\xi^p).$$

If $G(\tau)$ has a Taylor expansion in I (i.e. it is an analytic function), $F(\tau)$ is an analytic function in I.

2. If $|K| = 1$, it is necessary to assume $G(0) = 0$. To preserve uniqueness, it is necessary to assume $f(t)$ is continuous near $t = 0$.

3. If $|\xi| = 1$, there is no problem if $\xi = 1$, $K \neq -1$;

$$F(\tau) = G(\tau)/(1 + K).$$

4. If $\xi = -1$, $|K| < 1$, then

$$K F(-\tau) + F(\tau) = G(\tau), \qquad K F(\tau) + F(-\tau) = G(-\tau),$$
$$F(\tau)(1 - K^2) = G(\tau) + K G(-\tau).$$

5. If $\xi = 1$, $|K| = 1$, the problem is either impossible or indeterminate.

Appendix II

The functional equation

$$f(t)+hf(mt)+Kf(nt)=g(t) \tag{B 1}$$

will be considered, where h, K, m and n are constants, and $|m|<1$, $|n|<1$, $|h|+|K|<1$.

Theorem: If $f(t)$ is uniformly bounded in a neighbourhood of $t=0$, and $g(t)$ is continuous in an interval I ($|t|\leqslant A$), there exists one and only one solution of (B 1) defined in I. $f(t)$ is a continuous function in I and, if $g(t)$ is continuously differentiable in I, $f(t)$ is also continuously differentiable in I. The solution of (B 1) is

$$f(t)=\sum_{p=0}^{\infty}\sum_{q=0}^{\infty}(-1)^{p+q}h^pK^qg(m^pn^qt)(p+q)!/p!\,q!, \tag{B 2}$$

where this series is uniformly convergent.

First, formally consider the functions $g(m^pn^qt)$, where $p,q=0,1,2,3,\ldots$, and attempt a solution of (B 1) of the form

$$\sum_{p=0}^{\infty}\sum_{q=0}^{\infty}e_{p,q}\,g(m^pn^qt). \tag{B 3}$$

The series (B 3) is a solution of (B 1) if

$$\left.\begin{aligned} &e_{0,0}=1, \qquad e_{0,1}+Ke_{0,0}=0, \qquad e_{1,0}+he_{0,0}=0,\\ &e_{p,q}+he_{p-1,q}+Ke_{p,q-1}=0. \end{aligned}\right\} \tag{B 4}$$

Put $$e_{p,q}=(-1)^{p+q}d_{p,q}h^pK^q.$$

Then

$$d_{p,q}=d_{p-1,q}+d_{p,q-1}, \qquad d_{0,0}=1, \qquad d_{0,1}=d_{1,0}=1,$$

and therefore

$$d_{p,q}=(p+q)!/p!\,q!. \tag{B 5}$$

It is now necessary to show that (B 2) is actually the solution of (B 1) and that it is unique. Consider the operator L_r which is defined by

$$L_r\phi=\sum_{p=0}\sum_{q=0}(-1)^{p+q}h^pK^q\phi(m^pn^qt)(p+q)!/p!\,q!, \qquad p+q\leqslant r. \tag{B 6}$$

The application of this operator to (B 1) gives

$$f(t)-L_rg(t)=\sum_{p+q=r+1}\sum h^pK^q[hf(m^{p+1}n^qt)+Kf(m^pn^{q+1}t)](-1)^{p+q}\frac{(p+q)!}{p!\,q!},$$

$$|f-L_rg|=\sum_{p+q=r+1}\sum[|h||f(m^{p+1}n^qt)|+|K||f(m^pn^{q+1}t)|]|h|^p|K|^q\frac{(p+q)!}{p!\,q!}.$$

Since f is to be uniformly bounded in a neighbourhood of $t=0$, it is possible to find r large enough so that

$$|f(m^pn^{q+1}t)|<M, \qquad |f(m^{p+1}n^qt)|<M,$$

where M is a constant. Therefore

$$|f-L_rg|<M\sum_{p+q=r+1}\sum|h|^p|K|^q(p+q)!/p!\,q!. \tag{B 7}$$

As $r\to\infty$, the right-hand side approaches zero and

$$f(t) = L_\infty g(t) = \sum_{p=0}^{\infty} \sum_{q=0}^{\infty} (-1)^{p+q} h^p K^q g(m^p n^q t)(p+q)!/p!\,q!\,. \quad \text{(B 8)}$$

As g is uniformly bounded in I, say $|g(t)| < N$, $|t| \leqslant A$, the series

$$N[1+|h|+|K|]^{-1} = N \sum_{p=0}^{\infty} \sum_{q=0}^{\infty} (-1)^{p+q} |h|^p |K|^q (p+q)!/p!\,q! \quad \text{(B 9)}$$

is a dominant series for (B 8), and (B 8) is uniformly convergent. It has been tacitly assumed that $|h| + |K| < 1$. For other values of h and K, f must be analytically continued. This question will not be discussed here.

If $g(t) = t^r$, $f(t) = t^r(1 + hm^r + Kn^r)^{-1}$. Thus, if $g(t)$ may be approximated by $\sum_{r=1}^{p} a_r t^r$, $f(t)$ may be approximated by

$$\sum_{r=1}^{p} b_r t^r [1 + hm^r + Kn^r]^{-1}.$$

If $g(t)$ is an analytic function in I, $f(t)$ is an analytic function in I.

Appendix III. Table of perturbations

From the equations which govern the flow, many relations between the perturbed quantities may be obtained. A few of these are tabulated below, where all perturbations will be denoted by a bar, e.g. $\bar{c}_1$ where the basic quantity is c_1.

$$c_1^2 = \gamma \exp[(s_1 - s^*)/c_v]\rho_1^{\gamma-1}, \qquad \bar{\rho}_1 = 2\rho_1 \bar{c}_1/c_1(\gamma-1) - \rho_1 \bar{s}_1/c_v(\gamma-1). \quad \text{(I)}$$

$$c_1^2 = \gamma P_1/\rho_1, \qquad \gamma \bar{P}_1 = c_1^2 \bar{\rho}_1 + 2c_1 \rho_1 \bar{c}_1. \quad \text{(II)}$$

$$\frac{P_2}{P_1} = \frac{\rho_2 - \theta\rho_1}{\rho_1 - \theta\rho_2}, \qquad \frac{\bar{P}_2}{P_2} - \frac{\bar{P}_1}{P_1} = \frac{\bar{\rho}_2 - \theta\bar{\rho}_1}{\rho_2 - \theta\rho_1} - \frac{\bar{\rho}_1 - \theta\bar{\rho}_2}{\rho_1 - \theta\rho_2}. \quad \text{(III)}$$

$$P_2/P_1 = (1+\theta)|u_1 - W|^2/c_1^2 - \theta. \quad \text{(III')}$$

$$\frac{\bar{P}_2 + \theta\bar{P}_1}{P_2 + \theta P_1} - \frac{\bar{P}_1}{P_1} = 2\left[\frac{\bar{u}_1 - \bar{W}}{u_1 - W} - \frac{\bar{c}_1}{c_1}\right],$$

$$\text{or } \frac{\bar{P}_2}{P_2} - \frac{\bar{P}_1}{P_1} = \frac{2(P_2 + \theta P_1)}{P_2}\left[\frac{\bar{u}_1 - \bar{W}}{u_1 - W} - \frac{\bar{c}_1}{c_1}\right]. \quad \text{(IV)}$$

$$\frac{\rho_2}{\rho_1} = \frac{v_1}{v_2}, \qquad \frac{\bar{\rho}_2}{\rho_2} + \frac{\bar{u}_2 - \bar{W}}{u_2 - W} = \frac{\bar{\rho}_1}{\rho_1} + \frac{\bar{u}_1 - \bar{W}}{u_1 - W}. \quad \text{(V)}$$

$$(1-\theta)(W-u_1)^2 - (u_2 - u_1)(W - u_1) = (1-\theta)c_1^2.$$

$$2(1-\theta)(W-u_1)(\bar{W} - \bar{u}_1) - (u_2 - u_1)(w - u_1) \times \left[\frac{\bar{u}_2 - \bar{u}_1}{u_2 - u_1} + \frac{\bar{W} - \bar{u}_1}{W - u_1}\right] = 2(1-\theta)c_1 \bar{c}_1. \quad \text{(VI)}$$

$$P = \exp[(s - s^*)/c_v]\rho^\gamma, \qquad c^2 = \gamma P/\rho = \gamma P^{(\gamma-1)/\gamma} \exp[(s - s^*)/c_v].$$

$$2\bar{c}_1/c_1 = (1 - \gamma^{-1})\bar{P}_1/P_1 + \bar{s}_1/\gamma c_v. \quad \text{(VII)}$$

$$v_2 v_1 = c_*^2 = \theta v_1^2 + (1-\theta)c_1^2 = \theta v_2^2 + (1-\theta)c_2^2.$$

$$(u_1 - W)(\bar{u}_2 - \bar{W}) + (u_2 - W)(\bar{u}_1 - \bar{W}) = 2\theta(u_1 - W)(\bar{u}_1 - \bar{W}) + (1-\theta)2c_1\bar{c}_1 = 2\theta(u_2 - W)(\bar{u}_2 - \bar{W}) + (1-\theta)c_2\bar{c}_2. \quad \text{(VIII)}$$

In some problems, it is convenient to express all perturbed quantities in terms of one parameter, e.g. as in the problem of § 4 where $\bar{W}$ was used as the parameter. Another convenient parameter, which leads to a concise representation of the perturbed quantities, is $M = |v|/c$. From relation III′ above,

$$\frac{\bar{P}_2}{P_2} - \frac{\bar{P}_1}{P_1} = \frac{4\gamma M_1 \bar{M}_1}{2\gamma M_1^2 - (\gamma - 1)}, \tag{IX}$$

Now
$$\frac{\rho_2}{\rho_1} = \frac{P_2/P_1 + \theta}{1 + \theta P_2/P_1} = \frac{2\gamma M_1^2/(\gamma+1)}{1 + \theta\{2\gamma M_1/(\gamma+1) - \theta\}}$$

implies that

$$\frac{\bar{\rho}_2}{\rho_2} - \frac{\bar{\rho}_1}{\rho_1} = \frac{4\bar{M}_1}{M_1[2 + (\gamma-1)M_1^2]} = -\frac{\bar{v}_2}{v_2} + \frac{\bar{v}_1}{v_1} \tag{X}$$

in view of the relation $\rho_2 v_2 = \rho_1 v_1$. From $c^2 = \gamma P/\rho$,

$$2\bar{c}_2/c_2 - 2\bar{c}_1/c_1 = \bar{P}_2/P_2 - \bar{P}_1/P_1 - [\bar{\rho}_2/\rho_2 - \bar{\rho}_1/\rho_1],$$

or

$$\frac{\bar{c}_2}{c_2} - \frac{\bar{c}_1}{c_2} = 2(\gamma-1)\frac{\bar{M}_1}{M_1}\frac{(1+\gamma M_1^4)}{(2\gamma M_1^2 - \gamma + 1)[2 + (\gamma-1)M]_1^2}. \tag{XI}$$

From (III′),

$$2\gamma M_1/(\gamma+1) - \theta = [-\theta + 2\gamma M_2^2/(\gamma+1)]^{-1},$$

or
$$\bar{M}_1 M_1(\gamma - 1 - 2\gamma M_2^2) = \bar{M}_2 M_2(2\gamma M_1^2 - \gamma + 1). \tag{XII}$$

From the equation of state,

$$\exp[(s_2 - s_1)/c_v] = (P_2/P_1)(\rho_1/\rho_2)^\gamma,$$

or
$$\frac{\bar{s}_2 - \bar{s}_1}{c_v} = \frac{\bar{P}_2}{P_2} - \frac{\bar{P}_1}{P_1} - \gamma\left[\frac{\bar{\rho}_2}{\rho_2} - \frac{\bar{\rho}_1}{\rho_1}\right],$$

it follows that
$$\bar{s}_2 - \bar{s}_1 = \frac{4\gamma c_v(\gamma-1)(1-M_1^2)\bar{M}_1}{M_1[2\gamma M_1^2 - \gamma + 1][2 + (\gamma-1)M_1^2]}. \tag{XIII}$$

From $M_2 = v_2/c_2$,

$$\bar{M}_2 = (v_2/c_2)[(\bar{v}_2/v_2) - (\bar{c}_2/c_2)], \tag{XIV}$$

$$\bar{v}_2 = \tilde{u}_2 - \bar{W}, \qquad \bar{v}_1 = \tilde{u}_1 - \bar{W}. \tag{XV}$$

For a particular shock problem, the basic flow (i.e. all terms without bars) and the perturbed flow (subscript 1) are assumed known. If the problem is to be solved in terms of $\bar{M}_1$, equations (IX) to (XIII) yield $\bar{P}_2$, $\bar{\rho}_2$, $\bar{c}_2$, $\bar{M}_2$, $\bar{s}_2$. From (XIV), $\bar{v}_2$ is obtained, and $\tilde{u}_2$ follows from (XV).

References

Chester, W. 1953 *Quart. J. Mech. Appl. Math.* **6**, 440.

Chester, W. 1954 *Phil. Mag.* **45**, 1293.

Germain, P. & Gundersen, R. 1955 *C.R. Acad. Sci., Paris*, **241**, 925.

Gundersen, R. 1954 *Brown University Report* AF-1021/1.

Lighthill, M. J. 1948 *Proc. Roy. Soc.* A, **198**, 454.

An experiment on free thermal convection of water in saturated permeable material

By R. A. WOODING

*Applied Mathematics Laboratory, Department of Scientific and Industrial Research, Wellington, New Zealand**

(*Received* 3 *September* 1957)

SUMMARY

A small-scale experimental model has been constructed for the study of steady-state slow free convection of water in saturated sand. The convection field is confined between coaxial cylinders maintained at constant temperature difference, and the upper and lower boundaries consist of planes with thermal and fluid insulation. Measurements of the temperature distribution within the convection space have been obtained for average boundary temperature differences $(T_1 - T_0)$ of (I) 18·40° A, (II) 32·70° A, and (III) 46·68° A. Theoretical temperature values predicted from perturbation theory have been fitted by least squares. The first-order estimates of $\eta/(T_1 - T_0)$, where η is the convection parameter or modified Rayleigh number, do not differ significantly from a constant value ($\pm 3\%$ S.D.) for the three given values of $T_1 - T_0$, indicating good agreement between theoretical and experimental results. First-order estimates are made also of the temperature coefficient of thermal conductivity b of the sand–water mixture, and of the coefficient of radiation loss c at the upper insulated boundary, but these estimates are less reliable. Separate determinations of $\eta/(T_1 - T_0)$, b, c by direct physical measurement are in good agreement with the least-squares estimates.

1. INTRODUCTION

In a recent paper (Wooding 1957), the equations governing slow free convection of liquid in saturated homogeneous permeable material have been solved approximately, using perturbation expansions of the dependent variables (temperature and stream function) in powers of a convection parameter η. The method is very closely related to the technique of expansion in powers of the Rayleigh number

$$R = \frac{\alpha(T_1 - T_0)gd^3}{\kappa_0 \nu_0}, \tag{1}$$

* Now at the Cavendish Laboratory, Cambridge.

which has been applied to problems of free convection in fluids (Batchelor 1954), and in fact

$$\eta = \frac{k\alpha(T_1 - T_0)gd}{(K_m/K_w)_0 \kappa_0 \nu_0} = \frac{N(\Delta/d)^2}{(K_m/K_w)_0} R. \tag{2}$$

Under non-isothermal conditions each of these parameters arises naturally when the corresponding equation of motion is reduced to dimensionless form—the Navier–Stokes equation in the case of R and the Darcy equation in the case of η. Hence η may be termed a modified Rayleigh number.

In equation (1), α is the linear coefficient of thermal volume expansion of the liquid, T_0 and T_1 are two reference temperatures on the absolute scale, g is the acceleration due to gravity, d is a representative linear dimension of the convection field, κ_0 is the thermal diffusivity of the liquid at temperature T_0, and ν_0 is the kinematic viscosity at temperature T_0. In equation (2), $(K_m/K_w)_0$ is the value at T_0 of the ratio of the thermal conductivity of the permeable solid–liquid mixture to the thermal conductivity of the liquid; Δ is a linear dimension proportional to the particle or pore size of the solid, and N is a dimensionless constant dependent upon the geometrical shape of the particles. The permeability k $(= N\Delta^2)$ is assumed to be constant.

Under given boundary conditions, the value of the convection parameter η may be estimated in several ways. For instance: (*a*) by physical measurement of the quantities involved in the definition of η (equations (1) and (2)), (*b*) by measurement of the distortion of the temperature field caused by convective flow of liquid, the observations being compared with a perturbation model of the form

$$\theta = \theta_0 + \eta\theta_1 + \eta^2\theta_2 + \ldots, \tag{3}$$

where θ is a temperature parameter and $\theta_0, \theta_1, \theta_2, \ldots$ are coefficients calculated from perturbation theory, (*c*) by measurement of the liquid flow rates at selected points of the convection field, the observations being compared with a corresponding perturbation model involving the stream function ψ. Methods (*b*) and (*c*) are applicable only over the range of small η for which perturbation theory is valid.

This paper describes the measurement of η by methods (*b*) and (*a*) respectively, the former method using an experimental model with water-saturated sand as the convection medium, while for the latter method, separate measurements of the fluid permeability and thermal conductivity of the saturated sand are obtained.

A particularly simple arrangement with cylindrical symmetry is chosen for the boundary conditions of the model. No attempt is made to use boundary conditions resembling those of a geothermal area, and, in fact, the latter task has been carried out recently by Mr John Elder in the Cavendish Laboratory, Cambridge. The present model, in addition to providing a preliminary check of the perturbation theory, serves to indicate a practical method of measuring directly the ratio $(K_m/K_w)_0 \kappa_0 \nu_0/k$ (see

equation (2)) for samples of material obtained in geothermal areas, although the effect of large-scale fissuring, which is normally present in active parts of such areas, would be neglected by the method.

To facilitate an accurate fit of the perturbation convection model to the experimental data, a refinement to the equation of energy transport, involving modification of the coefficient of thermal conductivity of the mixture, will be considered. This is the variation with temperature of the thermal conductivity of the solid–liquid mixture. The law of temperature dependence can be taken to be

$$K_m = (K_m)_0\{1 + b(T - T_0)\}, \tag{4}$$

where K_m, $(K_m)_0$ are the values of the thermal conductivity of the saturated permeable material at the temperatures T and T_0 respectively, and the constant b is the linear coefficient of thermal conductivity. As b can be assumed to be small, its effect for small temperature differences can be treated by first-order perturbation theory.

The diffusion or dispersion of heat due to percolation of the liquid about the sand grains can be expected to be a small effect, although it could become significant in cases of appreciably high fluid flow speeds about coarse solid particles. The phenomenon closely resembles Brownian motion in that a given fluid particle performs small random motions which are superimposed upon the main fluid motion $\mathbf{q}$. From the analogy with the classical theory of random flights (Rayleigh 1899, Chandrasekhar 1943), it is a simple matter to show that the magnitude D of the 'thermal dispersion coefficient' will obey the relation

$$D = O(\rho c \Delta |\mathbf{q}|), \tag{5}$$

where Δ is a typical dimension of the solid particles or of the pores, ρc is the heat capacity of the fluid, and $|\mathbf{q}|$ is the main flow speed. Then the apparent thermal conductivity of the saturated permeable material, for isotropic thermal dispersion, becomes $K_m + D$. If the dispersion effect is non-isotropic, its coefficient assumes a complicated tensor form (Chandrasekhar 1943). However, for very small Δ in comparison with the boundary dimensions, and with very slow fluid flow, as in the present experiment, it can be shown from (5) that D is negligible in comparison with K_m and the effect of dispersion can therefore be neglected.

For purposes of the experiment, it is necessary to consider briefly the influence of the dynamic boundary layer associated with each rigid boundary which is immersed in permeable solid material. Darcy-type flow solutions cannot satisfy the 'non-slip' condition at a rigid boundary, whence it becomes necessary to neglect the region of boundary layer flow. This approximation is justified when the Reynolds number of the flow is very small. Then all fluid velocities in the pore spaces are of laminar (Poiseuille) type, and the shape of each velocity profile across a pore space, or normal to a rigid boundary, is independent of the kinematic viscosity ν and of the main fluid flow rate $|\mathbf{q}|$. It follows that the typical thickness δ of the boundary layer depends on only the typical solid particle (or pore) size Δ, and that the ratio

δ/Δ is of order unity. This follows from the particular form of the Navier–Stokes equations for which the inertia terms are negligible, gradients perpendicular to the boundary are large compared with those parallel, and the pressure gradient is given by Darcy's law. If X is a coordinate measured along an impermeable rigid boundary immersed in saturated permeable material and Y is measured along the normal, one has

$$(\text{pressure gradient})/\rho = -\frac{\nu}{k}|\mathbf{q}| = \nu u_{YY},$$

where u is the X-component of the flow, and $|\mathbf{q}|$ is the speed of the main stream outside the boundary layer. Since $u_{YY} = O(|\mathbf{q}|/\delta^2)$, this gives

$$\delta = O(k^{1/2}) = O(\Delta), \tag{6}$$

from the relation $k = N\Delta^2$ (Slichter 1899).

2. Approximate solution of differential equations

As in a previous paper (Wooding 1957), the differential equations of slow steady flow may be expressed in dimensionless units. The temperature parameter θ is defined by

$$\theta = (T - T_0)/(T_1 - T_0), \tag{7}$$

where T_0, T_1 are two typical boundary temperatures. The 'equivalent flow' vector $\mathbf{q}_0$ is defined from the continuity relation

$$\rho\mathbf{q} = \rho_0\mathbf{q}_0, \tag{8}$$

in which it will be assumed that the density ρ of the liquid is related to the temperature by the approximate expression

$$\rho = \rho_0\{1 - \alpha(T_1 - T_0)\theta - \beta(T_1 - T_0)^2\theta^2\}, \tag{9}$$

ρ_0 being the density at temperature T_0, and α, β being constants. The modified Péclet number $\boldsymbol{\zeta}$ is given by

$$(K_m/K_w)_0\boldsymbol{\zeta} = \mathbf{q}_0 d/\kappa_0, \tag{10}$$

where κ_0 is the thermal diffusivity of the liquid at temperature T_0, d is a typical length derived from the boundary dimensions, and $(K_m/K_w)_0$ is, as before, the ratio at T_0 of the thermal conductivity of the mixture to the thermal conductivity of the liquid.

Since the boundary conditions of the experiment have cylindrical symmetry, it is convenient to take axes in dimensionless units r, z, with Or horizontal and Oz directed vertically upwards, and to define Stokes' stream function ψ by

$$\boldsymbol{\zeta} = \mathbf{i}\psi_z/r - \mathbf{k}\psi_r/r, \tag{11}$$

$\mathbf{i}$, $\mathbf{k}$ being vectors in the directions Or, Oz respectively. The suffices in r, z signify partial differentiation.

Then, for slow steady motion of water in a saturated homogeneous permeable solid, the equations of energy and motion give in cylindrical

coordinates a pair of simultaneous partial differential equations for $\theta(r, z)$ and $\psi(r, z)$,

$$\theta_{rr}+\frac{1}{r}\theta_r+\theta_{zz}+b(T_1-T_0)\frac{1}{r}\{(r\theta\theta_r)_r+(r\theta\theta_z)_z\}=\frac{1}{r}(\psi_z\theta_r-\psi_r\theta_z)$$
$$=\frac{1}{r}\frac{\partial(\theta,\psi)}{\partial(r,z)}, \quad (12)$$

$$\psi_{rr}-\frac{1}{r}\psi_r+\psi_{zz}-\frac{a(T_1-T_0)}{1+a(T_1-T_0)\theta}(\theta_r\psi_r+\theta_z\psi_z)+$$
$$+\eta r\{1+a(T_1-T_0)\theta\}\{1+(2\beta/\alpha)(T_1-T_0)\theta\}\theta_r=0, \quad (13)$$

where

$$a=(T_0-260)^{-1}\,(^\circ\mathrm{A})^{-1} \quad (14)$$

is a temperature coefficient for viscosity.

For the approximate solution of equations (12) and (13) it will be assumed that η, b are small, and that θ and ψ may be expanded in power series involving these quantities. (Also, for convenience in later analysis, we introduce the notation $m=\eta/(T_1-T_0)$, the parameter m being independent of T_1-T_0.) Then the perturbation models will be written as

$$\theta=\theta_0+m(T_1-T_0)\theta_1+b(T_1-T_0)\theta^{(1)}+m^2(T_1-T_0)^2\theta_2+\ldots, \quad (15)$$

$$\psi=m(T_1-T_0)\psi_1+m^2(T_1-T_0)^2\psi_2+\ldots. \quad (16)$$

Here, the second-order term (in m^2) will be calculated in order to estimate the magnitude of the second-order correction. The second-order terms in mb, b^2 will be ignored, on the assumption that only the linear term in b has significance. The series solution (15) and (16) of the equations (12) and (13) may be fitted to suitable experimental data to obtain estimates of the parameters m and b.

Substitution of equations (15) and (16) into (12) and (13) gives a series of partial differential equations for the perturbation coefficients θ_0, ψ_1, θ_1, ψ_2, θ_2 and $\theta^{(1)}$,

$$(\theta_0)_{rr}+\frac{1}{r}(\theta_0)_r+(\theta_0)_{zz}=0, \quad (17)$$

$$(\psi_1)_{rr}-\frac{1}{r}(\psi_1)_r+(\psi_1)_{zz}-\gamma\{(\theta_0)_r(\psi_1)_r+(\theta_0)_z(\psi_1)_z\}+$$
$$+r\{1+a(T_1-T_0)\theta_0\}\{1+(2\beta/\alpha)(T_1-T_0)\theta_0\}(\theta_0)_r=0, \quad (18)$$

$$(\theta_1)_{rr}+\frac{1}{r}(\theta_1)_r+(\theta_1)_{zz}=\frac{1}{r}\frac{\partial(\theta_0,\psi_1)}{\partial(r,z)}, \quad (19)$$

$$(\psi_2)_{rr}-\frac{1}{r}(\psi_2)_r+(\psi_2)_{zz}-\gamma\{(\theta_0)_r(\psi_2)_r+(\theta_0)_z(\psi_2)_z\}-$$
$$-\gamma\{(\theta_1)_r(\psi_1)_r+(\theta_1)_z(\psi_1)_z\}+\gamma^2\theta_1\{(\theta_0)_r(\psi_1)_r+(\theta_0)_z(\psi_1)_z\}+$$
$$+r\{1+a(T_1-T_0)\theta_0\}\{1+(2\beta/\alpha)(T_1-T_0)\theta_0\}(\theta_1)_r+$$
$$+r[\{1+a(T_1-T_0)\theta_0\}(2\beta/\alpha)(T_1-T_0)\theta_1+$$
$$+\{1+(2\beta/\alpha)(T_1-T_0)\theta_0\}a(T_1-T_0)\theta_1](\theta_0)_r=0, \quad (20)$$

where $\gamma = a(T_1 - T_0)\{1 + a(T_1 - T_0)\theta_0\}^{-1}$,

$$(\theta_2)_{rr} + \frac{1}{r}(\theta_2)_r + (\theta_2)_{zz} = \frac{1}{r}\frac{\partial(\theta_0, \psi_2)}{\partial(r, z)} + \frac{1}{r}\frac{\partial(\theta_1, \psi_1)}{\partial(r, z)}, \tag{21}$$

$$\theta^{(1)}_{rr} + \frac{1}{r}\theta^{(1)}_r + \theta^{(1)}_{zz} + \{(\theta_0)^2_r + (\theta_0)^2_z\} = 0. \tag{22}$$

These are readily transformed into finite-difference equations by the usual procedures, taking a square mesh of element dimension h, and relaxation techniques may be applied in order to obtain approximate numerical solutions for the coefficients.

3. Description of apparatus and experimental procedure

Figure 1 illustrates in diagrammatic form the arrangement of temperature and flow boundaries chosen for the experimental work. Oz is the axis of two concentric cylinders AD, BC which have radii in the ratio 2:7. In

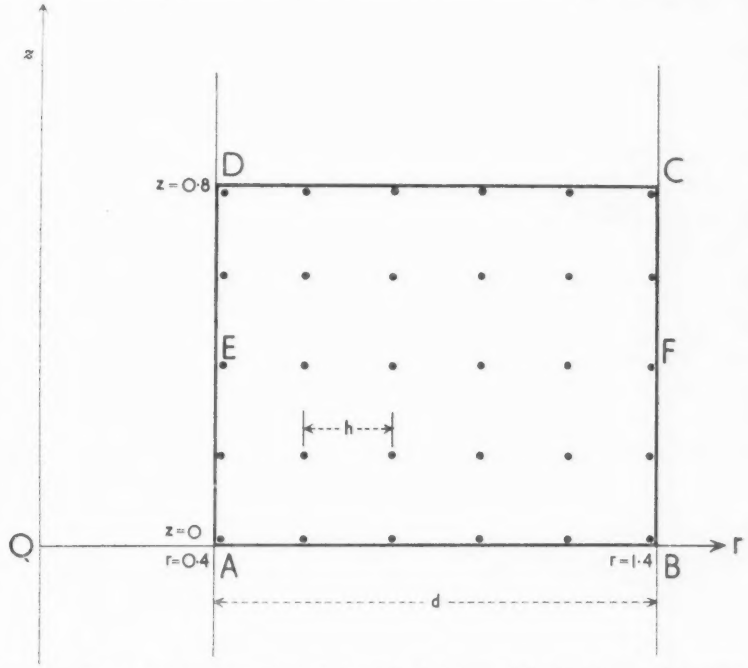

Figure 1. Boundary configuration of the cylindrical model, showing mesh points of the relaxation net.

the dimensionless system the length unit is taken as $d = AB$, giving the dimensionless r, z values shown for the various boundaries. The 30 points arranged in a square mesh represent points of the relaxation net, from which it will be seen that $h = \frac{1}{5}$ in dimensionless units. These points correspond to thermocouple positions in the experimental arrangement.

The cylinders AD and BC are held at constant temperatures T_1 and T_0 respectively ($T_1 > T_0$), while the boundaries AB, CD satisfy conditions of nearly complete thermal insulation. All four boundaries are impermeable to liquid. Consequently, the boundary conditions for the numerical calculations may be described ideally as follows:

$$\text{on } BC, \qquad \theta = 0;$$

$$\text{on } DA, \qquad \theta = 1;$$

$$\text{on } AB,\ CD, \qquad \theta_z = 0; \tag{23}$$

$$\text{on } AB,\ BC,\ CD,\ DA, \quad \psi = 0. \tag{24}$$

A feature of these boundary conditions is that $(\theta_0)_z$ vanishes throughout equations (17) to (22).

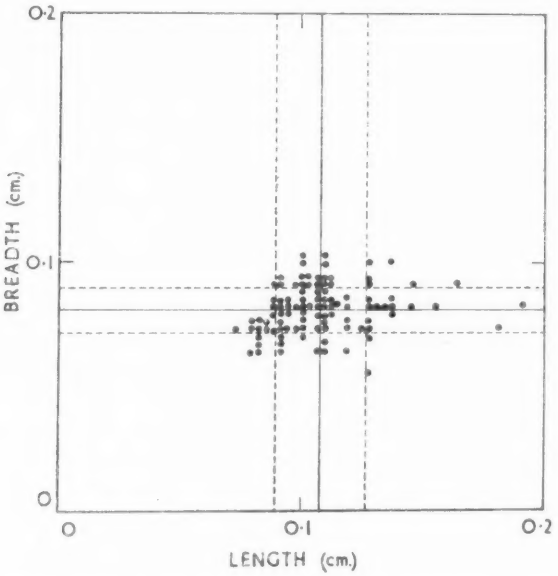

Figure 2. Length-breadth distribution of 100 grains of quartz sand. The regression lines and standard deviation have been calculated from a total sample of 233 grains.

In the experimental arrangement, two copper cylinders of radii 3·8 cm and 13·3 cm are arranged coaxially to represent boundaries DA and BC respectively. The outer cylinder is surrounded by a water jacket, while the inner cylinder forms the sides of a water-tight container. Constant, practically uniform, temperatures are maintained on the boundary cylinders by means of circulating water with thermostatic control.

The space between the temperature-controlled copper cylinders, of width $d = 9{\cdot}5$ cm, is filled with standard graded quartz sand (porosity 0·4

approximately) to a depth of $0{\cdot}8d$. Figure 2 is a scatter diagram showing the length–breadth relation for a sample of 100 sand grains, based on the assumption that each grain is approximately ellipsoidal. (Since these results have been obtained from a single photomicrograph, measurements are not available for the depth of each grain.) The sample is seen to be satisfactorily homogeneous, and if Δ is a typical dimension for grain size it follows that $\Delta/d = O(10^{-2})$.

A thin sheet of bakelite mounted vertically and radially supports copper–constantan thermocouples in the 30 positions shown in figure 1, the thermocouple leads being carried circumferentially for several centimetres from the junctions to reduce conduction errors. Each thermocouple junction is arranged to project about 0·4 cm beyond the bakelite sheet, and is supported by gluing the copper and constantan wires to the sheet For the thermocouples adjacent to the boundaries corresponding to BC and DA, extra support can be afforded by the cylinder walls, as these are in effective thermal contact with the thermocouples.

Although a boundary layer exists close to the vertical bakelite sheet, its effect upon the thermocouple readings can be considered negligible provided that $\delta \doteqdot \Delta \ll 0{\cdot}4$ cm, where δ is the thickness of the layer (§ 1). From figure 2 it appears that this condition is practically satisfied.

Thin sheets of bakelite sealed with a rubber-based glue render the upper and lower boundaries impermeable to moisture, and are backed by layers 3 cm thick of Perspex 'honeycomb' to provide thermal insulation. Compression applied to the top of the upper layer of insulating material is transmitted throughout the assembly, and ensures that (except for possible packing irregularities) the sand should have an approximately constant fluid permeability and thermal conductivity within the convection space.

After the convection space has been filled with boiled water, care being taken to exclude all air bubbles, the inner and outer boundaries are adjusted to have a suitable temperature difference which is maintained as nearly constant as possible. A period of up to four hours elapses before steady-state conditions are approached.

Three different values of the boundary temperature difference have been employed, the experimental average values of $T_1 - T_0$ being (I) 18·40° A, (II) 32·70° A, (III) 46·68° A. In each case, T_0 is held close to (273 + 20)° A, for which $\alpha = 2{\cdot}25 \times 10^{-4}\,(^\circ\mathrm{A})^{-1}$, $\beta = 3{\cdot}75 \times 10^{-6}\,(^\circ\mathrm{A})^{-2}$ in equation (9), and $a = 1/33\,(^\circ\mathrm{A})^{-1}$ in equation (14).

Experimental values θ_e of the convection temperature parameter are computed from the measured temperatures T (° A) using the formula (7). The results for the three experiments are given in table 1.

Steady-state conditions are found to be attainable on each cylindrical boundary to within $\pm 0{\cdot}05$° A for experiments I and II, and to within $\pm 0{\cdot}20$° A for experiment III. These results are obtained by observation of several boundary thermocouple outputs whilst the thermostats controlling the boundary temperatures pass through several 'on–off' cycles. It is easily shown from formula (7) that resultant variations in time of the

parameter θ_c are less than $\pm 0{\cdot}005$ for experiments I and II, and less than $\pm 0{\cdot}010$ for experiment III. Corresponding time variations in the interior thermocouples are much reduced, owing to the short period (five to eight minutes) of the boundary variations, which are lagged by the saturated sand.

Expt. I	*D*	999	(1)	686	(3)	472	(2)	275	(2)	119	(3)	*C* −7 (7)
		986	(14)	681	(4)	459	(2)	279	(1)	119	(1)	0 (0)
	E	1010	(−10)	673	(−1)	445	(0)	263	(0)	112	(0)	*F* 1 (−1)
		1004	(−4)	655	(−1)	416	(0)	243	(0)	100	(−1)	1 (−1)
	A	998	(2)	645	(0)	399	(0)	241	(0)	103	(−2)	*B* 6 (−6)
Expt. II	*D*	1003	(−3)	735	(0)	514	(0)	313	(1)	148	(2)	*C* −6 (6)
		997	(3)	710	(0)	486	(0)	305	(0)	141	(1)	−2 (2)
	E	1009	(−9)	680	(−2)	440	(−1)	263	(−1)	124	(−2)	*F* 7 (−7)
		999	(1)	613	(0)	387	(0)	224	(−1)	101	(−1)	−1 (1)
	A	993	(7)	587	(2)	353	(0)	210	(−1)	98	(−1)	*B* 2 (−2)
Expt. III	*D*	1020	(−20)	791	(−8)	593	(−4)	368	(−3)	189	(−3)	*C* 3 (−3)
		1008	(−8)	742	(−5)	533	(−3)	293	(−3)	166	(−3)	5 (−5)
	E	1009	(−9)	660	(−3)	437	(−1)	262	(−1)	123	(−2)	*F* 8 (−8)
		991	(9)	559	(4)	347	(2)	197	(2)	86	(3)	−7 (7)
	A	973	(27)	509	(10)	295	(4)	172	(3)	76	(5)	*B* −10 (10)

Table 1. Experimental values of the temperature parameter $10^3\theta_c$. Corresponding values of the boundary correction term $10^3\theta^{(0)}$ are shown in parentheses.

However, in the steady state, small spatial temperature variations occur in the Oz-direction along the boundaries DA and BC (table 1). These appear to be due to the finite effective conductivity of each cylindrical boundary system, emphasized perhaps by the presence of a steady flow pattern within the circulating water.

4. Analysis of results

As noted at the end of § 3, the steady-state values of θ_c obtaining on boundaries BC and DA vary by small amounts from the theoretical values of θ given by (23). The theoretical boundary conditions will now be fitted to the experimental values by applying a perturbation $\theta^{(0)}$ to θ, such that

$$\text{on } BC,\ DA,\ 1-\theta^{(0)} = \theta_c;$$
$$\text{on } AB,\ CD, \qquad \theta_z^{(0)} = 0. \tag{25}$$

Also, let the definition of $\theta^{(0)}$ be such that

$$\theta - \theta^{(0)} = \theta_c \tag{26}$$

within the convection space. Here, θ can be assumed to be represented by the perturbation series (15). As $\theta^{(0)}$ is very small, cross-product terms

involving $m(T_1 - T_0)\theta_1 \theta^{(0)}$, etc., will be neglected, whence it is readily shown that $\theta^{(0)}$ is harmonic to first order in the convection space. Values of $\theta^{(0)}$ calculated by relaxation methods are given in parentheses in table 1.

A further correction to the boundary conditions arises from the possibility of thermal radiation through the insulation at the boundaries AB, CD. Since the external ambient temperature is normally close to T_0, it is possible to assume that the radiation boundary conditions take the form

$$\text{on } CD,\ \theta_z = c\theta;$$
$$\text{on } AB,\ \theta_z = c'\theta. \tag{27}$$

With the assumption that the radiation constants c, c' are very small, it is possible to take first-order perturbations in θ of form

$$c\theta^{(2)} + c'\theta^{(3)}, \tag{28}$$

this expression being combined with (15).

$10^3\theta_0$	D	1000	677	447	269	123	C	0
$10^3\psi_1$	D	0	0	0	0	0	C	0
		0	−41	−52	−48	−32		0
	E	0	−51	−67	−62	−42	F	0
$10^4\theta_1$	D	0	131	136	96	47	C	0
		0	90	94	67	33		0
	E	0	0	0	0	0	F	0
$10^5\psi_2$	D	0	0	0	0	0	C	0
		0	8	−30	−46	−38		0
	E	0	0	0	0	0	F	0
$10^5\theta_2$	D	0	−25	2	17	13	C	0
		0	−27	−5	11	10		0
	E	0	−28	−11	5	7	F	0
$10^3\theta^{(1)}$	D	0	112	126	100	55	C	0
$10^3\theta^{(2)}$	D	0	144	146	105	52	C	0
		0	68	80	62	32		0
	E	0	35	45	37	20	F	0
		0	21	28	24	13		0
	A	0	17	23	20	11	B	0

Table 2. Numerical values of the perturbation coefficients calculated by relaxation methods for experiment I. The given values of θ_0, $\theta^{(1)}$ and $\theta^{(2)}$ apply for experiments I, II and III.

Tables 2, 3 and 4 give numerical values of the coefficients θ_0, ψ_1, θ_1, ψ_2, θ_2 and $\theta^{(1)}$, calculated by relaxation methods from equations (17) to (22) respectively, and using the boundary conditions derived by substitution of (15) into (23) and (16) into (24). Also tabulated are values of $\theta^{(2)}$, which are calculated from Laplace's equation with boundary conditions derived

by substituting (28) into (27). In all cases the relaxation net of figure 1 is used. In general, it is necessary to tabulate only part of the calculated field for each case, as both θ_0 and $\theta^{(1)}$ are constant with respect to z, while ψ_1 and θ_2 are symmetrical about the horizontal plane EF, and θ_1 and ψ_2

$10^3\psi_1$	D	0	0	0	0	0	C	0
		0	−59	−70	−60	−38		0
	E	0	−74	−91	−79	−50	F	0
$10^4\theta_1$	D	0	184	184	127	61	C	0
		0	126	127	88	43		0
	E	0	0	0	0	0	F	0
$10^5\psi_2$	D	0	0	0	0	0	C	0
		0	0	−77	−93	−65		0
	E	0	0	0	0	0	F	0
$10^5\theta_2$	D	0	−44	9	33	24	C	0
		0	−49	−4	22	19		0
	E	0	−53	−16	12	14	F	0

Table. 3. Numerical values of the perturbation coefficients calculated by relaxation methods for experiment II.

$10^3\psi_1$	D	0	0	0	0	0	C	0
		0	−80	−90	−74	−44		0
	E	0	−100	−117	−97	−58	F	0
$10^4\theta_1$	D	0	245	238	160	75	C	0
		0	167	164	111	52		0
	E	0	0	0	0	0	F	0
$10^5\psi_2$	D	0	0	0	0	0	C	0
		0	−22	−158	−165	−101		0
	E	0	0	0	0	0	F	0
$10^5\theta_2$	D	0	−70	23	58	39	C	0
		0	80	0	40	31		0
	E	0	−90	−22	23	23	F	0

Table 4. Numerical values of the perturbation coefficients calculated by relaxation methods for experiment III.

are antisymmetrical about EF. $\theta^{(2)}$ does not possess symmetry of this type, but $\theta^{(3)}$ and $\theta^{(2)}$ are related antisymmetrically about EF. Finally, the functions θ_0, $\theta^{(1)}$ and $\theta^{(2)}$ have the same values for experiments I, II and III.

Because of the small scale of the apparatus used, the sand grains are of appreciable size ($\Delta/d = O(10^{-2})$) and the spatial temperature gradient is

high, with resultant scatter in the experimental temperature readings. It is preferable, therefore, to use statistical methods (least squares) in fitting the theoretical model to the data of table 1 for the three values of the boundary temperature difference which are employed, and to use significance tests in evaluating the adequacy of the model.

Combination of equations (15) and (28) shows that the statistical temperature model will be of the form

$$\theta-\theta_0 = m(T_1-T_0)\theta_1+b(T_1-T_0)\theta^{(1)}+c\theta^{(2)}+c'\theta^{(3)}+m^2(T_1-T_0)^2\theta_2+\epsilon, \quad (29)$$

to the order of accuracy considered, where all of the parameters m, b, c and c' should be constant for varying values of T_1-T_0. Point values of the residual error variable ϵ will be assumed to be distributed approximately normally and independently of each other with zero mean. Since not all terms in the analysis are necessarily significant, and since the complete model would prove unwieldy when obtaining a least-squares fit, a series of partial models will be used, each model involving not more than three of the parameters on the right-hand side of (29). For future reference, each partial model will be labelled H_i, with residual variable ϵ_i and a corresponding suffix will be used to identify the parameters retained.

Table 5 gives the numerical results obtained with a number of partial models for the three cases I, II and III by the usual least-squares methods. In table 5, entries from the left are in terms of model number i, parameters retained in model i, degrees of freedom ν_i, experiment number (I, II or III), optimal parametric estimates, and standard error of estimates. The significance of each added parameter is estimated by means of the variance ratio F_{ij}, computed from the residual sums of squares $\sum(\epsilon_i^2)$, $\sum(\epsilon_j^2)$ for the ith and jth models respectively ($i>j$), from the formula

$$F_{ij} = F(Q_F\ \nu_j-\nu_i,\ \nu_j) = \frac{\{\sum(\epsilon_j^2)-\sum(\epsilon_i^2)\}/(\nu_j-\nu_i)}{\sum(\epsilon_i^2)/\nu_i}, \quad (30)$$

(Pearson & Hartley 1954). Each tabulated value of Q_F gives the probability of exceeding the observed F-ratio by chance. Thus, a very small value of Q_F implies that the added parameter is significant.

The models H_1, H_2 and H_3, ($i=1, 2, 3$ in table 5), are intended to test the significance of the convection effect to first and second orders respectively. However, H_3 cannot be tested against H_2 by the usual significance tests, since m, m^2 are not independent parameters. A conservative test for *non*-significance of m^2 may be obtained by replacing m^2 with an independent parameter l (H_4), and testing H_4 against H_2. Thus, if this test shows that the effect of l is non-significant, then the effect of m^2 will be non-significant also.

Values of the parametric estimates $\hat{m}_2=\hat{\eta}_2/(T_1-T_0)$, $\hat{c}_5$, $\hat{b}_6$ from table 5 are plotted in figure 3 (*a*), (*b*) and (*c*) respectively, these being chosen since they represent values estimated from the simplest models.

i	Parameters retained	ν_i	Expt.	Parametric estimates	Standard errors of estimates	F_{ij}	Q_F
1	—	20	I	—	—	—	—
			II	—	—	—	—
			III	—	—	—	—
2	m	19	I	$\hat{m} = 0{\cdot}118\ (^\circ\mathrm{A})^{-1}$	$0{\cdot}016\ (^\circ\mathrm{A})^{-1}$	$F_{21} = 57$	$\ll 10^{-3}$
			II	0·126	0·006	255	
			III	0·120	0·006	410	
3	m, m^2	19	I	—	—	—	—
			II	—	—	—	—
			III	—	—	—	—
4	m, l	18	I	—	—	$F_{42} = 0$	N.S.*
			II	—	—	2	N.S.
			III	—	—	6	$\leqslant 0{\cdot}025$
5	m, c	18	I	$\hat{c} = -0{\cdot}16$	0·03	$F_{52} = 35$	$< 10^{-3}$
			II	−0·16	0·02	50	$< 10^{-3}$
			III	−0·17	0·07	7	$\leqslant 0{\cdot}025$
6	m, b	18	I	$\hat{b} = -0{\cdot}0046\ (^\circ\mathrm{A})^{-1}$	$0{\cdot}0008\ (^\circ\mathrm{A})^{-1}$	$F_{62} = 37$	$< 10^{-3}$
			II	−0·0025	0·0004	61	$< 10^{-3}$
			III	−0·0023	0·0007	11	$< 0{\cdot}025$
7	m, c, b	17	I	—	—	$F_{76} = 0$	N.S.
			II	—	—	2	N.S.
			III	—	—	1	N.S.

(* N.S. = not significant.)

Table 5. Statistical results obtained by fitting perturbation models to the separate groups of experimental data I, II and III.

Also shown in figure 3 are overall estimates $\hat{m}_2'$, $\hat{c}_5'$, $\hat{b}_6'$, which are obtained by assuming the hypothesis that the quantities m, c, b are constant for experiments I, II and III, and obtaining least-squares estimates using the combined data. These results are summarized in table 6, and are distinguished from the results of table 5 by dashes. The variance ratio F_{ij}'

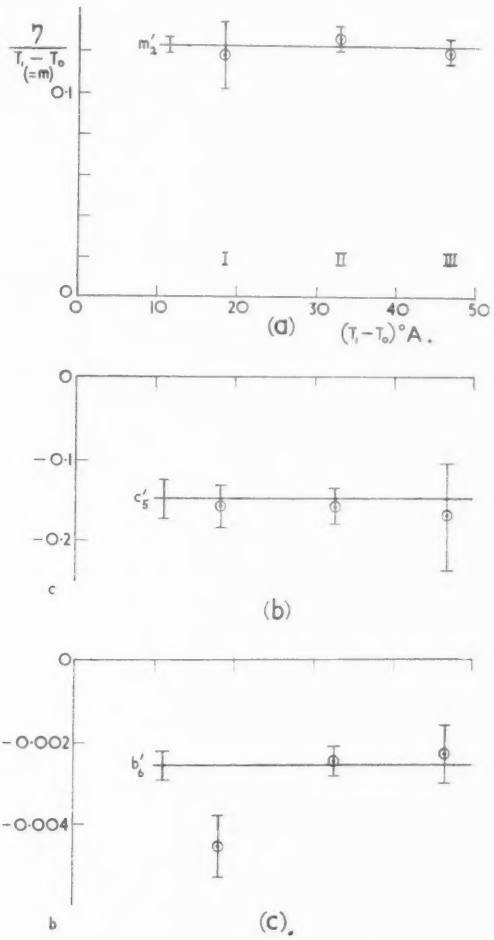

Figure 3. Values of the parametric estimates from table 5 for experiments I, II and III, and the overall estimates from table 6 for (*a*) m_2, (*b*) c_5, (*c*) b_6.

is used to examine the significance of the effect of each added parameter m_i', b_i', c_i', and the variance ratio F_{ii}' is used to examine the significance of the increase in the residual sum of squares $\sum(\epsilon_i'^2)$ over the sum of the three individual sums of squares $\sum(\epsilon_i^2)$ given for the ith model in table 5.

i, i'	Parameters retained	ν_i'	$\sum_3 \nu_i^*$	Parametric estimates	Standard errors of estimates	F_{ij}'	Q_F'	F_{ii}'	Q_F
1	—	60	60	—	—	—	—	—	—
2	m	59	57	$\hat{m} = 0{\cdot}122\,(^\circ\,\mathrm{A})^{-1}$	$0{\cdot}004\,(^\circ\,\mathrm{A})^{-1}$	$F_{21}' > 1000$	$\ll 10^{-3}$	$F_{22}' = 0$	N.S.
5	m, c	58	54	$\hat{m} = 0{\cdot}121$ $\hat{c} = -0{\cdot}15$	$0{\cdot}003$ $0{\cdot}02$	$F_{52}' = 38$	$\ll 10^{-3}$	$F_{55}' = 1$	N.S.
6	m, b	58	54	$\hat{m} = 0{\cdot}122$ $\hat{b} = -0{\cdot}0026\,(^\circ\,\mathrm{A})^{-1}$	$0{\cdot}003$ $0{\cdot}0004\,(^\circ\,\mathrm{A})^{-1}$	$F_{62}' = 52$	$\ll 10^{-3}$	$F_{66}' = 0$	N.S.
6*a*	m, m^2, b	58	54	$\hat{m} = 0{\cdot}119$ $\hat{b} = -0{\cdot}0023$	— —	—	—	—	—
7	m, b, c	57	51	$\hat{m} = 0{\cdot}124$ $\hat{c} = -0{\cdot}03$ $\hat{b} = -0{\cdot}0021$	$0{\cdot}004$ $0{\cdot}04$ $0{\cdot}0007$	$F_{75}' = 9$ $F_{76}' = 1$	$\ll 0{\cdot}005$ N.S.	$F_{77}' = 1$	N.S.

($^*\sum_3 \nu_i$ = sum of degrees of freedom for I, II and III from table 5.)

Table 6. Statistical results obtained by fitting perturbation models to the combined data of experiments I, II and III.

5. Discussion of statistical results

In table 5 for $i = 1, 2$, the values of F_{21} show that the parameter $m = \eta/(T_1 - T_0)$ in the first-order model has a very high significance, which increases with $(T_1 - T_0)$ as the convection effect becomes increasingly dominant over secondary effects. Hence the null hypothesis $H_1(\theta - \theta_0 = \epsilon_1)$ must be rejected, and the presence of a convection phenomenon appears to be well established. However, from F_{42} the effect of the second-order term (m^2) is not significant in experiments I and II, and the effect in III is probably not significant. Presumably, the term in m^2 would become significant for larger values of $(T_1 - T_0)$ than are available in these experimental data.

Separate tests of the effects of the parameters m, c and m, b against m (F_{52}, F_{62} respectively) show comparable significance for the reduction in residual sums of squares in the two cases. However, with the effect of m, c, b tested against m, b (F_{76}), there is not a significant reduction in residual sum of squares. It appears that this result is due to the similarity, analogous to a high correlation, between the coefficients of c and b. In physical terms, the effect of radiation through the upper insulated boundary (coefficient c) is very similar in form to the effect of variation in thermal conductivity due to the negative temperature coefficient (b) of the quartz sand. Both phenomena tend to reduce the temperature within the convection field, and since each effect is small, the present method of analysis is not able to resolve them completely.

An additional test, of the parameters m, c, c' against m, c, shows that c' has no significance. It follows that radiation through the lower boundary surface is negligible.

To examine the significance of the dispersion term (§ 1), a further test is formulated using m, b, c and an additional perturbation parameter representing the effect of simple isotropic dispersion. As the three values obtained for the coefficient of the additional parameter are scattered closely about zero, it can be concluded that there is negligible dispersion of heat by irregularities of the fluid motion.

Considerable heterogeneity of residual variance $\sum(\epsilon_i^2/\nu_i)$ has been found between the results of experiments I, II and III, much of the heterogeneity being due to a relatively large residual variance in III. Physically, it would appear that the higher temperatures involved in III have resulted in poorer stabilization, the residual standard error in the temperature measurements being given by (I) $\pm 0{\cdot}12^\circ$ A, (II) $\pm 0{\cdot}18^\circ$ A, (III) $\pm 0{\cdot}69^\circ$ A respectively, after m, b and c have been fitted. These values are larger than the time variations mentioned in § 3, since steady-state scatter in the thermocouple readings is present also. The effect of this heterogeneity of variance is to modify the distribution of the F'-values given in table 6 and the corresponding values of Q'_F may therefore be only an indication of the true values. Although it follows that the results of table 6 are statistically less reliable than the results of table 5, the Q'_F-values in table 6 are all either so large or so small that any numerical modification necessary is unlikely to alter their physical implications.

The results of the overall tests F'_{22}, F'_{55}, F'_{66}, F'_{77} (table 6) show that the hypothesis that m, b, c are constant is not disproved. The standard error of the estimate $\hat{m}'_2$ is about $\pm 3\%$. Constant values of these three parameters are expected, of course, since none is dependent upon $(T_1 - T_0)$, the quantity varied between the three experiments.

It will be seen that the test F'_{76} (which tests m, b, c against m, b) does not give significance. If the simpler model is desired, therefore, one could ignore boundary radiation and choose the model H'_6 in preference to H'_7.

A further hypothesis H'_{6a}, using the overall data to fit m to second order and b to first order as in equation (15), is found to give the same residual sum of squares as H'_6. Hence there is no preference for or against the second-order model when it is compared with the first-order model.

6. Supplementary observations and results

In order to calculate an approximate value for m by alternative means, it is necessary to measure the permeability of quartz sand under compression conditions resembling those of the convection experiment, and to measure the thermal conductivity of quartz sand at temperature T_0 in the absence of convection. A standard permeability experiment of Darcy type (Muskat 1937) has been set up, the sand being carefully tapped down and compressed as in the convection model, and a value of

$$k = (2{\cdot}61 \pm 0{\cdot}05) \times 10^{-6} \text{ cm}^2 \tag{31}$$

has been obtained. For the conductivity measurement, water-saturated quartz sand is compressed between a pair of square horizontal plates, the upper plate being at the higher temperature. A conductivity value of

$$(K_m)_0 = (4{\cdot}60 \pm 0{\cdot}05) \times 10^{-3} \text{ c.g.s. units} \tag{32}$$

has been obtained at $(20 + 273)^\circ$ A. With these values for k and $(K_m)_0$, and with $\alpha = 2{\cdot}25 \times 10^{-4} (^\circ\text{A})^{-1}$, $d = 9{\cdot}5$ cm, $g = 980$ cm sec^{-2}, $\nu_0 = 0{\cdot}010$ cm^2 sec^{-1} units, equation (2) gives

$$m = \eta/(T_1 - T_0) = 0{\cdot}119 \pm 0{\cdot}003\,(^\circ\text{A})^{-1}. \tag{33}$$

This value is in very good agreement with the least-squares estimates of m in § 4, table 6. It will be seen that m has been determined with approximately the same standard error by either method.

From these values of m, it is a simple calculation to show that the ratio

$$(K_m/K_w)_0(\kappa_0 \nu_0/k) = 17{\cdot}5 \pm 0{\cdot}5 \text{ cm}^2 \text{ sec}^{-2} \tag{34}$$

for $T_0 = (273 + 20)^\circ$ A and for the particular water-saturated quartz sand used in the experimental work. This result, which is a property of the sand and water alone, is of more general usefulness than m, as it is independent of the boundary conditions used in the model.

A rough estimate of b has been obtained from the data on thermal conductivity of quartz published in the International Critical Tables

(National Research Council, U.S.A. 1929). In the temperature range 20° C to 70° C, the thermal conductivity of quartz can be represented approximately by

$$K_s = 0{\cdot}029\{1 - 0{\cdot}0037(T - T_0)\} \text{ c.g.s. units}$$

parallel to the principal axis of the crystal, and

$$K_s = 0{\cdot}016\{1 - 0{\cdot}0024(T - T_0)\} \text{ c.g.s. units}$$

perpendicular to the principal axis, where $T_0 = (273 + 20)°$ A. If the directions of the principal axes of the sand grains can be assumed to have a spherical distribution, and if the quartz contributes the major share of the thermal conductivity, the average value of the temperature coefficient would be approximately

$$b = -0{\cdot}0028(°\text{A})^{-1}. \tag{35}$$

This is to the same order as the values of b estimated in § 4, table 6.

r (non-dimensional)	0·6	0·8	1·0	1·2
$q \times 10^3$ (cals cm^{-2} sec^{-1})	5 ± 2	5 ± 2	3 ± 2	3 ± 2

Table 7. Measurement of flux of heat output through upper insulation.

An independent estimate of c can be obtained from the approximate formula

$$\frac{2\pi d}{(K_m)_0(T_1 - T_0)} \int_{0{\cdot}4}^{1{\cdot}4} qr\, dr = -2\pi c \int_{0{\cdot}4}^{1{\cdot}4} \theta_z^{(2)} r\, dr, \tag{36}$$

where q is the outflux of heat per unit area in c.g.s. units, and $\theta^{(2)}$ is the coefficient of c in the perturbation formulae. To measure q, a series of four differential thermocouples (calibrated as heat flux meters) are placed on the upper insulation at radii r corresponding to points of the relaxation net. The results are given in table 7, using the boundary conditions as for experiment I. After the integrals in (36) have been evaluated approximately, a value of

$$c = -0{\cdot}10 \pm 0{\cdot}05 \tag{37}$$

is obtained. This result is to the same order as the values of c estimated in § 4, table 6.

7. Conclusions

Evidently the first-order perturbation scheme provides a satisfactory fit to the convection data for the range of boundary temperature differences $(T_1 - T_0)$ chosen. Its range of validity extends from $\eta = m(T_1 - T_0) = 0$ to the point where the second-order term becomes significant in comparison with the term of first order. Presumably terms of higher order can be calculated, with increasing computational difficulty, but accuracy is not easily maintained owing to cumulative errors.

With the above limitation to first-order accuracy, it appears that the following additional conclusions have been justified experimentally.

(*a*) The motion of the liquid percolating through the sand under non-isothermal conditions is adequately described by Darcy's law for the low values of Reynolds number ($\ll 1$) applying here.

(*b*) The hypothesis that the packed sand behaves as an approximately homogeneous permeable medium is satisfactory.

(*c*) Near a fixed impermeable boundary, changes in sand packing due to the presence of a rigid surface might be expected to produce a thin layer of altered permeability. Neglect of this effect does not appear to introduce detectable errors: hence it is not of importance.

(*d*) Modifications to the apparent thermal conductivity at very low Reynolds numbers by fluid dispersion (§ 1) is negligible.

(*e*) The thickness of the fluid boundary layer adjacent to smooth rigid boundaries is small, probably close to the typical grain size.

The conditions (*a*) to (*e*) represent initial assumptions which are contained implicitly in the theoretical solutions. Departures from these conditions are negligible in comparison with the convection and other effects analysed above, since the residual variance after fitting m, b, c is very small.

While the analysis of thermal boundary loss and variation of thermal conductivity with temperature does not give accurate results, it is clear that these effects are small when compared with the convection effect. The estimate of m is not altered appreciably by their presence, and the general conclusions about the convection process are not affected.

The author wishes to thank the Director, Dominion Physical Laboratory, New Zealand Department of Scientific and Industrial Research, for making experimental facilities available, and Mr R. F. Benseman who was closely associated with the author in carrying out the experimental work. Thanks are due also to Dr J. H. Darwin and Mr A. McNabb of Applied Mathematics Laboratory for helpful suggestions, and to Mrs J. B. Wooding, who performed many of the numerical computations required in the analysis of the results.

References

Batchelor, G. K. 1954 *Quart. Appl. Math.* **12**, 209.

Chandrasekhar, S. 1943 *Rev. Mod. Phys.* **15**, 1.

Muskat, M. 1937 *The Flow of Homogeneous Fluids Through Porous Media.* Ann Arbor: Edwards.

National Research Council, U.S.A. 1929 *International Critical Tables*, Vol. 4. New York: McGraw-Hill.

Pearson, H. S. & Hartley, H. O. 1954 *Biometrika Tables for Statisticians*, Vol. 1. Cambridge University Press.

Rayleigh, Lord 1899 *Phil. Mag.* **47**, 246.

Slichter, C. S. 1899 *United States Geological Survey*, 19th annual report, part 2, p. 295.

Wooding, R. A. 1957 *J. Fluid Mech.* **2**, 273.

An approximate boundary layer theory for semi-infinite cylinders of arbitrary cross-section

By E. VARLEY
Division of Applied Mathematics, Brown University, Providence

(*Received* 21 *November* 1957)

SUMMARY

An estimate is given of the distribution of skin frictional force per unit length, and of displacement area, on the outside of a semi-infinite cylinder, of arbitrary cross-section, moving steadily in a direction parallel to its generators. A Pohlhausen method is employed with a velocity distribution chosen to yield zero viscous retarding force on the boundary layer approximations. (The smallness of the fluid acceleration far from the leading edge has been pointed out by Batchelor (1954).) Like the Rayleigh method, this method is expected to yield reasonable results at large distances from the leading edge. However, for a large class of cross-sections, which includes all convex cross-sections and locally concave cross-sections with re-entrant angles greater than $\frac{1}{2}\pi$, the method yields the expected square root growth of the boundary layer at the leading-edge, with a fairly close approximation to the coefficient, and it is supposed that the skin-frictional force and displacement area are given with reasonable accuracy along the whole length of the cylinder.

Results for the elliptic cylinder and the finite flat plate are given in closed form, valid for the whole length of the cylinder, and are expected to be in error by at most 20%. In addition, some estimate is given of the effect of corners on skin frictional force and displacement area.

1. INTRODUCTION

This paper deals with the boundary layer on a long cylinder of arbitrary cross-section in a stream parallel to the generators. The shape of the nose is immaterial, but it is supposed to be smooth enough not to cause separation. It is the growth of the boundary with distance x from the leading edge, and the distribution of skin friction along the cylinder, with which this paper is concerned.

The problem for the cylinder of arbitrary cross-section has been tackled by Batchelor (1954). His work is based on Rayleigh's (1911) method of inferring a rough answer from the analogous time-dependent heat-conduction problem of determining the temperature distribution in an infinite

homogeneous solid, initially at zero temperature, but with the internal boundary (an infinitely long cylinder) maintained for $t > 0$ at a constant non-zero temperature. The time t is then interpreted as x/U, the thermal diffusivity as ν, and the temperature as the departure of the velocity u from the free stream value U.

This method assumes that vorticity in the boundary layer is convected downstream with the free stream velocity instead of the local velocity u in the boundary layer. In consequence, the boundary layer thickness is underestimated and the skin friction is overestimated.

For the cylinder of arbitrary cross-section Batchelor finds that, for small values of $\nu x/U$, the local properties in the boundary layer are independent of the cylinder cross-section. They are as in the well-known Blasius layer, for which the boundary layer thickness varies like $(\nu x/U)^{1/2}$. For the Blasius layer, Batchelor, like Rayleigh (1911), obtains for the local skin friction $0{\cdot}564\mu U(\nu x/U)^{-1/2}$, when the true coefficient is 0·332. This is a serious overestimate.

At values of $\nu x/U$ for which the thickness of the boundary layer is comparable with a typical dimension l (taken to be the perimeter divided by 2π) of the cylinder cross-section, the effect of the cross-sectional shape is important. The first approximation for the effect of the shape of the cylinder on the force per unit length of cylinder is determined in terms of the number of corners and their angles in the cylinder cross-section; if there are no corners, the force on a unit length of the cylinder is the same, to this approximation, as that on a circular cylinder of the same perimeter. For large values of x/U the boundary layer thickness is large compared with l, and it is here that we expect the Rayleigh method to furnish reasonable results since conditions in a large part of the outer boundary layer approximate to free stream conditions. Batchelor shows that the bulk properties of the boundary layer for large values of x/U are the same as those for the circular cylinder which has the 'equivalent radius' c, such that the two cylinders, if given the same charge per unit length, would have the same electrostatic potential at large distances. Moreover, the rate of retardation of the fluid becomes very small.

Batchelor's solution for the general cylinder can be regarded as giving useful qualitative results, but is inadequate quantitatively except far downstream where it was shown by Glauert & Lighthill (1954) to be good.

Glauert & Lighthill (1954) investigated the boundary layer on a circular cylinder by using a Pohlhausen method with a velocity profile of the form $A(x)\log(r/c)$, where r is the distance from the axis of the circular cylinder. This profile has the virtue of satisfying conditions near the wall as accurately as possible, and of being the profile for which the viscous retarding force is identically zero. $A(x)$ was determined by substitution in the integrated momentum equation.

The results near the leading edge show good agreement with the exact solution (due to Seban & Bond (1951) and corrected by Kelly (1954)), in which the Stokes stream function is expanded in powers of $\{\nu x/(Ua^2)\}^{1/2}$.

The solution also agrees well with an asymptotic series solution, published in the same paper, which is valid far downstream.

To summarize: Batchelor has shown that for a cylinder of arbitrary cross-section far from the leading edge the viscous retarding force is very small, and in the outer part of the boundary layer where conditions are symmetrical the velocity profile is of the form $A(x)\log(r/c)$, where $A(x)$ depends upon the cylinder cross-section. Moreover Glauert & Lighthill have shown that for the case of a circular cylinder a Pohlhausen method with a velocity profile yielding zero viscous retardation gives good results along the whole length of the cylinder.

In the present paper a Pohlhausen method is again used with a velocity profile for which the viscous retarding force is identically zero along the whole length of the cylinder, and which agrees with the known solution far downstream. We expect the present method to furnish good results in the region where the boundary layer thickness is comparable with l, since in this region Batchelor shows that the viscous retarding force is small. To see whether the method, like that of Glauert & Lighthill, has value also near the nose, we expand the solutions for different shaped cross-sections at the nose and compare them with the expected Blasius solutions.

We assume the velocity profile is of the form $A(x)\phi(y, z)$, where y, z are Cartesian coordinates in the cross-sectional plane. It is further assumed that for a large distance r from an axis fixed in the cylinder boundary ϕ varies like $\log(r/c)$. The determination of ϕ is then seen to be reducible to a potential problem, the solution of which is known once we can determine the conformal mapping which transforms the exterior of the cross-section into the exterior of its 'equivalent circle', the modulus of the transformation being unity at infinity. This is the problem in electrostatics of determining the potential due to an infinite cylinder with a charge distribution of one unit of charge per unit length of the cylinder. $A(x)$ for a given cylinder is then determined from the momentum integral equation, Glauert & Lighthill's solution for a circular cylinder being a particular case.

It is shown that, only for flows down cylinders whose cross-sections contain a re-entrant angle of 90° or less, does this solution break down qualitatively at the leading edge by not giving initially the expected square-root law of boundary-layer growth with distance from the leading edge. Further for a large class of cross-sectional shapes, including circles, ellipses, convex polygons, and partly-concave polygons having re-entrant angles greater than $5\pi/8$, this method gives quantitative results at the leading edge for bulk properties, such as skin friction force per unit length, and displacement area, which are quite close to the known Blasius value, and much better than values obtained by the Rayleigh method. On the other hand, there is of course no attempt to predict velocity distributions in this or any other Pohlhausen method.

In addition, the results are expected to be good, like those given by the Rayleigh method, far downstream, because the assumption of a profile for which the viscous retarding force is zero becomes closer and closer to

the truth. Therefore, it is not unreasonable to suppose that the complete distribution of these bulk properties as functions of the distance from the leading edge is given satisfactorily.

Solutions in closed form are given for the flat plate of finite width and the elliptic cylinder. The skin frictional force and the displacement area for the flat plate are given with errors of 3% and 10% respectively at the leading edge, and for the circular cylinder errors of 13% and $\frac{1}{2}$% in the corresponding quantities. For the general elliptic cylinder the corresponding quantities are given with errors which lie between these two sets of values. (Rayleigh's method gives an error of 70% and 35% in the skin frictional force and displacement area respectively.) It is expected that the errors gradually become less, further downstream.

The solution of the problem for the general cylinder is given in the form of a double integral which is expanded in series both at the leading edge and far downstream. These solutions can, in general, be easily joined giving a solution valid along the whole length of the cylinder. The bulk properties of the flow are seen to depend on the cross-sectional perimeter at the leading edge, and on the 'equivalent radius' far downstream, the detailed shape of the cross-section being important in the intermediate region.

Results for the finite flat plate and the square cross-section are given in tabular and graphical form. In particular, the graph of momentum defect area enables easy readings of the total frictional drag of the cylinders of any length to be made. Some consideration is also given below to several other polygonal shapes.

2. General theory

If u is the velocity in the x direction parallel to the generators of the cylinder whose boundary is denoted by Γ, and v, w are the velocities parallel to Cartesian axes y, z fixed in the plane of the cylinder cross-section, then the boundary layer equations for the problem of this paper are

$$u\frac{\partial u}{\partial x}+v\frac{\partial u}{\partial y}+w\frac{\partial u}{\partial z}=\nu\left(\frac{\partial^2 u}{\partial y^2}+\frac{\partial^2 u}{\partial z^2}\right) \tag{1a}$$

and

$$\frac{\partial u}{\partial x}+\frac{\partial v}{\partial y}+\frac{\partial w}{\partial z}=0. \tag{1b}$$

Equations (1) are to be solved under the boundary conditions

$$\begin{aligned} &u=v=w=0 \quad \text{on } \Gamma,\\ &u\to U \quad \text{as } x\to 0 \qquad \text{or } y,z\to\infty. \end{aligned} \tag{2}$$

The method of this paper is a Pohlhausen method based upon a profile

$$u=A(x)\phi(y,z), \tag{3}$$

with ϕ chosen to yield zero viscous retarding force on the boundary layer approximations. $A(x)$ is determined for a given cylinder by substitution in the momentum integral equation

$$\rho U^2\frac{d(\cdot)}{dx}=F, \tag{4}$$

where

$$\theta = \frac{1}{U^2} \int_{\Sigma} u(U-u)\,dydz, \tag{5}$$

is the momentum defect area, Σ being the whole area outside the perimeter, and

$$F = \mu \oint_{\Gamma} \frac{\partial u}{\partial n}\,dr \tag{6}$$

(where dr, dn are elements of the perimeter Γ and of its outward normal) is the frictional force per unit length of the cylinder. Equation (4) may be obtained either by direct physical argument or by integrating (1 a) over the whole area outside Γ and using (1 b) to eliminate v and w.

The viscous retarding force given on the right-hand side of equation (1 a) vanishes for the profile (3) if

$$\frac{\partial^2 \phi}{\partial y^2} + \frac{\partial^2 \phi}{\partial z^2} = 0. \tag{7}$$

The particular solution of (7) with $\phi = 0$ on Γ which will be used is simply the electrostatic potential of a cylinder at zero potential and unit charge per unit length, so that

$$\int_{\Gamma} \frac{\partial \phi}{\partial n}\,dr = 2\pi. \tag{8}$$

The join between the profile chosen for the boundary layer and the constant value U, which u must take outside the boundary layer, is effected by writing $A(x) = U/\alpha(x)$, where $\alpha(x)$ is non-dimensional, and putting

$$\begin{aligned} u &= U\phi(y,z)/\alpha(x) \quad \text{for } 0 < \phi \leqslant \alpha, \\ u &= U \qquad\qquad\quad \text{for } \phi \geqslant \alpha. \end{aligned} \tag{9}$$

Then by (6) and (8)

$$F = 2\pi\mu A(x) = 2\pi\mu U/\alpha(x). \tag{10}$$

When ϕ has been determined, the variation of α with x follows from (4), which, with (8) and (10), gives

$$\frac{d}{dx} \iint_{u<U} \frac{\phi(\alpha-\phi)}{\alpha^2}\,dydz = \frac{2\pi\nu}{U\alpha(x)}. \tag{11}$$

Once the integral in (11) has been determined as a function of α, it is easy to obtain the relation between α and x by one further simple integration.

A seemingly objectionable feature of this method is the discontinuity in $\partial u/\partial n$ at the edge of the boundary layer (given by $\phi = \alpha$). However, Glauert & Lighthill have shown that this in itself does not lead to serious errors in a Pohlhausen treatment. Moreover, as $\nu x/(Uc^2)$ increases, the discontinuity (which is proportional to $1/\alpha$) decreases and we would expect the errors arising from it to decrease also.

It now remains to determine the integral on the left-hand side of (11) as a function of α for a given boundary shape Γ. The solution to the potential problem given by (7) and (8) has been found for a number of boundary

shapes. In particular for a circular cylinder of radius c the solution takes the form

$$\phi = \log(r/c), \tag{12}$$

and if $\zeta = re^{i\theta}$ then this can be written as

$$\zeta = ce^{\phi + i\theta} = ce^{s}, \quad \text{say.} \tag{13}$$

The solution of (7) and (8) for a given boundary Γ then reduces to finding the conformal mapping

$$w = f(\zeta), \quad \text{with } f(\zeta) \sim \zeta \quad \text{for large } \zeta, \tag{14}$$

which maps the exterior of the boundary Γ in the $w\,(= z + iy)$ plane on to the exterior of the equivalent circle of radius c in the ζ-plane. The solution of

$$w = f(ce^{s}) \tag{15}$$

then gives ϕ (the real part of s) as a function of y and z.

If we now change variables in (11) from the physical (y, z)-plane into the (θ, ϕ)-plane, noting that

$$dydz = |dw/ds|^2 \, d\theta d\phi, \tag{16}$$

the equation becomes

$$\frac{d}{dx} \int_0^{\alpha} \frac{\phi(\alpha - \phi)}{\alpha^2} d\phi \int_0^{2\pi} \left| \frac{dw}{ds} \right|^2 d\theta = \frac{2\nu\pi}{U\alpha}. \tag{17}$$

The mathematical problem is thus reduced to the calculation of the inner integral in (17).

A quantity of special interest is the displacement area

$$\Delta = \frac{1}{U} \iint_{\Sigma} (U - u)\, dydz \tag{18}$$

which represents the amount by which the fluid outside the boundary layer is displaced owing to the reduced flow inside. On the present theory (18) takes the form

$$\Delta = \int_0^{\alpha} \int_0^{2\pi} \frac{(\alpha - \phi)}{\alpha} \left| \frac{dw}{ds} \right|^2 d\theta d\phi, \tag{19}$$

which is a function of α. Once (17) has been solved numerically to give the variation of α with $(\nu x)/(Uc^2)$, equation (19) enables us to determine the variation of Δ with $(\nu x)/(Uc^2)$.

To check the accuracy of the method for a given cylinder we expand the solution at the leading edge in terms of the parameter $(\nu x)/(Ul^2)$ and compare it with the expected Blasius layer, where l is the perimeter divided by 2π, given in the present method by

$$l = \frac{1}{2\pi} \int_0^{2\pi} \left| \frac{dw}{ds} \right|_{\phi = 0} d\theta. \tag{20}$$

3. Flat plate of finite width

The well-known mapping which transforms the exterior of the finite flat plate of width $4c$ in the w-plane on to the exterior of its equivalent circle

of radius c in the ζ-plane is

$$w = \zeta + c^2/\zeta, \tag{21}$$

which can be transformed by using (13) into the required form

$$w = 2c\cosh s. \tag{22}$$

The form (22) shows that this method assumes that lines of constant velocity are confocal ellipses when at the leading edge they should be flat cylinders. This is a source of error at the leading edge, although the effects may well cancel out more or less on integrating round the perimeter.

On substituting the value of $|dw/ds|^2$ given by (22) it is easily deduced that, for a flat plate of width $4c$,

$$\int_0^{2\pi} |dw/ds|^2 \, d\theta = 2\pi c^2(e^{2\phi} + e^{-2\phi}), \tag{23}$$

which when substituted in (17) reduces the momentum integral equation to

$$\frac{d}{dx}\int_0^{\alpha} \frac{\phi(\alpha-\phi)}{\alpha^2}(e^{2\phi} + e^{-2\phi})\, d\phi = \frac{\nu}{Uc^2\alpha}. \tag{24}$$

The integral in (24) is

$$(1/\alpha^2)(\alpha\cosh\alpha - \sinh\alpha)\cosh\alpha,$$

whence (24) can be solved giving

$$\frac{\nu x}{Uc^2} = \frac{1}{2}\left[\cosh 2\alpha + 3 - \frac{2}{\alpha}\sinh 2\alpha + \int_0^{2\alpha} \frac{\cosh t - 1}{t}\, dt\right]. \tag{25}$$

The integral in (25) is a well-known exponential integral which has been copiously tabulated so that the variation of α with $(\nu x)/(Uc^2)$, and hence the skin frictional force per unit length $F = 2\pi\mu U/\alpha$, is easy to determine numerically.

For practical purposes the results are given in tabular and graphical form. The only means of finding if the solution is accurate up to the leading edge is to expand the solution in powers of $\{(\nu x)/(Ul^2)\}^{1/2}$ and compare the first term in the expansion for skin frictional force and displacement area with the expected exact values of Blasius. For the flat plate of finite width $4c$,

$$l = 4c/\pi. \tag{26}$$

The right-hand side of (25) may be expanded as

$$(\nu x)/(Uc^2) = \tfrac{1}{6}\alpha^2 + \tfrac{3}{20}\alpha^4 + O(\alpha^6)$$

which is easily inverted to give, using (26),

$$\frac{F}{2\pi\mu U} = \frac{1}{\alpha} = 0{\cdot}321\left(\frac{\nu x}{Ul^2}\right)^{-1/2} + 1{\cdot}40\left(\frac{\nu x}{Ul^2}\right)^{1/2} + 18{\cdot}8\left(\frac{\nu x}{Ul^2}\right)^{3/2} + O\left(\frac{\nu x}{Ul^2}\right)^{5/2}. \tag{27}$$

The exact coefficient of $\{(\nu x)/(Ul^2)\}^{-1/2}$ in (27) is given by Blasius as 0·332 showing that even at the leading edge the method of the present paper applied to a flat plate gives the frictional force with an error of 3%, although some cancelling of errors doubtlessly occurs. Since it is reasonable to

assume that the method becomes more accurate far downstream we see that the distribution of skin frictional force is given remarkably well along the whole length of the flat plate. In contrast the Rayleigh method gives the coefficient 0·564 which overestimates the skin frictional force by 70% at the leading edge.

$\log_{10}\left(\frac{\nu x}{Uc^2}\right)$	$\log_{10}\left(\frac{F}{2\pi\mu U}\right)$	$\log_{10}\left(\frac{\Theta}{2\pi c^2}\right)$	$\log_{10}\left(\frac{\Delta}{2\pi c^2}\right)$
−3·0	1·11	$\bar{2}$·43	$\bar{2}$·89
−2·5	0·86	$\bar{2}$·66	$\bar{1}$·14
−2·0	0·62	2·92	$\bar{1}$·39
−1·5	0·39	$\bar{1}$·17	$\bar{1}$·63
−1·0	0·19	$\bar{1}$·44	$\bar{1}$·88
−0·5	0·01	$\bar{1}$·73	0·12
0·0	$\bar{1}$·87	0·05	0·38
0·5	$\bar{1}$·75	0·39	0·67
1·0	$\bar{1}$·65	0·77	0·99
1·5	$\bar{1}$·57	1·16	1·35
2·0	$\bar{1}$·49	1·57	1·72
2·5	$\bar{1}$·42	1·99	2·12
3·0	$\bar{1}$·36	2·42	2·54

Table 1. Finite flat plate.

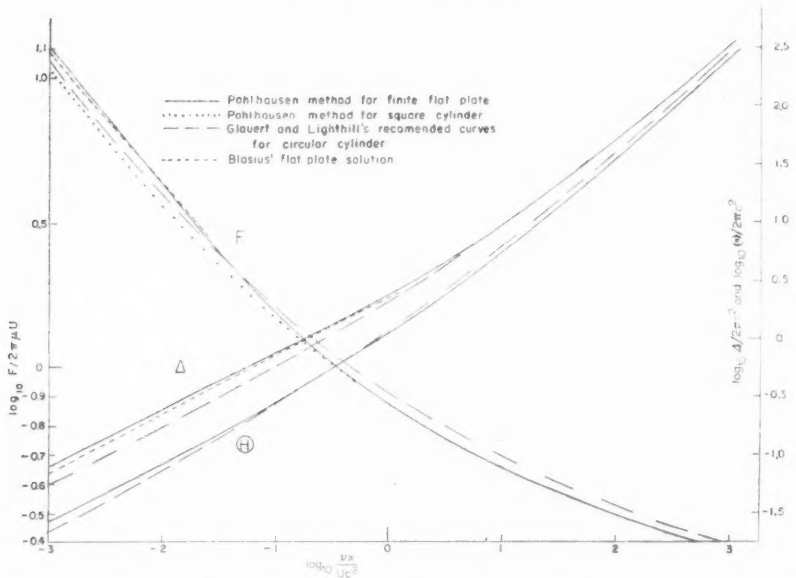

Figure 1. Frictional force F per unit length of cylinder, displacement area Δ and moment defect area Θ at distance x downstream from nose. (U = stream velocity, c = equivalent radius of cylinder.)

To determine the displacement area Δ we substitute (23) in (19) to give

$$\frac{\Delta}{2\pi c^2} = \int_0^{\alpha} \frac{\alpha - \phi}{\alpha} (e^{2\phi} + e^{-2\phi})\, d\phi = \frac{1}{2} \frac{\cosh 2\alpha - 1}{\alpha}. \tag{28}$$

Equation (28) together with (24) enables us to find numerically the variation of Δ with x. The results are given in graphical and tabular form in table 1 and figure 1.

For conditions at the leading edge we expand the right-hand side of (28) as

$$\Delta/(2\pi c^2) = \alpha + \tfrac{1}{3}\alpha^3 + O(\alpha^5). \tag{29}$$

When we substitute for α in (28) as a power series in $\{(\nu x)/(Ul^2)\}^{1/2}$ we obtain

$$\frac{\Delta}{2\pi l^2} = 1{\cdot}924\left(\frac{\nu x}{Ul^2}\right)^{1/2} - 2{\cdot}18\left(\frac{\nu x}{Ul^2}\right)^{3/2} + O\left(\frac{\nu x}{Ul^2}\right)^{5/2}. \tag{30}$$

Blasius gives 1·72 as the exact coefficient of $\{(\nu x)/(Ul^2)\}^{1/2}$, showing that at the leading edge the Pohlhausen method of the present paper gives an error of 11% in the displacement area. This can be compared with an error of 30% in the Rayleigh method which gives the coefficient as 1·13.

In addition to Δ, the momentum defect area $\Delta\Theta$ defined as in (5) will be considered. The integral in (5) has already been evaluated to give

$$\Theta/(2\pi c^2) = \alpha^{-2}(\alpha \cosh \alpha - \sinh \alpha)\cosh \alpha, \tag{31}$$

whence $\Theta/(2\pi c^2)$ may be plotted against $(\nu x)/(Uc^2)$.

No comparison with other solutions need be made as Θ is simply proportional to the integral of the skin friction F with respect to x. The graph of Θ as a function of x gives a convenient way of determining the drag $\rho U^2\Theta$ on a plate of length x.

4. Elliptic cylinder

The mapping

$$w = \zeta + c^2 k/\zeta \tag{32}$$

transforms the exterior of the ellipse with axes $c(1+k)$ and $c(1-k)$ in the w-plane on to the exterior of its equivalent circle of radius c in the ζ-plane. We may assume $0 < k < 1$ since this range of k gives all possible values of the ratio of major to minor axes.

Equation (32) together with the transformation (13) gives the solution of (7) and (8) in the form

$$w = c(e^s + ke^{-s}), \tag{33}$$

from which it is easily deduced

$$\int_0^{2\pi} |dw/ds|^2\, d\theta = 2\pi c^2(e^{2\phi} + k^2 e^{-2\phi}), \tag{34}$$

and

$$l = (2c/\pi)(1+k)E[2k^{1/2}(1+k)^{-1}] \tag{35}$$

where E is the complete elliptic integral of the second kind.

Substituting (34) in (17), the momentum integral equation becomes

$$\frac{d}{dx}\int_0^\alpha \frac{\phi(\alpha-\phi)}{\alpha^2}\,e^{2\phi}+k^2e^{-2\phi})\,d\phi = \frac{\nu}{Uc^2\alpha}, \tag{36}$$

which is easily solved to give

$$\frac{\nu x}{Uc^2} = \frac{1}{4}\left\{e^{2\alpha}+3-4\frac{e^{2\alpha}-1}{2\alpha}+\int_0^{2\alpha}\frac{e^t-1}{t}\,dt+ \right.$$
$$\left. +k^2\left[e^{-2\alpha}+3-4\frac{1-e^{-2\alpha}}{2\alpha}-\int_0^{2\alpha}\frac{1-e^{-t}}{t}\,dt\right]\right\}. \tag{37}$$

For conditions at the leading edge we expand the right-hand side of (37) to give

$$(\nu x)/(Uc^2) = \tfrac{1}{12}(1+k^2)\alpha^2+\tfrac{1}{9}(1-k^2)\alpha^3+\tfrac{3}{40}(1+k^2)\alpha^4+O(\alpha^5), \tag{38}$$

which is easily inverted to give together with (35), for the skin frictional force F,

$$\frac{F}{2\pi\mu U} = \frac{1}{\alpha} = 0{\cdot}455\frac{(1+k^2)^{1/2}}{(1+k)E}\left(\frac{\nu x}{Ul^2}\right)^{-1/2}+0{\cdot}667\frac{1-k^2}{1+k^2}+$$
$$+0{\cdot}995\frac{(1+k)E}{(1+k^2)^{1/2}}\left(\frac{\nu x}{Ul^2}\right)^{1/2}+O\left(\frac{\nu x}{Ul^2}\right)^{3/2}. \tag{39}$$

The coefficient of $\{(\nu x)/(Ul^2)\}^{-1/2}$ is a monotonically increasing function of k and varies between 0·289 for a circular cylinder ($k = 0$) and 0·321 for a flat plate of finite width ($k = 1$). Since for any cylinder cross-section we expect the error in this method to decrease far downstream it is not unreasonable to suppose that for the case of a general elliptic cylinder the frictional force is given everywhere with an error less than 13%.

We can determine the displacement area Δ in a similar manner to that given for the flat plate and find

$$\frac{\Delta}{2\pi c^2} = \frac{1}{2}\left\{\frac{e^{2\alpha}-1}{2\alpha}-1+k^2[1-\tfrac{1}{2}(1-e^{-2})]\right\}. \tag{40}$$

The right-hand side of (40) can be expanded to give

$$\Delta/(2\pi c^2) = \tfrac{1}{2}(1+k^2)\alpha+\tfrac{1}{3}(1-k^2)\alpha^2+O(\alpha^3), \tag{41}$$

which, with the solution of (38), gives

$$\frac{\Delta}{2\pi l^2} = 1{\cdot}73\frac{(1+k^2)^{1/2}}{(1+k)E}\left(\frac{\nu x}{Ul^2}\right)^{1/2}+O\left(\frac{\nu x}{Ul^2}\right)^{3/2}. \tag{42}$$

The coefficient of $\{(\nu x)/(Ul^2)\}^{1/2}$ is a monotonically increasing function of k and varies between 1·73 for $k = 0$ and 1·92 for $k = 1$, showing that it is not unreasonable to assume that the displacement area Δ is everywhere given with an error less than 10%.

In addition the momentum displacement area Θ is given as

$$\frac{\Theta}{2\pi c^2} = \frac{1}{4\alpha^2}[(\alpha-1)e^{2\alpha}+(\alpha+1)+k^2\{(\alpha+1)e^{-2\alpha}+(\alpha-1)\}]. \tag{43}$$

5. Polygon cross-sections

We now consider the application of the present method to flow down cylinders whose cross-sections are n-sided, closed polygons with exterior angles $\pi\alpha_r$ $(r = 1, ...n)$. Suppose that we can determine the a's of the Schwarz–Christoffel transformation

$$dw/dt = A(t-a_1)^{\alpha_1}...(t-a_n)^{\alpha_n}/(1+t^2)^2, \tag{44}$$

with

$$\sum_{r=1}^{n}\alpha_r = 2, \qquad \sum_{r=1}^{n}\alpha_r/(a_r^2+1) = 1, \qquad \sum_{r=1}^{n}\alpha_r a_r/(a_r^2+1) = 0, \tag{45}$$

which transforms the exterior of the closed polygon in the w-plane on to the lower half of the t-plane, where A is a constant and conditions (45) ensure the polygon is closed and that the solution of (44) is single-valued. Then introducing the bi-linear transformation

$$t = i(\zeta-c)/(\zeta+c), \tag{46}$$

which maps the lower half t-plane on to the exterior of the circle of radius c in the ζ-plane and which with (13) can be written

$$t = \tan(is/2), \tag{47}$$

we see that the solution of (7) and (8) reduces to solving

$$\frac{dw}{ds} = B\prod_{r=1}^{n}\sin^{\alpha_r}\tfrac{1}{2}(\theta+B_r-\phi i), \tag{48}$$

if the constant B is suitably chosen, where

$$a_r = \tan(\tfrac{1}{2}\beta_r) \qquad (r = 1, ...n). \tag{49}$$

The conditions (45) become

$$\sum_{r=1}^{n}\alpha_r = 2, \qquad \sum_{r=1}^{n}\alpha_r\cos\beta_r = \sum_{r=1}^{n}\alpha_r\sin\beta_r = 0. \tag{50}$$

From (48) it is easily deduced

$$\left|\frac{dw}{ds}\right| = B'\cosh\phi\prod_{r=1}^{n}\left\{1-\frac{\cos(\theta+\beta_r)}{\cosh\phi}\right\}^{\alpha_r/2}. \tag{51}$$

Since we seek the solution of (55) with

$$|dw/ds| \sim ce^{\phi} \quad \text{for large } \phi, \tag{52}$$

we see that $B' = 2c$.

For conditions far downstream we expand

$$\int_0^{2\pi}|dw/ds|^2\,d\theta \tag{53}$$

in (17) and (19) in a series valid for large ϕ which can always be written, by (50) and (51), as

$$\int_0^{2\pi}|dw/ds|^2\,d\theta = 2\pi c^2(e^{2\phi}+\sum_{m=1}^{\infty}A_m e^{-m\phi}). \tag{54}$$

If we use the form (54) the solution of the momentum integral equation giving the variation of α, and hence of frictional force, with $(\nu x)/(Uc^2)$ is

$$\frac{\nu x}{Uc^2} = \frac{1}{4}\left[e^{2\alpha}+3-4\left(\frac{e^{2\alpha}-1}{2\alpha}\right)+\int_0^{2\alpha}\frac{e^t-1}{t}\,dt\right]+\sum_{m=1}^{\infty}A_m G(\alpha,m), \tag{55}$$

where

$$G(\alpha, m) = \frac{1}{m^2}\left[e^{-m\alpha} + 3 - 4\frac{1-e^{-m\alpha}}{m\alpha} - \int_0^{m\alpha}\frac{1-e^{-t}}{t}\,dt\right]. \tag{56}$$

In addition the variation of Δ with large α, and hence by (55) with large $(\nu x)/(Uc^2)$ is given in the series form

$$\Delta/2\pi c^2 = (1/4\alpha)(e^{2\alpha} - 2\alpha - 1) + \sum_1^\infty A_m M(\alpha, m), \tag{57}$$

where

$$M(\alpha, m) = (1/m^2\alpha)(m\alpha + e^{-m\alpha} - 1). \tag{58}$$

For conditions at the leading edge we expand (53) in a series valid for small ϕ and solve equations (17) and (19) in series valid for small $(\nu x)/(Uc^2)$. In particular the expected square-root behaviour in the boundary layer at the nose occurs if the integral (53) converges for $\phi = 0$.

Regular polygon

For an n-sided regular polygon it is easily shown (Bickley 1929) that

$$\beta_r = \pi r/n \qquad (r = 1, \ldots n), \tag{59}$$

whence

$$|dw/ds| = 2^\lambda c|\sin(s/\lambda)|^\lambda, \tag{60}$$

where $\pi\lambda = 2\pi/n$ is the common exterior angle of the regular polygon. From (60) it is easily deduced that

$$\int_0^{2\pi}\left|\frac{dw}{ds}\right|^2 d\theta = 2^{\lambda+1}c^2\cosh(2\phi/\lambda)\int_0^\pi (1 - \operatorname{sech}(2\phi/\lambda)\cos\gamma)^\lambda\,d\gamma. \tag{61}$$

The integral on the right-hand side of (61) is a hypergeometric function which can be expanded in series valid for large and small ϕ.

For conditions far downstream we expand (61) in a series valid for large ϕ, namely

$$\int_0^{2\pi}\left|\frac{dw}{ds}\right|^2 d\theta = 2\pi c^2 e^{2\phi}\,F_2(-\lambda, -\lambda; 1; e^{-3\phi/\lambda}), \tag{62}$$

which is in the form given by (54) and enables us together with (55) and (57) to obtain numerically the variation of frictional force and displacement area with large distance x downstream.

At the leading edge we expand (61) in the form

$$\int_0^{2\pi}\left|\frac{dw}{ds}\right|^2 d\theta = 2\pi c^2 e^{2\phi}\left[\frac{(2\lambda!)}{(\lambda!)^2}F(-\lambda, -\lambda; -2\lambda; 1 - e^{-4\phi/\lambda}) + \right.$$

$$\left. + \frac{(\lambda!)^2}{2\pi(2\lambda+1)!}\tan\pi\lambda(1 - e^{-4\phi/\lambda})^{1+2\lambda}\,F(1+\lambda, 1+\lambda; 2+2\lambda; 1 - e^{-4\phi/\lambda})\right], \tag{63}$$

except for the case of a square cylinder ($\lambda = \frac{1}{2}$) when the integral on the right-hand side of (61) is an elliptic integral. The expansion of (61) given by (63) enables us to determine a series for the left-hand side of (61) valid

for small ϕ which when inserted in (17) and (19) readily gives for non-zero λ

$$\frac{F}{2\pi\mu U} = \frac{1}{\alpha} = 0{\cdot}289\left[\frac{(\lambda/2)!}{\lambda!}\right]^2 [(2\lambda)!]^{1/2}\left(\frac{\nu x}{Ul^2}\right)^{-1/2} + k_1(\lambda)\left(\frac{\nu x}{Ul^2}\right)^{\lambda} + \\ + k_2(\lambda)\left(\frac{\nu x}{Ul^2}\right)^{1/2} + O\left(\frac{\nu x}{Ul^2}\right)^{1+\epsilon}, \quad (64)$$

and

$$\frac{\Delta}{2\pi l^2} = 1{\cdot}73\left[\frac{(\lambda/2)!}{\lambda!}\right]^2 (2\lambda)!\left(\frac{\nu x}{Ul^2}\right)^{1/2} + D_1(\lambda)\left(\frac{\nu x}{Ul^2}\right)^{1+\lambda} + \\ + D_2(\lambda)\left(\frac{\nu x}{Ul^2}\right)^{3/2} + O\left(\frac{\nu x}{Ul^2}\right)^{2+\epsilon}, \quad (65)$$

where for a regular polygon

$$l = c\lambda!/(\lambda/2)! \quad (66)$$

and

$$\epsilon = \lambda, \qquad \lambda \leqslant \tfrac{1}{2}, \\ \epsilon = \tfrac{1}{2}, \qquad \lambda \geqslant \tfrac{1}{2}. \quad (67)$$

The coefficients of $\{(\nu x)/(Ul^2)\}^{-1/2}$ in (64) and of $\{(\nu x)/(Ul^2)\}^{1/2}$ in (65) vary between the limits given for a flat plate ($\lambda = 1$) and a circular cylinder ($\lambda = 0$), whence it is not unreasonable to suppose the skin frictional force per unit length and the displacement area are given everywhere with errors less than 13% and 10% respectively.

An indication is given in (64) and (65) of the effect of flow outside an angle $\pi(1-\lambda)$ on skin frictional force and displacement area at the leading edge. For small values of λ the coefficients of the fourth terms in (64) and (65) are so large compared with the second and third coefficients that the contributions of the second and third terms are well below the level of the fourth. For values of $\lambda \sim \frac{1}{2}$ the second and third terms effectively cancel in both (63) and (64), while for values of $\lambda \sim 1$ the third terms give the effective first approximation.

The results given so far for skin frictional force agree qualitatively with a result given by Batchelor, namely: "The friction on cylinders (with inward curvature everywhere) with corners is always less than the friction on cylinders with smooth boundaries; to turn a corner sharply is more economical on drag than to do it gently with the same perimeter". The results do however disagree quantitatively with Batchelor by not predicting a finite effect for corners at the nose.

In addition a similar result holds for displacement area which can be stated: "The displacement area on cylinders (with inward curvature everywhere) with corners is always greater than the friction on cylinders with smooth boundaries; to turn a corner slowly is more economical on displacement area than to do it quickly with the same perimeter".

The values of $F/(2\pi\mu U)$ for a cylinder of square cross-section are plotted in figure 1. For $(\nu x)/(Uc^2) > 1$ they are indistinguishable from those for a flat plate or circular cylinder of the same equivalent radius c. Glauert & Lighthill's recommended curve, obtained by adding 9% on to the Pohlhausen values, is probably a close approximation for all shapes in this range.

n-pronged cross

To investigate the application of the method of this paper to flows down cylinders whose cross-sections contain re-entrant angles we consider the case of the cylinder with a cross-section formed by n equal, equally spaced prongs, whence the common re-entrant angle is $2\pi/n = \pi\lambda$. The solution of (7) and (8) is such that

$$|dw/ds|^2 = 2^{\lambda}c|\sin(s/\lambda)]^{\lambda-1}|\cos(s/\lambda)|, \tag{68}$$

whence

$$l = 2^{\lambda+1}c/(\pi\lambda) \tag{69}$$

and

$$\int_0^{2\pi} |dw/ds|^2\, d\theta = 2\pi c^2 e^{2\phi}[F(-\lambda, -\lambda; 1; e^{-4\phi/\lambda}) + \\ + 4(1-\lambda)e^{-4\phi/\lambda} F(2-\lambda, 1-\lambda; 2e^{-4\phi/\lambda})]. \tag{70}$$

The right-hand side of (70) can be written

$$2\pi c^2 e^{2\phi} \sum_{r=0}^{\infty} A_r e^{-4r\phi/\lambda}, \tag{71}$$

where

$$A_r = (\lambda-1)^2 - (\lambda-r+1)^2(\lambda-2r)^2/(r!)^2, \tag{72}$$

which is in the form of (54) and enables us to find the distribution of skin frictional force and displacement area far downstream.

To obtain a check on the accuracy of the method at the leading edge we continue (71) analytically for small ϕ and obtain

$$\int_0^{2\pi} \left|\frac{dw}{ds}\right|^2 d\theta = 2\pi c^2\left[\frac{(2\lambda)!}{(\lambda!)^2(2\lambda-1)} + B\phi^{2\lambda-1} + O(\phi^{\lambda})\right]. \tag{73}$$

The right-hand side of (73) shows that only for re-entrant angles greater than 90° ($\lambda < \frac{1}{2}$) does the method of this paper yield results which are qualitatively correct at the leading edge since they give the expected square-root growth of boundary layer with distance. For re-entrant angles less or equal to 90° the surfaces of constant velocity assumed by this method at the leading edge are so different from those in reality that the momentum defect is seriously overestimated, whence the skin frictional force is overestimated. However, for re-entrant angles lying between π (flat plate) and $5\pi/8$ the skin frictional force is overestimated by between 3% and 21% while the displacement area is overestimated by between 11% and 40%. These results are better than those given by the Rayleigh method.

The greater part of this paper was written at Manchester University as a M.Sc. thesis; it was completed at Brown University under the Air Force Contract AF–49(638)–232. The author is grateful to Professor Lighthill for his helpful suggestions.

References

Batchelor, G. K. 1954 *Quart. J. Mech. Appl. Math.* **7,** 179.

Bickley, W. G. 1929 *Phil. Trans.* A, **228,** 235.

Glauert, M. B. & Lighthill, M. J. 1955 *Proc. Roy. Soc.* A, **230,** 188.

Kelly, H. R. 1954 *J. Aero. Sci.* **21,** 634.

Rayleigh, Lord 1911 *Phil. Mag.* (6) **21,** 697.

Seban, R. A. & Bond, R. 1951 *J. Aero. Sci.* **18,** 671.

Cavitating flow about a wedge at incidence

By A. D. COX and W. A. CLAYDEN
Ministry of Supply, Armament Research and Development Establishment, Fort Halstead, Kent

(*Received* 10 *October* 1957)

SUMMARY

A mathematical model is constructed for cavitating flow past a wedge with sides of equal length but with its axis of symmetry placed at an angle to the incident stream. The model involves a subsidiary cavity with a re-entrant jet at the vertex. Only the case of zero cavitation number is considered. The flow field is worked out in some detail for small angles of incidence, and the lift, drag and moment coefficients are calculated as far as first-order terms in the angle of incidence. It is shown that the effect of the rate of loss of momentum in the re-entrant jet on these force coefficients is negligible to this order.

Experimentally, it is shown that the secondary cavity does exist under suitable conditions, and the force coefficients obtained agree with the theory.

1. INTRODUCTION

The problem of two-dimensional steady cavitating flow with zero cavitation number past a symmetrical wedge in an infinite stream, neglecting external forces, has in the past been solved exactly, using complex variable techniques, for the particular case of a non-yawed wedge (see Lamb 1932, or Milne-Thomson 1949).

Milne-Thomson has also derived a solution involving a yawed wedge. He found, however, that for the flow pattern considered it is not possible to specify arbitrarily the ratio of the lengths of the two wedge faces. This ratio is determined as a function of the wedge and yaw angles, and is unity only for zero yaw; so that, in particular, Milne-Thomson's method fails to solve the problem of a symmetric wedge at non-zero yaw.

To be able to specify the ratio of the lengths of the wedge faces independently of the wedge angle and yaw angle, it is necessary to relax the conditions determining Milne-Thomson's problem, and it is clear that the non-essential condition imposed is that which requires the vertex of the wedge to be a stagnation point. This is borne out by considering the special case of a yawed semi-infinite flat plate, whereon the stagnation point is not in general in a symmetric position (see Milne-Thomson 1949).

It is by discarding this condition that the following solution is found, involving a flow pattern which is of a sufficiently novel type to appear to

merit description in some detail. The novel feature of the flow—a subsidiary cavity in the lee of the wedge vertex—is shown experimentally to exist under certain conditions.

2. The physical model of the flow

The method of solution used will be that of the complex variable, and for this we need to assume potential flow and neglect viscosity.

It is convenient to adopt the convention that the angle of incidence is positive, so that the 'lower' face of the wedge is inclined to the stream at a greater angle than the 'upper' face. By analogy with the behaviour in the case of the flat plate, we should expect the stagnation point to move to the lower face of the wedge.

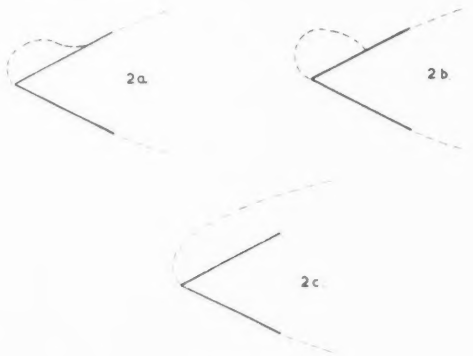

Figure 2.

The dividing streamline through this stagnation point will, on the downstream side, follow the wedge face until it reaches the rear of the wedge and will then become the lower free-streamline of the main or 'rear' cavity. On the upstream side of the stagnation point the dividing streamline will reach the vertex of the wedge and would then, in the absence of a stagnation point, need to attain an infinite fluid velocity to turn round the sharp corner of the wedge. However, owing to the inability of real fluids to sustain pressures less than vapour pressure, a rise in velocity above a certain finite value, in this case taken to be the main stream velocity, is impossible. We shall assume in our model that a cavity will form, bounded by a free-streamline which is the smooth continuation of the dividing streamline. Besides the rear cavity, therefore, we have a 'bubble' cavity formed on the upper face of the wedge; this certainly exists under suitable conditions, as is shown by the photograph (figure 1, plate 1) taken in the A.R.D.E. Cavitation Tunnel.

The free-streamline springing from the vertex must either rejoin the upper face of the wedge or else continue to infinity. The first case might conceivably occur as illustrated in figure 2. If, however, the re-attachment

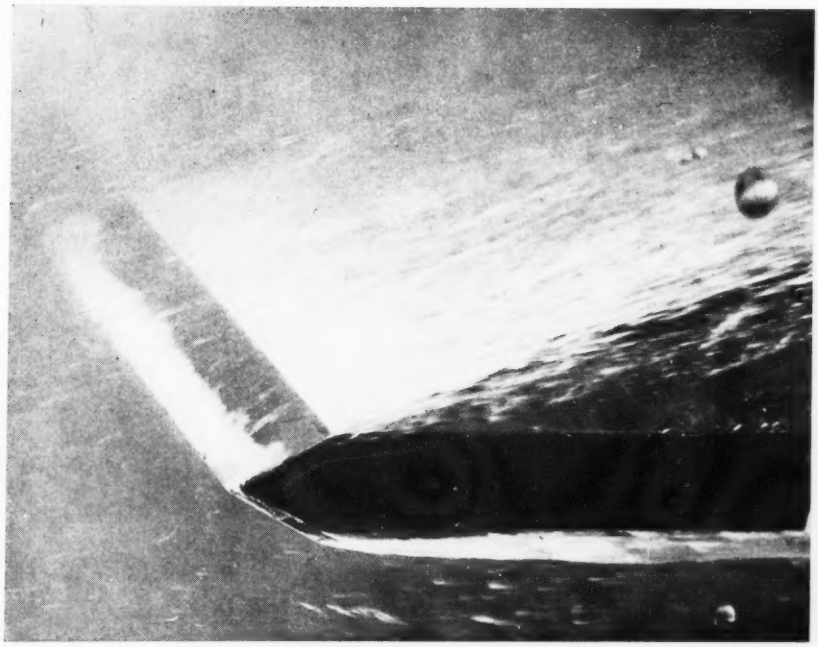

Figure 1. 30° semi-angle wedge.
Angle of incidence = 10°, cavitation number = 0·003.

were effected tangentially, as in figure 2(*a*), the free-streamline would contain a point of inflection, which is impossible because the pressure gradient, and therefore the streamline curvature, must always be directed towards the cavity. If the re-attachment were other than tangential, as in figure 2(*b*), it would involve a stagnation point, which again is impossible on a free-streamline.

If, on the other hand, the free-streamline continues to infinity downstream, so that the upper face of the wedge is included in the cavity, as in figure 2(*c*), then the flow is simply that past a yawed flat plate. This flow pattern will indeed occur under suitable conditions, which may easily be defined from the exact general solution of this type of flow (see Milne-Thomson 1949).

When the dimensions and orientation of the wedge preclude the possibility of 'yawed flat plate' flow, we are left with the possibility that the flow continues to infinity in some other direction. This apparently unreal configuration, involving a double-sheeted flow pattern, is similar to the familiar re-entrant jet models occurring in the solutions obtained by Kreisel (1946) and Shiffman (1949) for non-yawed wedges at non-zero cavitation number.

While Gilbarg & Rock (1946) have shown by numerical methods that drag forces are remarkably insensitive to the assumptions made as to the flow pattern at the rear of the cavity, at least when this region of the flow is far removed from the wetted nose of the body, we cannot quote this as sufficient justification for the model now proposed, since the re-entrant jet is here postulated as forming on the face of the wedge itself. The justification will rest partly on the degree of agreement achieved with experimental results, and partly on the mathematical demonstration that the rate of loss of momentum in the re-entrant jet is of smaller order of magnitude than the drag and lift forces on the wedge, at least for small angles of yaw.

We now consider the assumed mathematical model in detail. Referring to figure 3, we have a symmetrical wedge DCD' of semi-angle β in an infinite stream which makes an angle α with the axis of symmetry of the wedge. As is customary, the uniform stream is considered to be due to a source system at A, the point at infinity (A_1, A_2, etc. all refer to the unique point at infinity in this plane and are labelled differently for the purpose of identification of individual streamlines).

The streamline A_1B divides at the stagnation point B on the lower wedge face CD'. A_1BD' becomes the lower bounding free-streamline $D'A_2$ of the main cavity and A_1BC breaks away smoothly from the vertex C to form the bounding free-streamline CQE of the subsidiary cavity. The free-streamline CQE and part of the flow to its left turn almost completely round and flow to infinity as a separate jet, bounded on one side by the extension of the wedge face DC and on the other side by the free-streamline CQE. The point at infinity on this jet is denoted by E and is quite distinct from A, the point at infinity in the main stream. Since the streamlines

in the jet cut across the streamlines of the main flow pattern, it is necessary to visualize the flow as occurring on a double-sheeted Riemann surface, one sheet of which carries the main flow pattern, while the jet crosses on to the second sheet. The cut dividing one sheet from the other is somewhat. arbitrary, but it can be said to have the form $GQPA_3$ shown in figure 3. Since part of the flow to the left of A_1B flows upstream and the rest flows downstream, forming the upper wall of the main cavity, there must be a stagnation point H on the upper face CD of the wedge. The dividing streamline A_5H will, on the downstream side, become the upper bounding free-streamline DA_4 of the main cavity.

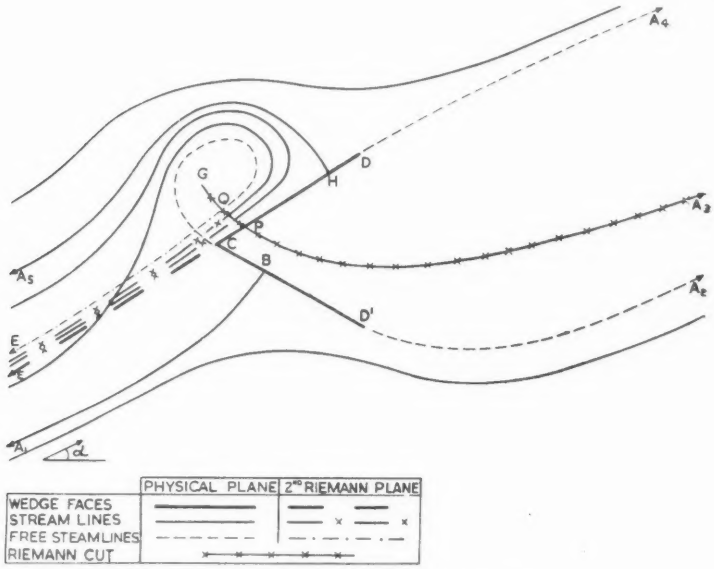

Figure 3. Assumed model of the flow.

Thus, of the fluid flowing from A, that lying to the right of A_1B returns to A, and that to the left of A_1B and to the right of A_5H flows to E and is 'lost', while that to the left of A_5H returns to A.

3. The solution of the problem

We use the standard technique of obtaining conformal transformations between suitable complex variables to determine the flow pattern and all physical quantities.

For the physical plane as represented in figure 3, we use the variable $z = x+iy$, where x and y are rectangular Cartesian coordinates parallel and perpendicular respectively to the plane of symmetry of the wedge, the direction of increasing x being downstream. Next, we define the complex

velocity potential $w = \phi + i\psi$, where ϕ is the velocity potential and ψ the stream function. The velocity vector (u, v) is given by

$$u = \frac{\partial \phi}{\partial x} = \frac{\partial \psi}{\partial y}, \qquad v = \frac{\partial \phi}{\partial y} = -\frac{\partial \psi}{\partial x}.$$

By a suitable choice of scale in the w-plane, in respect to the as yet undetermined length scale, we arrange that

$$u_\infty^2 + v_\infty^2 = 1,$$

where (u_∞, v_∞) is the velocity vector of the flow at infinity. Then

$$dw/dz = u - iv = qe^{-i\theta},$$

where $$q^2 = u^2 + v^2 \quad \text{and} \quad \theta = \tan^{-1} v/u.$$

The w-plane is illustrated in figure 4. All the streamlines, since they are by definition lines of constant ψ, become lines parallel to the ϕ-axis. The pair of streamlines HDA, HE and the pair BCE, $BD'A$ should each actually be represented by a single straight line but are shown separated for convenience.

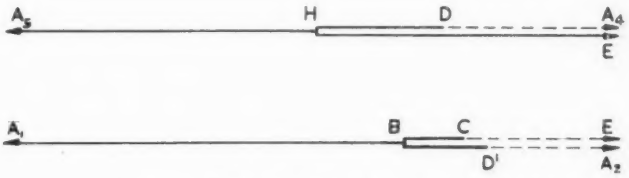

Figure 4. The complex velocity potential.

The next variable is the logarithmic hodograph variable Ω defined by

$$\Omega = \log(dw/dz) = \log q - i\theta.$$

This variable is plotted in figures 5 (*a*) and (*b*). The free-streamlines $D'AD$ and CQE are lines of constant speed q, this constant speed being equal to that at infinity so that, by our choice of scale, we have $q = 1$ (i.e. $\log q = 0$) on the free-streamlines. Thus in the Ω-plane they become portions of the imaginary axis. Since the wedge faces CB, BD' and DH, HE are lines of constant θ, they become lines parallel to the real Ω-axis with a discontinuity of amount π in the imaginary part of Ω at H and B, where $Re(\Omega) = -\infty$.

It is found on tracing the other streamlines that the Ω-plane is doubly-covered. To overcome this we make a cut in the Ω-plane from the point R, where $d\Omega/dz$ vanishes, to the point at infinity in the Ω-plane in a negative direction, and then consider the Ω-plane as a Riemann surface with two sheets cross-joined along this line.

Then the streamlines are as shown in figures 5 (*a*) and (*b*), where, for convenience, we have separated the two Riemann sheets. The streamlines themselves show how the four half-planes are joined. The images of all streamlines between the dividing streamlines A_1B and A_5H of figure 3 lie between AX_1 and AX_2 in figure 5 (*a*); after crossing the cut they remain on the second sheet, eventually terminating at E in figure 5 (*b*).

In order to obtain the requisite conformal transformations between these variables, we define an auxiliary variable τ by requiring that the streamlines DAD', $D'BC$, CQE, EHD become the sides of the rectangle

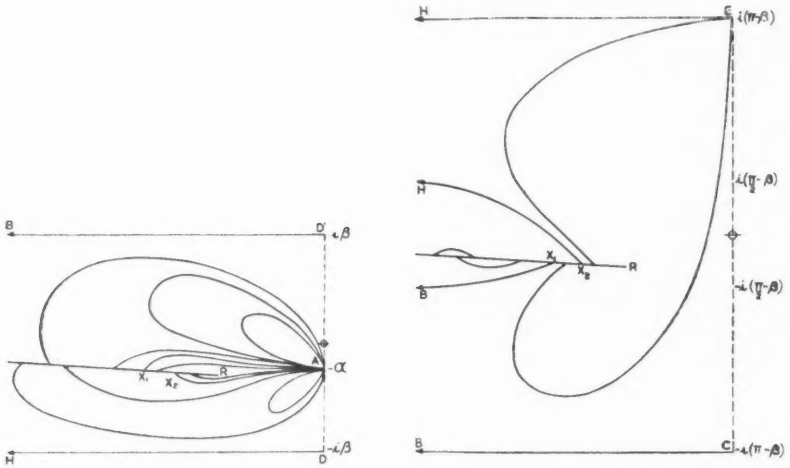

Figure 5. The logarithmic hodograph.

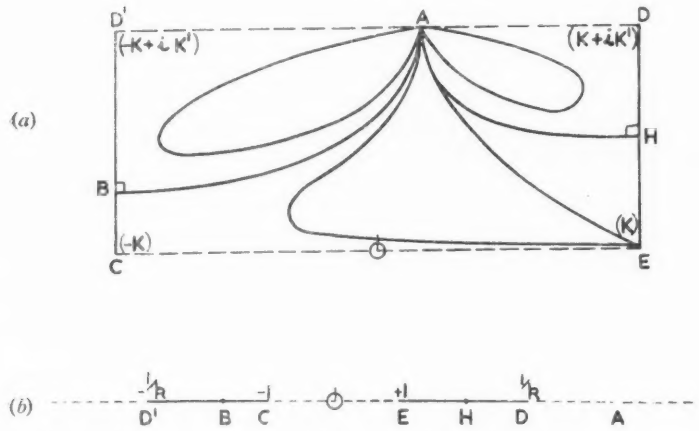

Figure 6. (*a*) τ-plane, (*b*) t-plane.

formed by the four points $\tau = \pm K, \pm K + iK'$, the orientation of the lines being as shown in figure 6(*a*). We also suppose the points H, B, A to be represented by

$$\left.\begin{aligned} \tau_H &= +K + ih, \\ \tau_B &= -K + ib, \end{aligned}\right\} \qquad K' \geqslant h, b \geqslant 0$$

$$\tau_A = iK' + a, \qquad -K \leqslant a \leqslant K.$$

In this plane the streamlines are as shown in figure 6(*a*), the behaviour near A being precisely as in figure 5(*a*) apart from a change of orientation.

We now find by inspection the conformal transformations which transform the lines DAD', $D'BC$, CE, EHD and AB, AH into their images in the w- and Ω-planes. From this we shall find a parametric relation between w and dw/dz, and hence the problem is solved.

The Ω–τ transformation

The functions to be used in this and the following transformation, as has been foreshadowed by choice of the τ-plane, are the Jacobian elliptic functions, for the definitions and properties of which reference may be made to Neville (1951), Jahnke & Emde (1948), Milne-Thomson (1950), and Whittaker & Watson (1940). Although Neville's notation is certainly the more elegant, we have used that of Whittaker & Watson as being the more familiar.

The function $d\Omega/d\tau$ must have a simple pole at τ_H and τ_B and must also be purely imaginary all along the boundary rectangle in the τ-plane. It must also be finite and non-zero at τ_A. The transformation

$$\frac{d\Omega}{d\tau} = \frac{T_1 \operatorname{sn}\tau}{\operatorname{sn}\tau - \operatorname{sn}\tau_H} + \frac{T_2 \operatorname{sn}\tau}{\operatorname{sn}\tau - \operatorname{sn}\tau_B} + iN, \tag{1}$$

where N is real and T_1, T_2 are purely imaginary, satisfies all these requirements since $\operatorname{sn}\tau$ is real all along the rectangle in the τ-plane. The function $d\Omega/d\tau$ can be shown to have only one zero inside the rectangle and this must obviously be at τ_R, where R is the branch point illustrated in figure 5.

To ensure that the transformation gives the correct scales as well as directions we have to impose further conditions. The first two are that Ω must have a discontinuity of $i\pi$ at τ_H and τ_B, and these are easily seen to lead to

$$T_1 = \operatorname{cn}\tau_H \operatorname{ds}\tau_H, \qquad \text{and} \quad T_2 = \operatorname{cn}\tau_B \operatorname{ds}\tau_B.$$

The other conditions are

$$\Omega_D = -i\beta, \quad \Omega_{D'} = i\beta, \quad \Omega_C = -i(\pi-\beta), \quad \Omega_E = i(\pi-\beta), \quad \Omega_A = -i\alpha,$$

and these must be applied to the integrated form of equation (1). Integrating, we get

$$\Omega = \Pi(\tau, \tau_H - iK') + \Pi(\tau, \tau_B - iK') - \\ - \tfrac{1}{2}\log\left\{\frac{\operatorname{cd}\tau_H + \operatorname{cd}\tau}{\operatorname{cd}\tau_H - \operatorname{cd}\tau}\,\frac{\operatorname{cd}\tau_B + \operatorname{cd}\tau}{\operatorname{cd}\tau_B - \operatorname{cd}\tau}\right\} + iN\tau, \tag{2}$$

where

$$\Pi(x,y) = \int_0^x \frac{k^2 \operatorname{sn} y \operatorname{cn} y \operatorname{dn} y \operatorname{sn}^2 u}{1 - k^2 \operatorname{sn}^2 y \operatorname{sn}^2 u}\, du,$$

as defined by Whittaker & Watson (1940). The constant of integration in (2) is zero due to the skew symmetry of the conditions at C and E.

The first four conditions imply that

$$NK = (\pi-\beta) + i[\Pi(K, \tau_H - iK') + \Pi(K, \tau_B - iK')],$$

and

$$\beta K' = \tfrac{1}{2}\pi(h+b). \tag{3}$$

The fifth condition gives

$$-i\alpha = \Pi(a, \tau_H - iK') + \Pi(a, \tau_B - iK') + ia\{Z'(h) + Z'(b)\} - \\ - i\left\{\tan^{-1}\frac{k\,\mathrm{sc}'b}{\mathrm{dc}\,a} - \tan^{-1}\frac{k\,\mathrm{sc}'h}{\mathrm{dc}\,a}\right\} + \\ + i\tan^{-1}\left\{-\frac{(k')^2\,\mathrm{sn}\,a\,\mathrm{sn}'h\,\mathrm{cn}'h}{\mathrm{cn}\,a\,\mathrm{dn}\,a\,\mathrm{dn}'h}\right\} + \\ + i\tan^{-1}\left\{-\frac{(k')^2\,\mathrm{sn}\,a\,\mathrm{sn}'b\,\mathrm{cn}'b}{\mathrm{cn}\,a\,\mathrm{dn}\,a\,\mathrm{dn}'b}\right\}, \quad (4)$$

where the prime indicates that the co-modulus k' replaces the modulus k, and $Z(x)$ is the Jacobian zeta function.

The w–τ transformation

This transformation is more easily found by considering a further auxiliary variable t defined by $t = \mathrm{sn}\,\tau$. Since $\mathrm{sn}\,\tau$ is real all along the rectangle in the τ-plane, the t-plane is as in figure 6 (b).

Then, using the Schwartz–Christoffel theorem, we see that we require the following conditions for dw/dt:

(i) It should have a simple zero at t_H, t_B.

(ii) It should have a simple pole at t_E and a triple pole at t_A.

Thus we get

$$\frac{dw}{dt} = \frac{P(t-t_H)(t-t_B)}{(t-t_E)(t-t_A)^3},$$

or, in terms of τ,

$$\frac{dw}{d\tau} = \frac{P\,\mathrm{cn}\,\tau\,\mathrm{dn}\,\tau(\mathrm{sn}\,\tau - \mathrm{sn}\,\tau_H)(\mathrm{sn}\,\tau - \mathrm{sn}\,\tau_B)}{(\mathrm{sn}\,\tau - 1)(\mathrm{sn}\,\tau - \mathrm{sn}\,\tau_A)^3} \quad (5)$$

since $$\mathrm{sn}\,\tau_E = \mathrm{sn}\,K = 1.$$

The constant P determines the length scale in the problem, and it is in relation to this that we choose the scale in the w-plane so that $q_\infty = 1$.

Equation (5) may be integrated to give w as a function of τ. Also, since $\Omega = \log(dw/dz)$, equations (2) and (5) together yield an expression for $dz/d\tau$ which can again be integrated to give z as a function of τ. Thus we can determine w and z parametrically in terms of τ, and hence find the flow pattern. From these we can determine all the physical quantities required.

4. Determination of parameters

There are four parameters a, b, h and k in the problem. Equations (3) and (4) show that specifying the wedge semi-angle and the angle of yaw will provide two equations. The other two conditions to be imposed are the following:

(i) The lengths of the sides of the wedge must be in a predetermined ratio. In particular we shall consider a symmetrical wedge.

(ii) In general C will not lie on the continuation of DH. Ensuring that it does provides the fourth condition and makes the solution determinate.

Conditions (i) and (ii) can be expressed in the mathematical form

$$DD' = 0 + 2i|CD'|\sin\beta, \tag{6}$$

where DD' and CD' are conveniently calculated by integrating $dz/d\tau$ along the sides of the rectangle in the τ-plane. The real and imaginary parts of this equation, together with equations (3) and (4), provide the four equations necessary for determining the four parameters of the problem.

In general these quantities will have to be determined numerically, but in certain cases, and in particular when k is small, the calculations can be carried out analytically as far as first-order terms. Since it can be shown that small k combined with certain other assumptions corresponds to small angles of yaw, a situation of particular interest, we shall consider this case in more detail.

5. The limiting case of small angles of yaw: the flow pattern in the large

As the yaw tends to zero, it is reasonable to suppose that the flow pattern studied here will tend to the familiar symmetrical flow pattern. In other words, the effect of the existence of the secondary cavity on the main cavity should tend to zero as the yaw tends to zero. Similarly the secondary cavity must become so small that its detailed geometry is unaffected by the main cavity. Thus the two free-streamlines must tend to become independent of one another, or, interpreting this in the τ-plane, $K'/K \to \infty$ as the yaw tends to zero. From the theory of Jacobian elliptic functions, this implies that k tends to zero.

Now, writing $2\beta/\pi = \epsilon$, where $0 < \epsilon < 1$, equation (3) becomes

$$h + b = \epsilon K',$$

and, since $h, b \geqslant 0$,

$$h \leqslant \epsilon K', \qquad b \leqslant \epsilon K'. \tag{7}$$

Writing $\sigma = iK' - \tau$, we transform the two fundamental equations (1) and (5) into the form

$$\frac{d\Omega}{d\sigma} = -\frac{\operatorname{cn}\sigma_H \operatorname{ds}\sigma_H}{1 - \operatorname{ns}\sigma_H \operatorname{sn}\sigma} - \frac{\operatorname{cn}\sigma_B \operatorname{ds}\sigma_B}{1 - \operatorname{ns}\sigma_B \operatorname{sn}\sigma} - iN, \tag{8}$$

and

$$\frac{dw}{d\sigma} = \frac{Pk \operatorname{sn}^3\sigma_A \operatorname{cn}\sigma \operatorname{dn}\sigma (1 - \operatorname{ns}\sigma_H \operatorname{sn}\sigma)(1 - \operatorname{ns}\sigma_B \operatorname{sn}\sigma)}{(1 + k \operatorname{sn}\sigma)(\operatorname{sn}\sigma_A - \operatorname{sn}\sigma)^3}. \tag{9}$$

When $k \to 0$, and provided σ lies on or near DAD', the following relations hold:

$$\operatorname{sn}\sigma = \sin\sigma[1 + O(k^2)], \qquad \operatorname{cn}\sigma = \cos\sigma[1 + O(k^2)], \qquad \operatorname{dn}\sigma = 1 + O(k^2).$$

Moreover, it is easily shown from (7) that

$$\operatorname{ns}\sigma_B = O(k^n), \qquad \operatorname{ns}\sigma_H = O(k^n),$$
$$\operatorname{cn}\sigma_B \operatorname{ds}\sigma_B = -i + O(k^{2\epsilon}), \qquad \operatorname{cn}\sigma_H \operatorname{ds}\sigma_H = -i + O(k^{2\epsilon}),$$

where $$1 > n = 1 - \epsilon > 0.$$

Equations (8) and (9) therefore reduce to the form

$$d\Omega/d\sigma = M - i\mu \sin\sigma + O(k^\gamma), \tag{10}$$

and

$$\frac{dw}{d\sigma} = \frac{S\cos\sigma}{(\sin\sigma + \sin a)^3}[1 + \mu\sin\sigma + O(k^\gamma)], \tag{11}$$

where $$\mu = -\operatorname{ns}\sigma_H - \operatorname{ns}\sigma_B = O(k^n),$$

and M, S, γ are constants, γ being chosen as the smaller of the two quantities 1 or $2n$.

Integrating (10), and applying the conditions at D and D', we obtain

$$e^{-\Omega} = e^{-i\epsilon\sigma}[1 - i\mu\cos\sigma + O(k^\gamma)]. \tag{12}$$

Since $\exp(-\Omega) = dz/dw$, we find that

$$\frac{dz}{d\sigma} = S\frac{\cos\sigma}{(\sin\sigma + \sin a)^3} e^{-i\epsilon\sigma}[1 - i\mu e^{i\sigma} + O(k^\gamma)].$$

Hence

$$DD'[1 + O(k^\gamma)] = S\oint_{-\pi/2}^{\pi/2} \frac{\cos\sigma}{(\sin\sigma + \sin a)^3}[e^{-i\epsilon\sigma} - i\mu e^{i\mu\sigma}]\, d\sigma, \tag{13}$$

the path of integration being the straight line from $-\pi/2$ to $\pi/2$, indented on the positive side by a small semi-circle described about $\sigma = -a$.

From the condition (6), expressing the equality of the wedge faces, it follows that $Re(DD') = 0$. Applying this condition to (13), we find that

$$a = \mu/t(\epsilon) = O(k^n),$$

the derivation of this formula, and the definition of $t(\epsilon)$, being given in Appendix I. The function $t(\epsilon)$ varies monotonically from $4/(4-\pi) = 4{\cdot}660$ at $\epsilon = 0$ to $5{\cdot}000$ at $\epsilon = 1$ (as shown in table 1, § 6).

When this condition is satisfied we have

$$|DD'| = S\sin(\tfrac{1}{2}\epsilon\pi)F(\epsilon)[1 + O(k^\gamma)],$$

where $F(\epsilon) = 1 + \epsilon + \frac{1}{2}\epsilon^2[\psi(1-\epsilon/4) - \psi(1/2 - \epsilon/4)]$, $\psi(x)$ being the digamma function ($\psi(x) = (d/dx)\Gamma(x)$). In particular, $F(0) = 1$ and $F(1) = 2 + \pi/2$.

In order to determine the forces on the wedge, let us consider a circle in the σ-plane, given by $\sigma = -a + re^{i\eta}$ (r small). In the z-plane this corresponds to a large contour completely surrounding the wedge and enclosing most of the flow, as shown in figure 7.

Then, equating the forces acting on this contour to the rate of change of momentum inside it, we have

$$(X, Y) = \rho\int(\mathbf{n}\,.\,\mathbf{q})\mathbf{q}\,\mathrm{d}s - \int p\mathbf{n}\,\mathrm{d}s + \mathbf{R},$$

where (X, Y) is the force per unit length acting on the wedge, $\mathbf{n}$ is the unit vector along the outward normal to the contour, s measures arc length

along the contour, ρ is the density, p is the pressure, $\mathbf{q}$ is the velocity vector (u, v), and $\mathbf{R}$ is the contribution of the fluid in the re-entrant jet.

Referring to figure 7, we know that on QSP, $\mathbf{q} = 0$, $p = p_\infty$; and on PRQ, $\mathbf{q}$ is known, $p = p_\infty + \frac{1}{2}\rho(1-q^2)$. Hence

$$(X, Y) = \rho \int_\Lambda (\mathbf{n}\,.\,\mathbf{q})\mathbf{q}\, ds - \tfrac{1}{2}\rho \int_\Lambda (1-q^2)\mathbf{n}\, ds + \mathbf{R},$$

where Λ is the semicircle $\sigma = -a + re^{i\eta}$, $0 \leqslant \eta \leqslant \pi$.

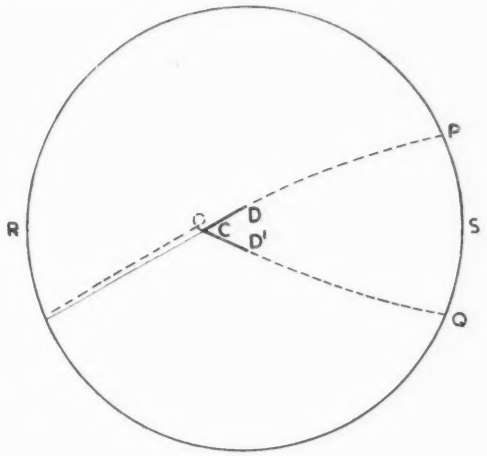

Figure 7.

Since the left-hand side of this equation is independent of r, so also is the right-hand side. Thus, on letting r tend to zero, we find

$$X = \tfrac{1}{2}\epsilon^2\pi S\rho + R_1 + O(a^2),$$

and

$$Y = \tfrac{1}{2}a\pi\rho S[-t + \epsilon(2t-1) - \epsilon^2 t + \epsilon^3] + R_2 + O(a^2),$$

where R_1 and R_2 are the components of $\mathbf{R}$.

From (12) we find, on putting $\sigma = -a$, that the angle of incidence α is given by

$$\alpha = a\{\epsilon - t\} + O(a^2).$$

Hence the drag force D and the lift force L per unit length are given by

$$D = X + O(\alpha^2) = \tfrac{1}{2}\epsilon^2\pi\rho S + R_1 + O(\alpha^2),$$

and

$$L = Y - X\alpha + O(\alpha^2) = \tfrac{1}{2}a\pi\rho S[-t + \epsilon(2t-1)] + R_2 - \alpha R_1 + O(\alpha^2).$$

In a similar manner we can find the pitching moment M per unit length, measured about the mid-point of the base of the wedge, and reckoned as positive for a destabilizing moment. Using the formula

$$M = \int p(x\, dx + y\, dy) - \rho \int (vx - uy)(u\, dx - v\, dy),$$

we find that

$$M = -\tfrac{1}{2}\rho\pi a S^2 p(\epsilon) + R_3 + O(\alpha^2) \tag{14}$$

where R_3 represents the term due to the re-entrant jet, and the function $p(\epsilon)$ is explained in Appendix III. In particular we have

$$p(0) = 3/(8-2\pi), \qquad \text{and } p(1) = -3/2.$$

The terms R_1, R_2 and R_3, representing the effect of the re-entrant jet, must be small if our mathematical model is to be physically realistic. In the next section we shall prove that they do, in fact, become negligible compared with the other terms in D, L and M as α tends to zero.

6. The flow pattern in the neighbourhood of the vertex and its effect on the forces acting on the wedge

The analysis of the preceding section was effected without making any assumptions regarding the behaviour of b and h as k tends to zero, apart from the restriction given in equation (7). It is now necessary to examine their behaviour in more detail, and it is clear that three possibilities arise:

(i) b and h both tend to infinity;

(ii) b remains finite; or

(iii) h remains finite.

The correct choice is governed by the fact that we have yet to satisfy the condition imposed by the imaginary part of equation (6), representing the fact that C must be collinear with D and H. (The real part of this equation has already been satisfied by the condition $\mu = a\,t(\epsilon)$ in the previous section.)

Since the analysis differs in detail for the three different possibilities, we shall reproduce here only that corresponding to case (iii) above, since, as we shall show, this is the case that enables equation (6) to be satisfied.

In this case it follows from (3) that $b/K' \to \epsilon$, and hence

$$\operatorname{ns}\tau_B \sim \operatorname{nc}\tau_B = O(k^{\epsilon}), \qquad \text{and } \operatorname{dn}\tau_B = 1 + O(k^{2n}).$$

Then on or near CE it can be shown, from (1), that

$$\frac{d\Omega}{d\tau} = \frac{\cos\tau_H}{\sin\tau - \sin\tau_H} + iZ + O(k^{\epsilon}),$$

where Z is a real constant.

Integrating, and applying the conditions at C and E, we find

$$e^{-\Omega} = -i\frac{\cos\frac{1}{2}(\tau+\tau_H)}{\sin\frac{1}{2}(\tau-\tau_H)}\, e^{-in\tau}[1+O(k^{\epsilon})].$$

Similarly, from (5),

$$\frac{dw}{d\tau} = +\frac{4^{\epsilon}Sk^{1+n}\cos\tau(\sin\tau-\sin\tau_H)}{2(\sin\tau-1)}\,[1+O(k^{\epsilon})].$$

Hence

$$\frac{dz}{d\tau} = +i4^{\epsilon}\frac{Sk^{1+n}}{2}\, e^{-in\tau}\,\frac{1+\sin\tau}{\cos\tau}\,[1+\cos(\tau+\tau_H)][1+O(k^{\epsilon})]. \tag{15}$$

Now the imaginary part of equation (6), implying the collinearity of C, D and H, may be replaced by the following condition:

$$Im\left\{\overrightarrow{CE}e^{-i\beta}\right\} = g, \tag{16}$$

where E is the point at infinity on the free-streamline of the re-entrant jet, and g is the width of the re-entrant jet at infinity.

But g may be readily evaluated by studying the behaviour of equation (15) in the neighbourhood of $\tau = K = \pi/2 + O(k^2)$; thus

$$g = \tfrac{1}{2} S k^{1+n} \pi [1 + \sin \tau_H][1 + O(k^6)]. \tag{17}$$

Substituting in (15), our condition becomes

$$\pi[\cosh h - 1][1 + O(k^6)] = \int_0^{\pi} (1 + \cos t)(\sin t)^{-1}(\sin nt - \\ - \cosh h \cos t \sin nt - \sinh h \sin t \cos nt)\, dt, \tag{18}$$

where we have written $\tau = \pi/2 - t$.

In Appendix II this equation is solved explicitly and then, using equation (15), the dimensions of the subsidiary bubble are calculated. However, as we shall now show, the effect of the value of h on the forces is negligible.

Equation (17) gives the value of g and it is obvious without actual evaluation that the values of R_1 and R_2 will both be equal to multiples of g, the multipliers being of order unity as α tends to zero. However, g itself is of order $\alpha^{1+1/n}$, so that we have

$$D = \tfrac{1}{2} \epsilon^2 \pi \rho S + O(\alpha^2), \tag{19}$$

$$L = \tfrac{1}{2} a \pi \rho S[-t + \epsilon(2t - 1)] + O(\alpha^2), \tag{20}$$

$$M = -\tfrac{1}{2} a \rho \pi S^2 p(\epsilon) + O(\alpha^2). \tag{21}$$

We now define a drag coefficient and lift and pitching moment slope coefficients, using the dynamic head as the reference pressure and the combined length of the wedge faces $c = |DD'| \operatorname{cosec} \beta$ as the reference length. An asterisk will be used to distinguish these coefficients from those which would be obtained by taking $|DD'|$ itself as the reference length. The advantage in taking c as reference length is that all these coefficients tend to finite limits as ϵ tends to zero.

Using an obvious notation, we obtain

$$C_D^* = \frac{D}{\tfrac{1}{2} \rho q_\infty^2 c} = \frac{\epsilon^2 \pi}{F(\epsilon)} + O(\alpha^2), \tag{19'}$$

$$\left[\frac{\partial C_L^*}{\partial \alpha}\right]_{\alpha = 0} = \lim_{\alpha \to 0} \left[\frac{L}{\tfrac{1}{2} \rho q_\infty^2 \alpha c}\right] = \frac{\pi[-t + \epsilon(2t - 1)]}{(\epsilon - t) F(\epsilon)}, \tag{20'}$$

$$\left[\frac{\partial C_M^*}{\partial \alpha}\right]_{\alpha = 0} = \lim_{\alpha \to 0} \left[\frac{M}{\tfrac{1}{2} \rho q_\infty^2 \alpha c^2}\right] = \frac{-\pi p(\epsilon)}{(\epsilon - t) F^2(\epsilon)}. \tag{21'}$$

It is interesting to compare these formulae with known limiting values as α tends to zero and as β tends to zero or $\pi/2$, bearing in mind, however, that the foregoing analysis is not strictly valid when β equals zero or $\pi/2$

For the case α equals zero (19′) agrees with the formula given by Perry (1952), while (20) and (21) give zero values for L and M as would be expected.

When ϵ tends to unity, corresponding to a flat plate nearly perpendicular to the stream, (20′) agrees with the value given by Milne-Thomson (1949), and (21′) with that given by Lamb (1932).

When ϵ tends to zero, corresponding to a flat plate nearly parallel to the stream, we find that (20′) gives a value π and (21′) a value $3\pi/8$. These do not agree with the classical values for cavitating flat plates, but this is to be expected since even in the limiting case both sides of the wedge are wetted. A more reasonable comparison is with a flat plate at incidence in fully wetted flow, with circulation chosen using the Joukowsky hypothesis of a finite velocity at the trailing edge. In this case Ramsey (1947) gives the value π for $[\partial C_L^*/\partial\alpha]_{\chi=0}$ and $3\pi/8$ for $[\partial C_M^*/\partial\alpha]_{\chi=0}$, so that again agreement is secured with classical theory.

Table 1 gives values of C_D^*, $[\partial C_L^*/\partial\alpha]_{\chi=0}$ and $[\partial C_M^*/\partial\alpha]_{\chi=0}$ and they are plotted in figures 8 and 9 respectively.

ϵ	$t(\epsilon)$	C_D^*	$\left[\frac{\partial C_L^*}{\partial\alpha}\right]_{\chi=0}$	$\left[\frac{\partial C_M^*}{\partial\alpha}\right]_{\chi=0}$
0	4·660	0	3·142	1·178
0·2	4·721	0·102	1·711	0·553
0·4	4·785	0·325	0·629	0·1 7
0·6	4·853	0·571	−0·138	−0·053
0·8	4·924	0·770	−0·628	−0·110
1·0	5·000	0·880	−0·880	−0·092

Table 1.

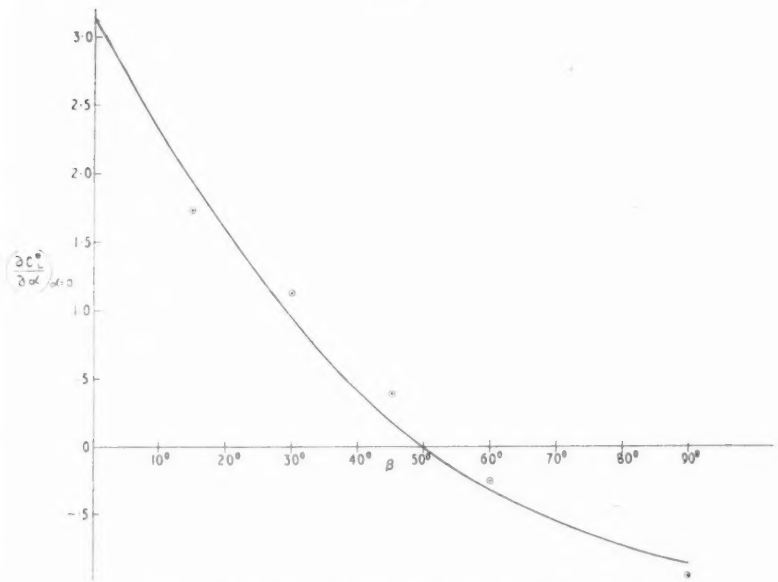

Figure 8. Modified lift slope coefficient as a function of β.

7. Experimental method

As a result of the foregoing theoretical study of cavitating flow about a wedge at incidence, experimental data were needed to verify the assumption

made concerning the existence of the subsidiary cavity formed on the upper face of the wedge, and also to measure the hydrodynamic forces acting on the wedge. These data were obtained in the A.R.D.E. cavitation tunnel (see Clayden 1954).

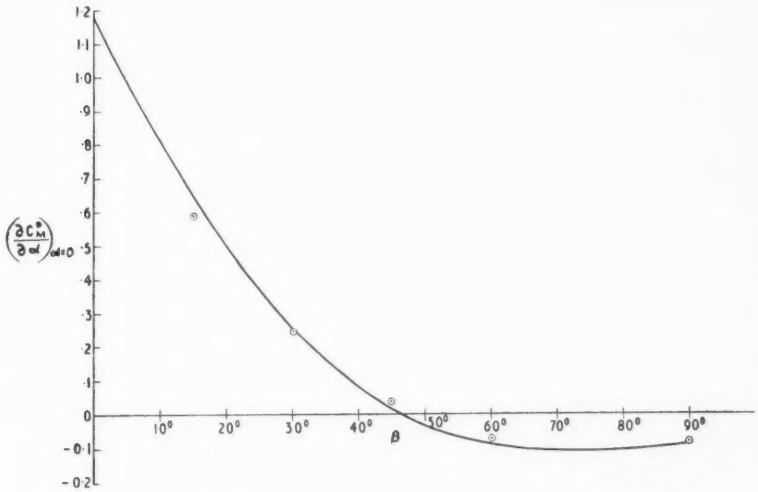

Figure 9. Modified moment slope coefficient as a function of β.

This tunnel is a re-circulating type with a rectangular 9×7 in. free jet working section with fixed vertical side walls and free top and bottom surfaces. The working section speed is nominally constant at 40 ft./sec, and the cavitation number is varied by varying the pressure. Very low cavitation numbers ($\sim 0{\cdot}01$) may be obtained in this manner. The basic instrumentation consists of the following:

(1) a horizontal beam manometer to measure the pressure across the contraction nozzle, which is used as a Venturi meter;

(2) a tilting dead weight manometer to measure the difference between the ambient and cavity pressure;

(3) a tilting dead weight manometer to measure the ambient pressure in the working section. This instrument is also used to operate a servo-mechanism to control the tunnel pressure in the range 1 atmosphere to 10 mm of mercury;

(4) a thermocouple thermometer; and

(5) a mechanical three-moment balance.

(The first four instruments give continuous recordings.)

The 30° semi-angle wedge shown in figure 1 (plate 1) was originally used to obtain design data for struts and model supports. It completely spanned the tunnel, but was attached only to the rear boundary wall of the working section. It was used to obtain photographs of the flow pattern, in preference to the family of wedges used to obtain force data, because it permitted an uninterrupted view.

The size of the models used to obtain the force data were as follows: for the wedge semi-angle $\beta = 15°$, the width of the base of the wedge was 0·5 in.; for $\beta = 30°$, 45°, 60° and 90°, the width of the base was 0·3 in. To obtain the force measurements, the wedges were pivoted on the front boundary of the free jet and were attached to the three-moment balance by a universal joint (figure 10). The three-moment balance was mounted on the back of the working section. (A more detailed description of the experimental rig was given by Clayden (1957).) A pressure tap was fitted in the boundary wall of the working section to measure the cavity pressure directly, since the cavity pressure is normally higher than the vapour pressure, due to a small quantity of air leaking through from the balance.

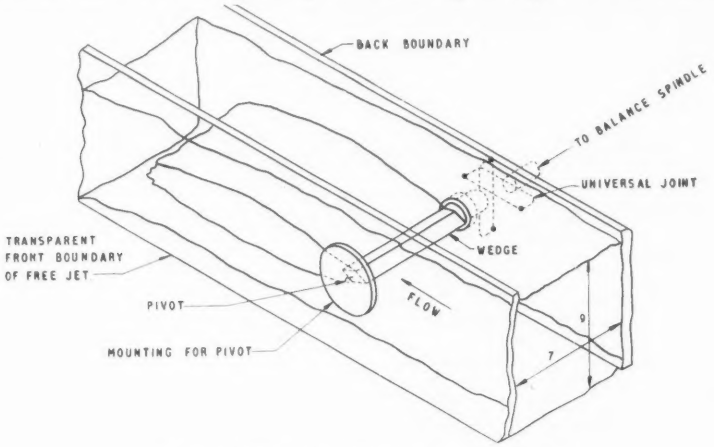

Figure 10. Test rig. Dimensions in inches.

For a typical series of tests the cavitation number was held constant whilst the balance was rotated from $-15°$ to $+15°$ with the horizontal, readings of the three moments being taken at intervals of 3°. Since the angle the free jet makes with the model is not precisely known, the position of zero incidence was determined as the position at which the measured lift force changed sign.

Although the tunnel is capable of achieving a cavitation number as low as 0·01, the lower limit in these tests was determined by the length of the cavity, which for the lowest cavitation numbers extended throughout the length of the working section.

8. Results

Observations and photographs of the flow about a yawed wedge indicated that the mathematical model, illustrated in figure 3, closely resembled a time average of the actual physical flow (figure 1, plate 1). The subsidiary cavity, however, oscillated considerably with a high frequency (a similar cyclic process has been observed and studied by Knapp (1956) for flow along a cylinder with a cavitating head). As the angle of yaw of the wedge

is increased so the subsidiary cavity becomes larger until it finally breaks away leaving the leeward face completely unwetted. The angle at which this occurs has been studied by Clayden (1957) for a family of wedges of varying vertex angles. The force measurements given in this paper are for small angles of incidence with the leeward face at least partially wetted (figure 3).

β	σ	C_{D0}	d	$\frac{\partial C_L}{\partial \alpha}$	$\frac{\partial C_M}{\partial \alpha}$
15°	0·067	0·291	0·00742	0·128	0·157
	0·096	0·300		0·126	0·163
	0·119	0·296		0·124	0·159
	0·170	0·345		0·130	0·163
	0·230	0·361		0·141	0·172
30°	0·059	0·517		0·0423	0·0182
	0·073	0·523	−0·000305	0·0389	0·0172
	0·112	0·536		0·0436	0·0192
	0·134	0·548		0·0435	0·0198
	0·183	0·590		0·0438	0·0198
	0·206	0·608		0·0431	0·0188
45°	0·081	0·681	−0·000342	0·0105	0·00180
	0·116	0·709		0·0097	0·00150
	0·149	0·727		0·0098	0·00212
	0·180	0·755		0·0088	0·00180
	0·260	0·794		0·0097	0·00242
60°	0·116	0·843	−0·00032	−0·00501	−0·00185
	0·122	0·864		−0·00523	−0·00214
	0·164	0·890		−0·00517	−0·00248
	0·210	0·885		−0·00578	−0·00302
	0·268	0·942		−0·00488	−0·00240
90°	0·104	0·945	−0·000170	−0·0171	−0·00214
	0·130	0·974		−0·0174	−0·00166
	0·145	0·991		−0·0170	−0·00148
	0·180	1·025		−0·0171	−0·00165
	0·220	1·056		−0·0168	−0·00231

Table 2.

The force measurements obtained from the three-moment balance were analysed to give C_D, C_L and C_M, the drag, lift and moment coefficients respectively. These results were fitted by the method of least squares to give the following relations for each combination of vertex angle and cavitation number:

$$C_L = (\partial C_L/\partial\alpha)\alpha, \qquad C_M = (\partial C_M/\partial\alpha)\alpha,$$
$$C_D = C_{D0}(1 + d\alpha^2) \qquad (d \text{ constant for a given vertex angle}),$$

where

$C_L = L/\frac{1}{2}\rho q_\infty^2 W$, $C_D = D/\frac{1}{2}\rho q_\infty^2 W$, $C_M = M/\frac{1}{2}\rho q_\infty^2 W^2$, $C_{D0} = C_D$ for $\alpha = 0$.

The results obtained for $\partial C_L/\partial\alpha$, $\partial C_M/\partial\alpha$, C_{D0} and d are tabulated in table 2.

These results are plotted in figures 11, 12 and 13. The values of C_{D0} are compared with theoretical values given by Perry (1952) in figure 11. In order to compare the experimental values of the lift slope coefficient $\partial C_L/\partial\alpha$,

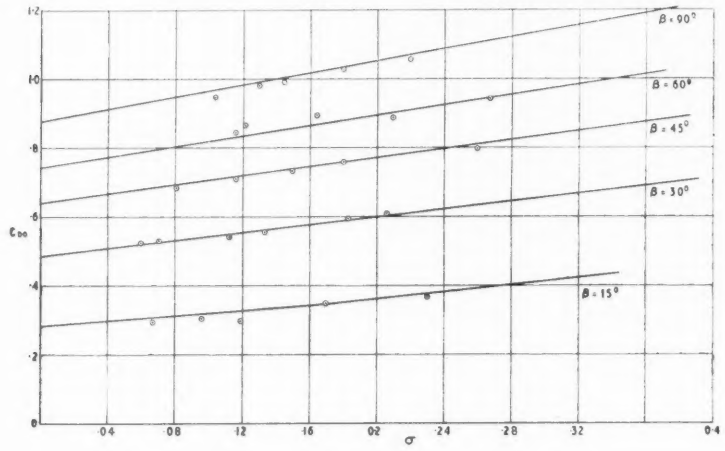

Figure 11. Measured drag coefficient as a function of σ.

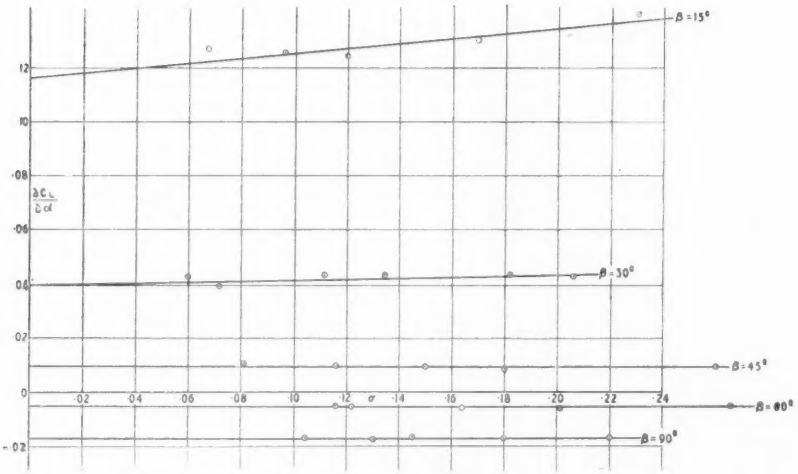

Figure 12. Measured lift slope coefficient as a function of σ.

with the theory developed in this paper, the results are extrapolated to give $(\partial C_L/\partial\alpha)$ for $\sigma = 0$. For values of $\beta = 90°$, $60°$ and $45°$, there does not appear to be any dependence on cavitation number and accordingly the

results are averaged. For $\beta = 30°$ and $15°$, however, there is a significant increase of $\partial C_L/\partial\alpha$ with the cavitation number σ, and a least squares fit is used to obtain $(\partial C_L/\partial\alpha)_{\sigma=0}$. The results for the moment coefficient are all fitted with a least squares fit to give $(\partial C_M/\partial\alpha)_{\sigma=0}$. The values of $(\partial C_L^*/\partial\alpha)_{\sigma=0}$ and $(\partial C_M^*/\partial\alpha)_{\sigma=0}$ are compared with theory in figures 8 and 9. These results are tabulated in table 3.

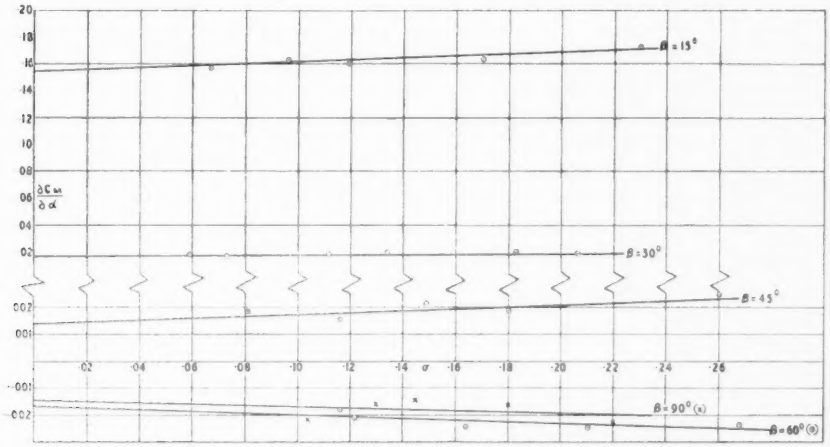

Figure 13. Measured moment slope coefficient as a function of σ.

β	$\dfrac{\partial C_L}{\partial\alpha}$	$\dfrac{\partial C_M}{\partial\alpha}$	$\left[\dfrac{\partial C_L^*}{\partial\alpha}\right]_{\sigma=0}$	$\left[\dfrac{\partial C_M^*}{\partial\alpha}\right]_{\sigma=0}$
15°	$0{\cdot}116+0{\cdot}093\sigma$	$0{\cdot}154+0{\cdot}085\sigma$	1·72	0·582
30°	$0{\cdot}0398+0{\cdot}0192\sigma$	$0{\cdot}0174+0{\cdot}0112\sigma$	1·14	0·248
45°	0·0097	$0{\cdot}00133+0{\cdot}0038\sigma$	0·392	0·038
60°	−0·0052	$-(0{\cdot}00165+0{\cdot}0030\sigma)$	−0·258	−0·071
90°	−0·0171	$-(0{\cdot}00148+0{\cdot}0023\sigma)$	−0·98	−0·085

Table 3.

9. Discussion of results

The drag results for zero incidence plotted in figure 11 show good agreement with theory. No theory is presently available for the dependence of the drag on the angle of incidence except for the case of a flat plate at zero cavitation number, when for a flat plate almost normal to the stream

the drag coefficient may be expressed as $C_D = C_{D0}(1 - 0{\cdot}000238\alpha^2)$ compared with an experimental value of $C_D = C_{D0}(1 - 0{\cdot}000171\alpha^2)$ for α in the range 0–15°.

Since the lift coefficient of a flat plate nearly normal to the stream may be expressed as $C_D \tan\alpha$ (neglecting skin friction), and as C_D behaves as $1+\sigma$, it would seem reasonable to suppose that the lift coefficient would behave in a similar manner. However, the experimental results do not show this trend, and the reason for this discrepancy is not yet apparent. The extrapolated values of the lift slope coefficient have been plotted in figure 8 for comparison with theory when it will be seen that agreement is fair, part of the difference between theory and experiment being accounted for by the fact that insufficient results were obtained to achieve great accuracy in the extrapolated values.

The values of the moment slope coefficient plotted in figure 9 show good agreement with theory. In particular, the negative moment for β greater than 45° is confirmed.

10. Conclusions

The analysis, for small angles of yaw, of the model described in § 2, has been shown to lead to a drag coefficient which differs only by second-order terms in the yaw from that given by the classical solution for a non-yawed wedge, and to lift and moment coefficients which have not previously been calculated, except for a flat plate, where agreement is again secured.

The experiments demonstrated the existence of a subsidiary cavity at the vertex which appeared to be of a cyclic nature, alternately filling with water, breaking away from the vertex, and reforming again. However, the steady state model described will give a first approximation to the time average of the forces, the quantities that were measured in the experiments.

The experiments could not be undertaken at zero cavitation number, but the extrapolated value of the lift slope and moment slope coefficients show reasonable agreement with theory developed in this paper. Good agreement between theory and experiment for the drag coefficient at zero incidence is also secured and experiments confirm the theoretical prediction that the drag for small angles of incidence differs only by small second-order terms in the angle of incidence from the drag at zero incidence.

Since the predictions of this theory are so well in accord with experiment, the theory has since been extended to cover the case of non-zero cavitation number (Cox 1957).

The authors wish to express their thanks to Mr A. H. Armstrong for his guidance and assistance and to Miss K. M. Stocks and her staff for carrying out the numerical work.

(Crown copyright reserved. Reproduced with the permission of the Controller, H.M.S.O.)

Appendix I

The evaluation of the integral I occurring in equation (13)

Expanding in powers of a by Taylor's theorem, and assuming that μ is of the same order of magnitude as a, we find that

$$I = i\sin(\tfrac{1}{2}\epsilon\pi)[1+\epsilon+\tfrac{1}{2}\epsilon^2\{\psi(1-\tfrac{1}{4}\epsilon)-\psi(\tfrac{1}{2}-\tfrac{1}{4}\epsilon)\}] + \\ +[-3aL_1+\mu L_2+3aL_3+\mu L_4]+O(a^2),$$

where $\psi(x) = (d/dx)\log\Gamma(x)$,

$$L_1 = \oint_{-\pi/2}^{\pi/2} \cos\sigma\cos\epsilon\sigma\sin^{-4}\sigma\, d\sigma,$$

$$L_2 = \oint_{-\pi/2}^{\pi/2} \cos\sigma\sin(1-\epsilon)\sigma\sin^{-3}\sigma\, d\sigma,$$

$$L_3 = \epsilon(1-\epsilon^2)\pi/6,$$

$$L_4 = (1-\epsilon)^2\pi/2.$$

By integrating L_2 twice by parts, we find that

$$L_2 = -\cos(\tfrac{1}{2}\epsilon\pi)-\tfrac{1}{4}(1-\epsilon)^2[I_{2-\epsilon}-I_\epsilon],$$

where

$$I_n = \int_{-\pi/2}^{\pi/2} \sin n\theta(\sin\theta)^{-1}\, d\theta,$$

$$= -\cos(\tfrac{1}{2}n\pi)[G(n)-G(-n)],$$

with $G(n) = \tfrac{1}{2}[\psi(\tfrac{1}{4}-\tfrac{1}{4}n)-\psi(\tfrac{3}{4}-\tfrac{1}{4}n)]$.

Thus we see that

$$L_2 = -\tfrac{1}{2}(1-\epsilon)^2\pi-\cos(\tfrac{1}{2}\epsilon\pi)[2-\epsilon+(1-\epsilon)^2G(\epsilon)].$$

Similarly, integrating L_1 twice by parts, we find that

$$L_1 = -\tfrac{2}{3}\cos(\tfrac{1}{2}\epsilon\pi)+\tfrac{1}{3}\epsilon L_2-\tfrac{1}{6}\epsilon(1-\epsilon)[I_\epsilon-I_{2-\epsilon}],$$

so that

$$L_1 = \epsilon(1-\epsilon^2)\pi/6-\tfrac{1}{3}\cos(\tfrac{1}{2}\epsilon\pi)[2-\epsilon^2-\epsilon(1-\epsilon^2)G(\epsilon)].$$

Thus, on applying condition (6), we find that

$$\mu = at(\epsilon),$$

where

$$t(\epsilon) = \frac{2-\epsilon^2-\epsilon(1-\epsilon^2)G(\epsilon)}{2-\epsilon+(1-\epsilon)^2G(\epsilon)}.$$

This result is consistent with our original assumption that μ and a are of the same order of magnitude.

Appendix II

(*a*) *The calculation of* $h = h(n)$

We have, from equation (18),

$$\pi[\cosh h-1] = J_1(n)-\cosh h\,J_2(n)-\sinh h\,J_3(n), \qquad \text{(II.1)}$$

where

$$J_1(n) = \int_0^\pi \frac{1+\cos t}{\sin t}\sin nt\, dt, \qquad J_2(n) = \int_0^\pi \frac{1+\cos t}{\sin t}\sin nt\cos t\, dt,$$

and

$$J_3(n) = \int_0^\pi \frac{1+\cos t}{\sin t}\cos nt\sin t\, dt.$$

The substitution $t = 2\mu$ leads immediately to

$$J_1(n) = \tfrac{1}{2}[I_{2n+1} + I_{2n-1}],$$

in the notation of Appendix I, and hence

$$J_2(n) + J_3(n) = J_1(n+1) = \tfrac{1}{2}[I_{2n+3} + I_{2n+1}],$$
$$J_2(n) - J_3(n) = J_1(n-1) = \tfrac{1}{2}[I_{2n-1} + I_{2n-3}].$$

Solving equation (II.1) for e^h, we find the values given in table 4.

(*b*) *The dimensions of the subsidiary cavity*

We have, from equation (15), on writing $2^{2\epsilon-2}Sk^{1+n}Z = ze^{-i\beta}$ and $\tau = \pi/2 - t$,

$$\frac{dZ}{dt} = -\frac{1+\cos t}{\sin t}\, e^{int}\,[1 - \cos(t - ih)].$$

If we write $Z = X + iY$, then X is the variable along the top face of the wedge and Y the variable perpendicular to it.

Then the maximum value Y_m of Y is the dimension of the subsidiary cavity perpendicular to the top face of the wedge, and is given by

$$Y_m = -\int_{\pi}^{t_m} \frac{1+\cos t}{\sin t}\,[\sin nt\,(1 - \cos t \cosh h) - \cos nt \sin t \sinh h]\, dt,$$

where t_m is the value of t where the expression in square brackets vanishes.

The variable X has, for $n > \frac{1}{2}$, two turning points X_1 and X_2 and the dimension of the cavity along the top wedge face is $|X_1 - X_2|$; while, for $n < \frac{1}{2}$, there is one turning point X_3, the dimension of the cavity then being X_3. It is seen that X_1, X_2, and X_3 are given by

$$X_1, X_2, X_3 = -\int_{\pi}^{t_1, t_2, t_3} \frac{1+\cos t}{\sin t}\,[\cos nt\,(1 - \cos t \cosh h) + \sin nt \sin t \sinh h]\, dt,$$

the appropriate value of t being taken as the upper limit.

Numerically we find the values in table 4.

n	e^{ih}	Y_m	$\lvert X_1 - X_2\rvert$	X_3
0	1·00000	0	—	2·000
0·2	1·19825	0·343	—	1·925
0·4	1·38439	0·693	—	1·767
0·6	1·54252	1·004	1·526	—
0·8	1·65503	1·221	1·296	—
1·0	1·70711	1·298	1·106	—

Table 4.

Appendix III

The function $p(\epsilon)$ occurring in equation (14) is defined by

$$p(\epsilon) = p_1(\epsilon) + t(\epsilon)p_2(\epsilon),$$

where

$$p_1(\epsilon) = -5\epsilon/24 - \epsilon^3/4 - \epsilon^5/6 + 3\epsilon^2 d_3(\epsilon) + \epsilon(1-\epsilon^2)a_3(\epsilon)$$
$$p_2(\epsilon) = 1/24 + \epsilon/6 - 3\epsilon^2/4 + \epsilon^3/2 - \epsilon^2 a_3(1-\epsilon) + (1-\epsilon)^2 a_3(\epsilon),$$

wherein

$$a_3(\lambda) = \tfrac{1}{3} + \int_{-\pi/2}^{0} \frac{\cos\sigma[\cos\lambda\sigma - 1 + \tfrac{1}{2}\lambda^2\sin^2\sigma]}{\sin^3\sigma}\, d\sigma$$

and

$$d_3(\lambda) = \lambda/3 + \int_{-\pi/2}^{0} \frac{\cos\sigma[\sin\lambda\sigma - \lambda\sin\sigma - \tfrac{1}{3}\lambda\{1-\lambda^2\}\sin^3\sigma]}{\sin^4\sigma} d\sigma.$$

Computed values of $a_3(\epsilon)$, $a_3(1-\epsilon)$ and $d_3(\epsilon)$ are given in table 5.

ϵ	$a_3(\epsilon)$	$a_3(1-\epsilon)$	$d_3(\epsilon)$
0·0	0·3333	0·4299	0·0000
0·2	0·3386	0·4034	0·0544
0·4	0·3537	0·3764	0·1122
0·6	0·3764	0·3537	0·1766
0·8	0·4034	0·3386	0·2498
1·0	0·4299	0·3333	0·3333

Table 5.

References

Clayden, W. A. 1954 *Unpublished Ministry of Supply Report.*

Clayden, W. A. 1957 *Unpublished Ministry of Supply Report.*

Cox, A. D. 1957 *Unpublished Ministry of Supply Report.*

Gilbarg, D. & Rock, D. H. 1946 On two theories of plane potential flow with finite cavities, *U.S. Naval Ordnance Lab. Mem.* no. 8718.

Jahnke, E. & Emde, F. 1948 *Tables of Functions*, 4th (rev.) Ed. Leipzig: Teubner.

Knapp, R. T. 1956 Further studies of the mechanics and damage potential of fixed type cavities, *Proc. Symposium on Cavitation in Hydrodynamics.* London: H.M.S.O.

Kreisel, G. 1946 Cavitation with finite cavitation number, *Admiralty Research Lab. Rep. U.B.R.C.* 52.

Lamb, H. 1932 *Hydrodynamics*, 6th Ed. Cambridge University Press.

Milne-Thomson, L. M. 1949 *Theoretical Hydrodynamics*, 2nd Ed. London: Macmillan.

Milne-Thomson, L. M. 1950 *Jacobian Elliptic Function Tables.* New York: Dover.

Neville, E. H. 1951 *Jacobian Elliptic Functions*, 2nd Ed. Oxford University Press.

Perry, B. 1952 Evaluation of the integrals occurring in the cavity theory of Plesset and Shaffer, *Cal. Inst. Tech. Hydrodynamics Lab. Rep.* no. 21–11.

Ramsey, A. S. 1947 *A Treatise on Hydromechanics*, Part II. London: Bell.

Shiffman, M. 1949 On free boundaries of an ideal fluid, Part II, *Comm. Pure Appl. Math.* **2**, 1.

Whittaker, E. T. & Watson, G. N. 1940 *A Course of Modern Analysis*, 4th Ed. Cambridge University Press.

A discussion of higher-order approximations for the flow field about a slender elliptic cone

By ROBERTO VAGLIO-LAURIN
Polytechnic Institute of Brooklyn, New York

and M. D. VAN DYKE
Ames Aeronautical Laboratory, National Advisory Committee for Aeronautics, Moffett Field, California

(*Received* 1 *November* 1957)

SUMMARY

A comparison is made between various methods for the calculation of the pressure distribution on an elliptic cone in supersonic flow. In particular, a criterion first put forward by Van Dyke (1956) is reconsidered. The paper is presented in two parts under separate authorship, taking the form of a discussion of some controversial aspects of this subject.

PART I. (By R. V.-L.)

In a recent paper Van Dyke (1956) derived the second-order slender-body solution for an unyawed elliptic cone in supersonic flow. Considering his results to be exact, he used them as a criterion for comparing various approximations in compressible flow theory. Among these the method of linearized characteristics (Ferri 1951) was discussed, in particular, its application to the analysis of the flow field about non-circular cones. This method in general proceeds by linearizing the departure between the flow field of interest and some known non-uniform flow close to the actual one; along these lines Ferri treated the particular problem mentioned above by superposing perturbations on the axisymmetric solution, the disturbance velocity components being expanded in Fourier series in the polar angle θ up to the tenth term. With this approach the entire flow field and the shock wave can be determined over a wide range of Mach numbers, in contrast to orthodox methods of linearization.

Van Dyke based his appraisal of Ferri's approximation on the two following numerical comparisons instituted for an elliptic cone of 3 : 1 axis ratio and area equivalent to a 10° circular cone, at $M = \sqrt{2}$:

(1) The law expressing the slender-body pressure distribution was expanded in a Fourier series, and the error introduced by termination of this series at $\cos 10\theta$ was evaluated.

(2) An approximation to the second-order slender-body solution was developed following Ferri's procedure of expanding the velocity components in a Fourier series in θ, while linearizing with respect to deviation of the cross-section from circular, and calculating pressure coefficients from the full relation; the resulting pressures were compared with the exact values.

Van Dyke suggested that the large discrepancies between his complete and approximate results gave a measure of the errors to be encountered in Ferri's method, supposedly due to termination of the series at $\cos 10\theta$ and to linearization of the boundary conditions. Since good accuracy is to be expected from the second-order slender-body theory for the example in question, and since Ferri (1951) reported good agreement with experiments for a similar case, it seemed interesting to ascertain the origin of these discrepancies. The matter has been the subject of private communications with Dr Van Dyke, who has provided many interesting comments and much information; these are gratefully acknowledged.

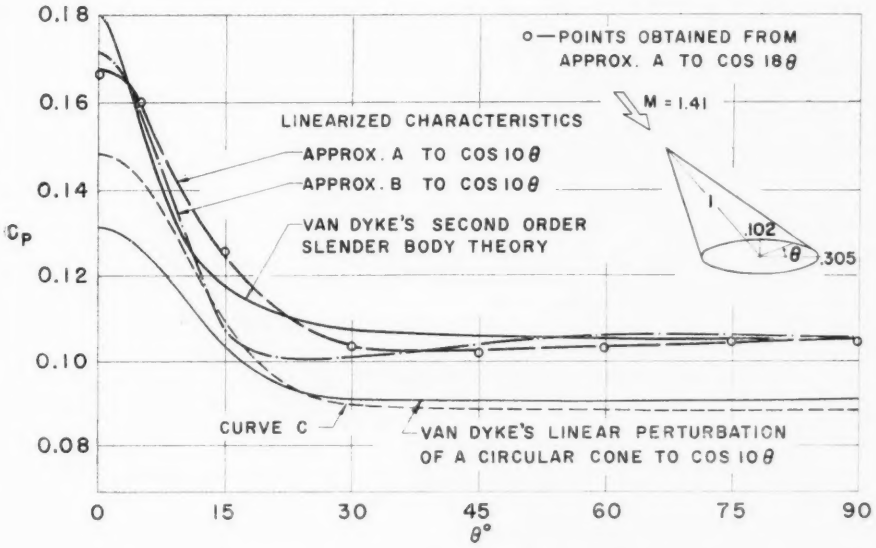

Figure 1. Comparison between various approximations to the pressure distribution around an elliptic cone.

It is shown in the present note that satisfactory results can be obtained from the method of linearized characteristics, even when only linear terms are retained in the boundary conditions, provided that an area rule requirement is satisfied. The pressure distribution predicted by this procedure for the aforementioned elliptic cone at $M = \sqrt{2}$ compares favourably with the second-order results (see figure 1); moreover, the experimental data presented in figure 3 of Van Dyke's paper indicate that the actual values in the region of small θ ($\tan\theta = b/a \tan\eta$ in the notation of his paper) should fall between the two predictions. Thus both analyses exhibit approximately the same accuracy at the surface of the body, even though the particular example (a slender body at fairly low Mach number) represents an unfavourable test for Ferri's method. It is also pertinent to

observe that Van Dyke's solution is not uniformly valid throughout the flow field and fails at the shock, where conversely the accuracy of the linearized characteristics method is best since the perturbations there are smallest.

The area-rule requirement for the expansion of the boundary conditions is justified by the following considerations. If, following Ferri, the shape of the body cross-section is expressed in polar coordinates (r, ψ, θ) as the Fourier series

$$\psi_b = \psi_{0b} + \sum_{n=1}^{\infty} \psi_{nb} \cos n\theta \tag{1}$$

with only linear terms retained in ψ_{nb}, and if ψ_{0b} refers to the basic circular cone, the velocity components at the surface of the actual body are given by

$$\left.\begin{aligned} v_r &= (v_{r0})_{\psi_{0b}} \left[1 + 2 \sum_{n=1}^{\infty} \psi_{nb} \left(\frac{v_{rn}}{v_{nn}} \right)_{\psi_{0b}} \cos n\theta \right], \\ v_v &= 0, \\ w &= 2(v_{r0})_{\psi_{0b}} \sum_{n=1}^{\infty} n\psi_{nb} \left(\frac{w_n}{v_{nn}} \right)_{\psi_{0b}} \sin n\theta. \end{aligned}\right\} \tag{2}$$

In the notation used by Ward (1955) the boundary conditions are

$$\frac{v_\nu}{v_z} = \frac{d\nu}{dz} \quad \text{or} \quad \int_C \frac{v_\nu}{v_z}\, d\tau = \int_C \frac{d\nu}{dz}\, d\tau = S'(z), \tag{3}$$

where ν is the distance along the direction normal to the body contour in a plane perpendicular to the free-stream direction z, and v_ν, v_z are the velocity components in the ν-direction and z-direction respectively. Within the approximation of the linearized characteristics method, we have

$$\left.\begin{aligned} v_\nu &= (v_{r0})_{\psi_{0b}} \sin \psi_{0b} \left\{ 1 + \sum_{n=1}^{\infty} \psi_{nb} \left[2 \left(\frac{v_{rn}}{v_{nn}} \right)_{\psi_{0b}} + \cot \psi_{0b} \right] \cos n\theta \right\}, \\ v_z &= (v_{r0})_{\psi_{0b}} \cos \psi_{0b} \left\{ 1 + \sum_{n=1}^{\infty} \psi_{nb} \left[2 \left(\frac{v_{rn}}{v_{nn}} \right)_{\psi_{0b}} - \tan \psi_{0b} \right] \cos n\theta \right\}. \end{aligned}\right\} \tag{4}$$

Substitution of these expressions into (3) yields

$$2\pi z \tan^2 \psi_{0b} = S'(z).$$

This result can alternatively be obtained by observing that in a neighbourhood $O[\psi_{nb}]$ of the body surface the following quantities are small of the same order (the symbol $O[\ ]$ indicating order of magnitude, and s entropy)

$$O[v_n] = O[w] = O\left[\frac{1}{\gamma R} \frac{\partial s}{\partial \psi} \right] = O[\psi_{nb}].$$

If terms $O[\psi_{nb}^2]$ are neglected, the equation of motion in spherical coordinates reduces to the incompressible form

$$\operatorname{div} \mathbf{v} = 2v_r + v_n \cot \psi + \frac{\partial v_n}{\partial \psi} + \frac{\partial w}{\sin \psi\, \partial \theta} = 0,$$

and the flow in the neighbourhood in question can be defined by an incompressible potential since the entropy is constant on the body and

the effect of $\partial s/\partial\psi$ on the velocities can be neglected, being $O[\psi_{nb}^2]$. Expansion of this potential in spherical harmonics and subsequent application of Gauss's theorem to a control volume delimited by the actual body, by the basic axisymmetric body and by two spherical surfaces of arbitrary radius leads to the same requirement for the zeroth term as quoted above. Therefore, the coefficients of the Fourier series representing the cross-section of the body within the approximation of the linearized characteristics method should be obtained by an expansion satisfying the requirement of equivalent areas. For the particular case of the elliptic cone at zero angle of attack, this can be obtained either (i) by determining b in the equation

$$\psi = \tan^{-1}\frac{b(a/b)}{[(a/b)^2\sin^2\theta+\cos^2\theta]^{1/2}},$$

so as to satisfy the condition $\pi\tan^2\psi_{0b} = S$ (approximation A in figure 1), or (ii) by determining ψ from the expansion

$$\tan^2\psi = \frac{a^2b^2}{a^2\sin^2\theta+b^2\cos^2\theta} = ab\left[1+2\sum_{n=1}^{\infty}\left(\frac{a-b}{a+b}\right)^n\cos 2n\theta\right],$$

which, within the linearized approximation, gives (approximation B in figure 1)

$$\tan^2\psi_{0b} = ab\,; \quad \psi = \psi_{0b}+\sin\psi_{0b}\cos\psi_{0b}\sum_{n=1}^{\infty}\left(\frac{a-b}{a+b}\right)^n\cos 2n\theta.$$

The expansion used in method (ii) has been suggested in a private communication by Van Dyke.

The poor accuracy exhibited by the results of Van Dyke's linear perturbation of a circular cone depended on the use of a direct Fourier expansion for the body geometry which yields $\psi_{0b} = 9{\cdot}27^\circ$ instead of $\psi_{0b} = 10^\circ$; in the chosen conical reference system, higher-order terms in ψ_{nb} were thus considered for the boundary conditions, while the linearized approximation was retained for the computation of the velocity components. In this connection it is interesting to observe the close agreement over the range $20^\circ < \theta < 90^\circ$ between Van Dyke's approximate results and the curve obtained by imposing his boundary conditions in the linearized characteristic analysis (curve C in figure 1). The increasing discrepancy between the aforesaid curves in the range $0^\circ < \theta < 20^\circ$ indicates that linear perturbations of the basic flow field lead to different accuracy in the two cases. This behaviour may in turn be attributed to the fact that the basic flow used in the linearized characteristics approach represents a uniformly valid solution, in contrast to the basic flow considered in Van Dyke's analysis.

The present example of a linearized characteristics calculation has also been extended to include terms up to $\cos 18\theta$ *. The results, which are

* Tables of the disturbance velocities up to $\cos 18\theta$ for a basic 10°-cone have been computed by the Research Department of the Grumman Aircraft Engineering Company.

included in figure 1, are practically identical to those obtained by the approximation as far as $\cos 10\theta$, and thus indicate that the question of convergence of the Fourier series in Ferri's method is related to the problem of representing the body cross-section rather than the problem of describing the perturbation flow field. It is believed that Van Dyke's expansion of the slender-body pressure distribution to $\cos 10\theta$ afforded a lower accuracy than that obtained in the present analysis because the disturbance velocities considered in the two cases are of different order of magnitude; indeed, the latter expands the differences in velocity components (referred to conical coordinates) between the actual and the basic non-linear conical flow, while the former involves the changes in velocity from free-stream magnitude and direction.

Part II. (By M. D. V. D.)

Professor Vaglio-Laurin makes the interesting suggestion that the range of applicability of Ferri's method may be increased by modifying it in accord with the equivalence (or 'area') rule due to Oswatitsch (1952). The modification involves the same linearization as Ferri's original method, differing from it only in higher-order terms; so that a demonstration of its superiority cannot be based on the linearized equations. Instead, one must compare with a more exact (non-linear) theory or with experiment, both of which will be done here.

First, in keeping with the spirit of my original paper (Van Dyke 1956), the second-order slender-body solution derived there has been used as the basis for a test of Vaglio-Laurin's proposal. That is, the second-order slender-body approximation is taken as a model of the full solution, and the simplifications of Ferri's method and Vaglio-Laurin's modification are introduced as additional approximations. The results are shown in figure 2 (which is the left half of figure 5 of my previous paper with two added curves). Vaglio-Laurin's approximation A is seen to give a definite improvement in the general level of pressure, though the peak is blurred (so that at this moderate Mach number simple slender-body theory is more accurate, as shown in figure 5 of my previous paper).

Second, Jorgensen (1957) has recently measured the pressures over an elliptic cone close in shape to that just considered. It has the same axis ratio of 3:1; and although its cross-sectional area is that of a 7·76° rather than a 10° circular cone, it was tested at a Mach number of 1·97 rather than 1·41, so that the supersonic similarity parameter (the ratio of cone angle to free-stream Mach angle) is actually somewhat higher. The results are shown in figure 3. Again the actual pressure peak is seen to be rounded off by approximation A.

Vaglio-Laurin's last paragraph is quite correct. Curtailment of the Fourier series at $\cos 10\theta$ introduces no appreciable error; and § 3.5 of my previous paper was wrong on this point for just the reason that he suggests. Hence my previous assessment of Ferri's method stands except that the

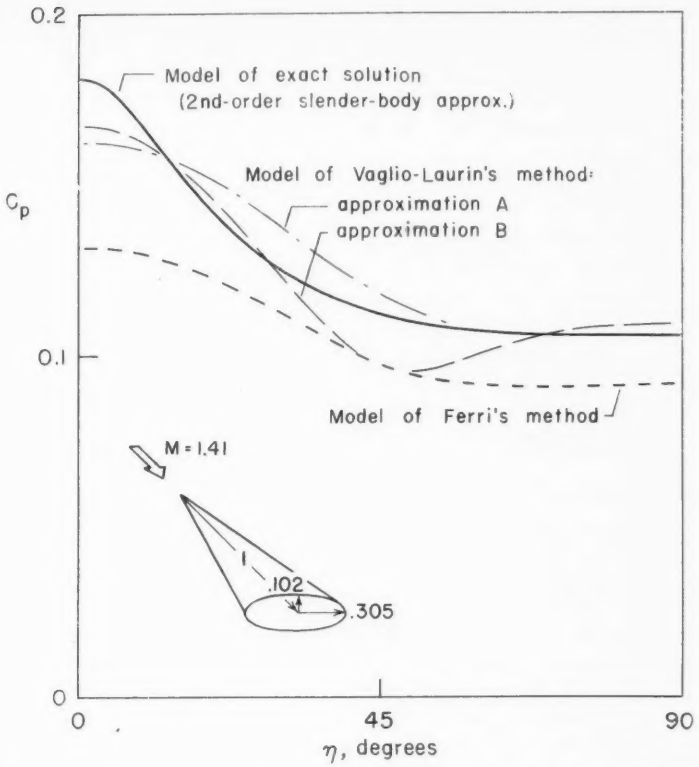

Figure 2. Further comparison between approximations to the pressure distribution around an elliptic cone.

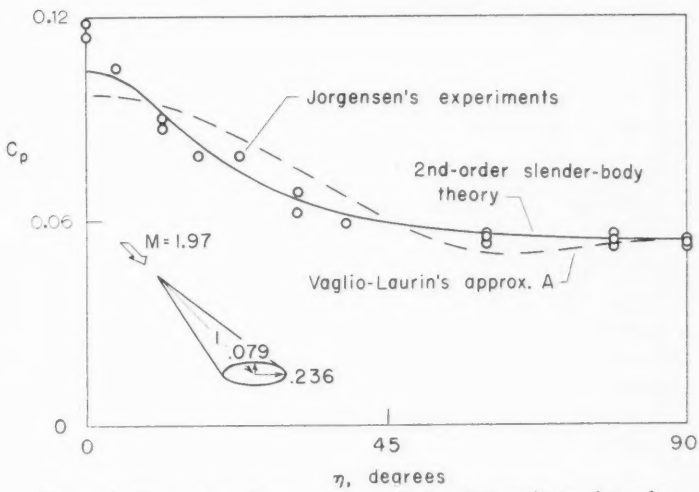

Figure 3. Comparison between theoretical and experimental results.

error is to be attributed almost entirely to non-linear effects rather than partly to the curtailment of the series. The method in its original form cannot reasonably be applied to cones whose cross-section differs from circular by as much as a 3 : 1 ellipse. For the modification suggested by Vaglio-Laurin, however, such eccentricity is seen to be perhaps tolerable at high supersonic Mach numbers where no more accurate theory exists. For less extreme eccentricities Vaglio-Laurin's method will yield good accuracy.

In view of this conclusion, the numerical results of Ferri, Ness & Kaplita (1953) must be regarded as unreliable except for nearly circular bodies. For example, the drag of an elliptic cone decreases much less with flattening than is suggested there. Indeed, Jorgensen's measurements at Mach numbers of 1·97 and 2·94 show that the decrease in wave drag is so slight as to be entirely offset by the increase in skin friction due to greater surface area.

References

Ferri, A. 1951 *Nat. Adv. Comm. Aero., Wash., Rep.* no. 1102.

Ferri, A., Ness, N. & Kaplita, T. 1953 *J. Aero. Sci.* **20,** 563.

Jorgensen, L. H. 1957 *Nat. Adv. Comm. Aero., Wash., Tech. note* no. 4045.

Oswatitsch, K. 1952 *Proc. 8th Intern. Congress Theor. & Appl. Mech., University of Istanbul,* **1,** 261.

Van Dyke, M. D. 1956 *J. Fluid Mech.* **1,** 1.

Ward, G. N. 1955 *Linearized Theory of Steady High-Speed Flow.* Cambridge University Press.

Some generalizations in steady one-dimensional gas dynamics

By J. A. SHERCLIFF
Department of Engineering, University of Cambridge

(*Received* 15 *November* 1957)

SUMMARY

In a stationary weak sound wave the four gas dynamical quantities, entropy, stagnation enthalpy, mass flow per unit area and impulse per unit area are constant. The six processes in which pairs of these four variables are kept constant are studied for the case of any single phase fluid or mixture of fluids in equilibrium, and it is shown that the remaining variables are stationary at sonic points. Such points are shown to occur once only in each process and are identified as maxima or minima, on the assumption that the fluid is a normal one which expands on heating at constant pressure and for which $(\partial^2 p/\partial v^2)_s$ is positive.

Newton's theory of sound assumed that the fluid temperature was invariant. Across a stationary Newtonian sound wave, the four quantities, temperature, mass flow and impulse per unit area, and a dynamical variant of the Gibbs function are constant. The six processes in which pairs of these four variables are kept constant are studied, and it is shown that the remaining variables are stationary at points where the fluid speed equals Newton's sound velocity. These points are shown to occur once only in each process and are identified as maxima or minima with the further proviso that $(\partial^2 p/\partial v^2)_T$ is positive.

The two sets of processes have one member in common, that usually referred to as the Rayleigh line. The Fanno line and the usual isentropic 'nozzle' process also belong to the first set.

Finally, the variation of stagnation temperature and pressure in some of the processes and in stationary shocks is investigated.

1. INTRODUCTION

Steady, one-dimensional gas dynamics has been analysed by many authors, particularly for the case of a perfect gas. A certain amount of work has also been done for arbitrary, single-phase fluids in equilibrium, with properties limited only by stability and the laws of thermodynamics (Courant & Friedrichs 1948; Kline & Shapiro 1954). It has been shown, for instance, that the speed of sound is a critical velocity for isentropic

nozzle flows, and for Rayleigh and Fanno processes, whatever the fluid. This is too striking a fact to be pure coincidence. It is the aim of this paper to construct a symmetrical mathematical treatment of these three and related processes, showing the dominant role of the sound speed.

The importance of studying arbitrary fluid dynamics is increasing since high-speed flows in which real gas behaviour, reaction, dissociation and ionization occur are becoming of practical interest. The theory of the arbitrary fluid in this and other papers is applicable to reactive gas mixtures provided only that at each section of flow investigated there is thermodynamic equilibrium. The speed of sound occurring in the analysis refers to the speed of waves of low enough frequency for chemical equilibrium to prevail. The theory cannot be applied to detonation waves in pre-mixed gases since there is true equilibrium on only one side of these waves. The flow behind and relative to a detonation wave can be sonic according to the Chapman–Jouguet rule, whereas behind a shock wave in a reactive gas mixture, which is in equilibrium on *both* sides of the wave, the flow must be subsonic. This last fact is evident from the work of Kline & Shapiro (1954), provided the gas mixture's properties are such that $(\partial^2 p/\partial v^2)_s$ and $(\partial p/\partial s)_v$ are constant in sign. p, v and s are pressure, specific volume and entropy, respectively.

Gases such as HCl which dissociate without total molal or volumetric change may be treated by perfect gas dynamical methods (Shapiro & Hawthorne 1947) with allowance for variation in effective specific heats.

2. The gas dynamical relations

Reactive or inert gas mixtures and single phase pure substances in equilibrium are usually characterized by the fact that any two independent properties define their thermodynamic state uniquely. As a generalization of this, the state of each section of flow in a one-dimensional gas dynamical process may be defined by *three* independent properties. One choice would be the velocity u together with any two independent thermodynamic ones. Another selection is F, G and H, in which

$$F = p + \rho u^2, \text{ the impulse per unit area,}$$

$$G = \rho u, \text{ the mass flow rate per unit area, and}$$

$$H = h + \tfrac{1}{2}u^2, \text{ the stagnation enthalpy.}$$

ρ and h denote density and specific enthalpy respectively. For convenience F is chosen equal to $p + \rho u^2$ rather than the more usual quantity

$$(p + \rho u^2) \times (\text{duct area of cross-section}).$$

F/G represents this latter quantity per unit rate of mass flow. The symbol H is chosen rather than h_0 to avoid complicated suffices. Note that $F = p + Gu$.

Specified values of F, G and H usually correspond to *two* possible states, such as occur on the two sides of a stationary shock wave. Across a stationary *weak* shock or acoustic wave, s is constant in addition to F, G and H, a very significant fact.

The familiar reversible, adiabatic 'nozzle' process and Rayleigh and Fanno processes each involve the invariance of two of the properties F, G, H and s. There are three other such processes. All six will be studied simultaneously. With suitable assertions regarding reversibility, adiabatic or other conditions, the six processes may be interpreted physically in various ways. Variation of G will be taken to correspond to duct area change, although it could equally well correspond to change in the mass flow due to injection or withdrawal of fluid. Typical interpretations of the six processes appear in table 1.

Constant	Typical interpretation
H, s	Reversible, adiabatic 'nozzle' process with area change.
F, G	Rayleigh process. Frictionless, constant area process with heat exchange or Ohmic heating, etc.
G, H	Fanno process. Adiabatic, constant area process with force in direction of motion due to wall friction, wire mesh, electromagnetic forces in ionized gas, etc. No external energy exchange.
G, s	Reversible, adiabatic work exchange in a duct of constant area by actuator discs, electromagnetic induction, etc.
F, s	Reversible, adiabatic process where work exchange and area change combine to keep F constant.
F, H	Adiabatic 'nozzle' process in which F is constant owing to friction.

Table 1.

The last two cases are rather artificial, and are more interesting mathematically than practically. There is difficulty in interpreting F when G is not constant. More artificial interpretations of the first four processes are also possible. For example, the Fanno process can represent a reversible process with suitably synchronized work and heat exchanges.

There being only three independent properties of a flow-section, F, G, H and s must be related. The differential equation expressing this relation is

$$dF+\rho T\,ds=\rho\,dH+u\,dG, \tag{1}$$

which follows from the definition of the variables and from the equilibrium relation $T\,ds=dh-dp/\rho$, T being the absolute temperature. Denoting the invariance of quantities by suffices, we then have

$$dF_{Hs}=u\,dG_{Hs}, \quad \text{etc.} \tag{2}$$

There are six such relations each involving two differentials. We shall proceed to relate all twelve differentials and show in particular that all vanish when the state is sonic. In a process with two of F, G, H and s constant, at points where the remaining two variables are stationary, the small change occurring between two closely adjacent flow-sections having the same values of F, G, H and s is virtually a stationary sound wave. Thus M, the local Mach number, must be unity. M, or u/a, where a is

the isentropic sound speed $\sqrt{(\partial p/\partial \rho)_s}$, is another gas dynamical property of each flow-section. A flow-section in a given state can be imagined as lying within any of innumerable processes, including the six currently under consideration.

From (1), $u = (\partial F/\partial G)_{Hs}$ and $\rho = (\partial F/\partial H)_{Gs}$, and hence

$$(\partial u/\partial H)_{Gs} = (\partial \rho/\partial G)_{Hs}. \tag{3}$$

There is a large array of these Maxwell-type relations, from which it is evident that all the differentials dH_{Gs}, dG_{Hs}, etc., will vanish simultaneously for flow-sections in certain states, provided there is no irregular behaviour of the quantities u, ρ, etc. Moreover, it is easily shown that

$$dG_{Hs} = \rho(1 - M^2)\, du, \tag{4}$$

so that sonic states are the relevant ones as expected.

To provide a firmer basis for the analysis, it is convenient to take u as the major independent variable. Quantities of the type $(\partial G/\partial u)_{Hs}$, written G'_{Hs}, will be studied and related.

From (3)

$$H'_{Gs} = G'_{Hs}\left(\frac{\partial u}{\partial \rho}\right)_{Hs} = -\frac{G'_{Hs}}{u}\left(\frac{\partial h}{\partial \rho}\right)_s = -\frac{uG'_{Hs}}{\rho M^2}. \tag{5}$$

All the differential coefficients may be related in this way or by shorter alternative methods.

It is easily shown with the help of (2) that

$$\frac{F'_{GH}}{F'_{Gs}} = \frac{(\partial H/\partial s)_{FG}}{(\partial H/\partial s)_{Gu}} = \frac{T}{(\partial h/\partial s)_\rho}, \tag{6}$$

and that

$$\frac{H'_{FG}}{H'_{Gs}} = \frac{(\partial F/\partial s)_{GH}}{(\partial F/\partial s)_{Gu}} = -\frac{\rho T}{(\partial p/\partial s)_\rho}. \tag{7}$$

Also,

$$G'_{Fs} = G'_{Hs} + \left(\frac{\partial G}{\partial H}\right)_{su} H'_{Fs} = G'_{Hs} + \left(\frac{\rho u}{a^2}\right)\left(-\frac{uG'_{Fs}}{\rho}\right).$$

Hence

$$G'_{Fs}(1 + M^2) = G'_{Hs}. \tag{8}$$

Similarly,

$$G'_{FH} = G'_{Hs} + \left(\frac{\partial G}{\partial s}\right)_{Hu} s'_{FH} = G'_{Hs} + \left\{-\rho T u\left(\frac{\partial \rho}{\partial p}\right)_h\right\}\left(\frac{uG'_{FH}}{\rho T}\right).$$

Hence

$$G'_{FH}\left\{1 + u^2\left(\frac{\partial \rho}{\partial p}\right)_h\right\} = G'_{Hs}. \tag{9}$$

Equations (2) and (4) to (9), now permit all the derivatives with respect to u to be evaluated. Table 2 lists them as multiples of $(1 - M^2)$. The example $H'_{Gs} = -u(1 - M^2)/M^2$ illustrates the use of the table.

It is necessary to study the behaviour of the quantities appearing in the table before the criticality of the sonic state can be clearly asserted. M^2 is well-behaved, as the speed of sound must always be defined in real substances. The quantity appearing in the (F, G) Rayleigh case is

$$T\left(\frac{\partial s}{\partial p}\right)_\rho = -\frac{c_p}{a^2}\left(\frac{\partial T}{\partial \rho}\right)_p, \tag{10}$$

which is well-behaved except at such rare points as water at 4° C at atmospheric pressure, where $(\partial T/\partial \rho)_p$ tends to infinity. C_p, the specific

Constant	G'/ρ	$F'/\rho u$	Ts'/u	H'/u
H, s (isentropic 'nozzle')	1	1	0	0
G, H (Fanno)	0	$-\dfrac{T}{M^2}\left(\dfrac{\partial s}{\partial h}\right)_\rho$	$\dfrac{T}{M^2}\left(\dfrac{\partial s}{\partial h}\right)_\rho$	0
F, G (Rayleigh)	0	0	$\dfrac{\rho T}{M^2}\left(\dfrac{\partial s}{\partial \rho}\right)_p$	$\dfrac{\rho T}{M^2}\left(\dfrac{\partial s}{\partial \rho}\right)_p$
G, s	0	$-M^{-2}$	0	$-M^{-2}$
F, s	$(1-M^2)^{-1}$	0	0	$-(1-M^2)^{-1}$
F, H	$\dfrac{1}{1+u^2(\partial \rho/\partial p)_h}$	0	$\dfrac{1}{1-u^2(\partial \rho/\partial p)_h}$	0

Table 2. Derivatives with respect to u as multiples of $(1-M^2)$.

heat at constant pressure, must be positive for stability. This is consistent with the findings of Kline & Shapiro (1954) who pointed out the criticality of the sign of $(\partial p/\partial s)_\rho$ and hence of $(\partial s/\partial p)_\rho$. The specific volume τ is the reciprocal of ρ. The quantity appearing in the (F, H)-case is

$$\left(\frac{\partial \rho}{\partial p}\right)_h = \frac{1}{a^2} - \frac{1}{\rho c_p}\left(\frac{\partial \rho}{\partial T}\right)_p, \tag{11}$$

of which both terms are positive, except in states where there is thermal contraction. Apart from this possibility, $(\partial \rho/\partial p)_h$ is finite, positive and non-zero. The quantity appearing in the (G, H) Fanno case,

$$T\left(\frac{\partial s}{\partial h}\right)_\rho = \frac{1}{a^2}\left(\frac{\partial p}{\partial \rho}\right)_h, \tag{12}$$

is seen to be finite and positive except conceivably in a thermal contraction region, by reference to (11) above. We may note that

$$\left(\frac{\partial h}{\partial s}\right)_\rho = T + v\left(\frac{\partial p}{\partial s_h}\right)_v,$$

which is the quantity studied by Kline & Shapiro (1954) in their discussion of Fanno processes. They considered it very unlikely that $T + v(\partial p/\partial s)_v$ would ever be negative for real fluids.

Summing up, we may say that if the above special states are excluded, the pair of the variables F, G, H and s that are not kept constant are stationary when and only when $M = 1$.

The next question to consider is whether these stationary values are maxima or minima. Kline & Shapiro (1954) have studied the (H, s), (F, G) and (G, H) cases and have shown separately in each case that the sign of $(\partial^2 p/\partial v^2)_s$ is the crucial factor. This also decides whether compressive acoustic waves steepen into shocks, and whether shocks must be compressive.

The six cases, keeping pairs of F, G, H and s constant, will now be treated in parallel to determine the nature of the stationary values as u varies. To fix the change of sign of F', G', H' or s' at the sonic state, it is necessary to study $\partial M^2/\partial u$ at the sonic state. It is found that $\partial M^2/\partial u$ takes the same value in all six cases when $M = 1$. This follows from the five equations:

$$\left.\begin{aligned}\left(\frac{\partial M^2}{\partial u}\right)_{GX} &= \left(\frac{\partial M^2}{\partial u}\right)_{Gs} + \left(\frac{\partial M^2}{\partial s}\right)_{Gu} s'_{GX},\\ \left(\frac{\partial M^2}{\partial u}\right)_{sX} &= \left(\frac{\partial M^2}{\partial u}\right)_{Gs} + \left(\frac{\partial M^2}{\partial G}\right)_{su} G'_{sX},\end{aligned}\right\} X = F \text{ or } H$$

and

$$\left(\frac{\partial M^2}{\partial u}\right)_{FH} = \left(\frac{\partial M^2}{\partial u}\right)_{Hs} + \left(\frac{\partial M^2}{\partial s}\right)_{Hu} s'_{FH},$$

in which the last terms vanish when $M = 1$, provided $(\partial M^2/\partial s)_{Gu}$, $(\partial M^2/\partial G)_{su}$, $(\partial M^2/\partial s)_{Hu}$ are not infinite when $M = 1$. These quantities are respectively equal to

$$-\frac{1}{a^2}\left(\frac{\partial a^2}{\partial s}\right)_\rho, \qquad -\frac{1}{a^3}\left(\frac{\partial a^2}{\partial \rho}\right)_s, \qquad -\frac{1}{a^3}\left(\frac{\partial a^2}{\partial s}\right)_h$$

when $M = 1$. Now

$$\left(\frac{\partial a^2}{\partial s}\right)_\rho = \frac{\partial^2 p}{\partial \rho\, \partial s} = v^2\left(\frac{\partial^2 T}{\partial v^2}\right)_s \quad \text{and} \quad \left(\frac{\partial a^2}{\partial \rho}\right)_s = \left(\frac{\partial^2 p}{\partial \rho^2}\right)_s,$$

and no singularity upon isentropics, such as would make these second derivatives infinite, appears to be possible. Furthermore,

$$\left(\frac{\partial a^2}{\partial s}\right)_h = \left(\frac{\partial a^2}{\partial s}\right)_\rho + \left(\frac{\partial a^2}{\partial \rho}\right)_s \left(\frac{\partial \rho}{\partial s}\right)_h \quad \text{and} \quad \left(\frac{\partial \rho}{\partial s}\right)_h = -\rho T\left(\frac{\partial \rho}{\partial p}\right)_h.$$

Equation (11) indicates that $(\partial \rho/\partial p)_h$ is not infinite, and so $(\partial a^2/\partial s)_h$ is not infinite.

We conclude that $\partial M^2/\partial u$ takes the same value when $M = 1$, whichever pair of F, G, H and s is kept constant. The common value is most easily evaluated in the (G, s) case, where u/v is constant:

$$\left(\frac{\partial M^2}{\partial u}\right)_{Gs} = \frac{v}{u}\frac{\partial}{\partial v}\left\{-\frac{u^2}{v^2}\frac{1}{(\partial p/\partial v)_s}\right\}_s = \frac{u}{v}\frac{1}{(\partial p/\partial v)_s^2}\left(\frac{\partial^2 p}{\partial v^2}\right)_s = \frac{v^3}{a^3}\left(\frac{\partial^2 p}{\partial v^2}\right)_s$$

when $M = 1$.

Kline & Shapiro (1954) indicated that $(\partial^2 p/\partial v^2)_s$ is positive for all single phase fluids for which accurate data are available. We therefore assume that $(\partial^2 p/\partial v^2)_s$ is positive, and also that there is no thermal contraction, in what follows. It is then possible, using (10), (11) and (12), to deduce the nature of the stationary values of F, G, H and s at sonic points from the change in sign in the relevant derivative with respect to u. Table 3 lists the results. It should be observed that the sonic points have the same nature as for a perfect gas.

Constant	Nature of sonic points
H, s (isentropic nozzle)	F max.; G max.
G, H (Fanno)	F min.; s max.
F, G (Rayleigh)	H max.; s max.
G, s	F min.; H min.
F, s	G max.; H min.
F, H	G max.; s max.

Table 3.

If we assume that the variation of M, F, G, H and s with u in the above cases is continuous, it follows that only one sonic point occurs in each process (if $(\partial^2 p/\partial v^2)_s$ is fixed in sign) since maxima and minima must occur alternately. (Sonic points of inflexion would require $\partial M^2/\partial u$ and $(\partial^2 p/\partial v^2)_s$ to vanish.) This fact was deduced by Kline & Shapiro (1954) from a different argument in the Fanno and Rayleigh cases.

3. The influence of the speed of Newtonian sound

Newton's calculation of the speed of sound in air proved to be too low because of his assumption that sound propagation was an isothermal process instead of an isentropic one. Nevertheless the speed of Newtonian sound, which will be denoted by n to distinguish it from the adiabatic sound speed a, proves to have some physical significance.

The symbol N will be used for the 'isothermal Mach number', the ratio u/n. The specific heat ratio γ is equal to N^2/M^2 because

$$\frac{a^2}{n^2} = \frac{(\partial p/\partial \rho)_s}{(\partial p/\partial \rho)_T} = \frac{(\partial s/\partial T)_p}{(\partial s/\partial T)_\rho} = \frac{c_p}{c_v} = \gamma.$$

γ is always greater than unity since $c_p - c_v = -T(\partial v/\partial T)_p^2(\partial p/\partial v)_T$ and $(\partial p/\partial v)_T$ must be negative for stability. γ reaches unity only at points of zero thermal expansion where $(\partial v/\partial T)_p$ vanishes. In passing, it it worth noting that the speeds of adiabatic and Newtonian sound are $(\gamma p/\rho)^{1/2}$ and $(p/\rho)^{1/2}$ for any fluid which obeys Boyle's law, $p/\rho = f(T)$. A reactive gas mixture whose mean molecular weight changes does not satisfy this condition.

It is well known that, for a perfect gas undergoing a Rayleigh process, the temperature has a stationary value when $M = \gamma^{-1/2}$ and $N = 1$. This,

however, is a general result, applicable to all single phase fluids in equilibrium, for

$$u^2 = \left(\frac{\partial p}{\partial \rho}\right)_{FG} \quad \text{and} \quad a^2 = \left(\frac{\partial p}{\partial \rho}\right)_s.$$

It follows that

$$\left(\frac{\partial T}{\partial p}\right)_s \left(\frac{\partial p}{\partial s}\right)_{FG} = M^2 \left(\frac{\partial T}{\partial \rho}\right)_s \left(\frac{\partial \rho}{\partial s}\right)_{FG}$$

and hence that

$$\left(\frac{\partial T}{\partial s}\right)_{FG} - \left(\frac{\partial T}{\partial s}\right)_p = M^2 \left\{\left(\frac{\partial T}{\partial s}\right)_{FG} - \left(\frac{\partial T}{\partial s}\right)_\rho\right\}.$$

From this we have

$$\left(\frac{\partial T}{\partial s}\right)_{FG} = \frac{T}{c_p} \frac{1-\gamma M^2}{1-M^2},$$

which vanishes when $M = \gamma^{-1/2}$. If the fluid is a reactive gas mixture, γ must be taken as the *effective* specific heat ratio, allowing for reaction.

A flow-section such that $N = 1$, i.e. capable of sustaining a weak steady Newtonian sound wave in which F, G and T do not change significantly, obviously corresponds to a state where T is stationary if F and G are fixed as in a Rayleigh process. It also corresponds to the section when G and the duct area have stationary values in a reversible, isothermal nozzle process. In fact there are again six simple processes for which n is the critical speed. A unified, symmetrical treatment is again possible if a new property Z, a dynamic form of Gibbs function, is introduced such that

$$Z = H - Ts = \zeta + \tfrac{1}{2}u^2,$$

ζ being the usual Gibbs function per unit mass, $h - Ts$. Z is not the stagnation Gibbs function, which is $H - T_0 s$, where T_0 is the stagnation temperature. Z has no obvious physical significance except in isothermal cases where its change measures reversible work exchanges (see § 4). Thus Z is constant in the reversible, isothermal nozzle process. The lack of significance of Z is related to the fact that the datum for s is arbitrary and therefore Z contains an arbitrary multiple of T when T varies. The two cases where Z, but not T, is constant will not be considered further.

Constant	Typical interpretation
F, G	Rayleigh process, as already discussed.
T, Z	Isothermal, reversible ' nozzle ' process with area change.
G, T	Isothermal, constant area process with state change produced by wall friction or work exchange.
F, T	Isothermal process in which area change and wall friction or work exchange combine to keep F constant.

Table 4.

The four variables F, G, T and Z are related by the equation

$$dF = \rho\, dZ + \rho s\, dT + u\, dG. \tag{13}$$

The four significant cases in which pairs of the variables are kept constant are interpreted in table 4.

This situation may be analysed in a manner completely analogous to that in the foregoing section. For brevity, only the main results will be presented. Again u is taken as the main independent variable and primes denote differentiation with respect to u. Table 5 lists these derivatives as multiples of $(1 - N^2)$.

Constant	G'/ρ	$F'/\rho u$	sT''/u	Z'/u
T, Z (isothermal 'nozzle')	1	1	0	0
F, G (Rayleigh)	0	0	$\frac{\rho s}{N^2}\left(\frac{\partial T}{\partial p}\right)_\rho$	$-\frac{\rho s}{N^2}\left(\frac{\partial T}{\partial p}\right)_\rho$
G, T	0	N^{-2}	0	$-N^{-2}$
F, T	$(1-N^2)^{-1}$	0	0	$-(1-N^2)^{-1}$

Table 5. Derivatives with respect to u as multiples of $(1 - N^2)$.

It is necessary to study the behaviour of the quantities appearing in table 5 before the criticality of the Newtonian sonic state can be clearly asserted. N^2 is well behaved, since two-phase states in which $(\partial p/\partial \rho)_T$ and n^2 vanish are excluded. Also,

$$(\partial T/\partial p)_\rho/N^2 = -(\partial T/\partial \rho)_p/u^2,$$

which is positive and finite if thermal contraction is excluded. Note that the factor s also occurs in the quantity sT''/u so that its sign is irrelevant to the behaviour of T in the Rayleigh case.

The conclusion is that with the above restrictions the pair of the variables F, G, T and Z that are not kept constant are stationary when and only when $N = 1$. The nature of these stationary points depends upon the sign of $\partial N^2/\partial u$ there.

In the (G, T) case, it is easily shown that

$$\frac{\partial N^2}{\partial u} = \frac{v^3}{n^3}\left(\frac{\partial^2 p}{\partial v^2}\right)_T \quad \text{when } N = 1. \tag{14}$$

It is also easily demonstrated that $\partial N^2/\partial u$ takes this same value at the Newtonian sonic point in all four cases. The analysis is similar to that in § 2, with N, n, T, Z and ζ replacing M, a, s, H and h. The condition for $\partial N^2/\partial u$ to be identical is found to be that $(\partial n^2/\partial T)_\rho$, which is equal to $-v^2(\partial^2 s/\partial v^2)_T$, and $(\partial n^2/\partial \rho)_T$, which is equal to $(\partial^2 p/\partial \rho^2)_T$, should not be infinite. No singularity upon isothermals such as would make these quantities infinite appears to be possible. We conclude that in all four cases (14) holds. The derivative $(\partial^2 p/\partial v^2)_T$ is usually positive, but can become negative near the critical point for pure fluids. If we assume that

the positive sign prevails, and that there is no thermal contraction, we can ascertain the nature of the stationary values when $N = 1$. The results appear in table 6. The behaviour is qualitatively like that of a perfect gas for substances for which there is no thermal contraction and for which $(\partial^2 p/\partial v^2)_T$ is positive.

Constant	Nature of Newtonian sonic points
F, G (Rayleigh)	T max.; Z min. (if $s \to 0$)
T, Z (isothermal nozzle)	F max.; G max.
G, T	F min.; Z min.
F, T	G max.; Z max.

Table 6.

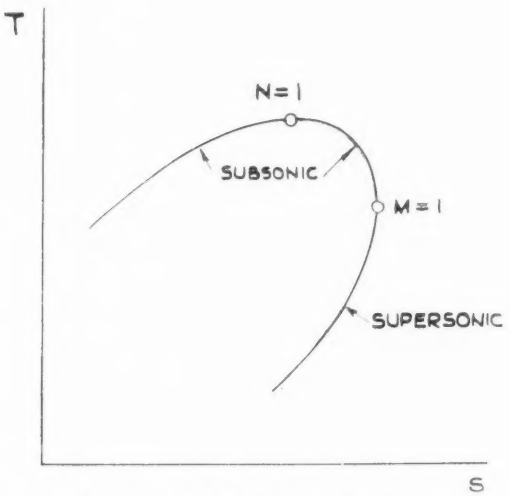

Figure 1. The Rayleigh Line, for the case $(\partial^2 p/\partial v^2)_{s \text{ or } T} > 0$, $(\partial \rho/\partial T)_p < 0$.

If we assume that the variation of F, G, T and Z with u in the above cases is continuous, it follows that only one point at which $N = 1$ occurs in each process (if $(\partial^2 p/\partial v^2)_T$ is fixed in sign) since maxima and minima must occur alternately and points of inflexion would require $(\partial^2 p/\partial v^2)_T$ to vanish.

This, and the corresponding result for points at which $M = 1$, constrains a Rayleigh line on the (T, s)-plane always to have the form familiar for the perfect gas case, illustrated in figure 1. The subsonic and supersonic branches cannot cross because this would imply two flow-sections with the

same values of T and s, and hence in the same thermodynamic state with the same values of a and p, but with differing Mach numbers and velocities. But $F = p + Gu$, F and G being constant, which shows that for a given value of p, u can have only one value. Thus a crossing is precluded.

4. Some other considerations

When propulsive effort is the prime concern, the quantity

$$(p + \rho u^2) \times (\text{duct area of cross-section})$$

is of interest. This quantity is represented by F/G per unit rate of mass flow, $1/G$ being the area per unit rate of mass flow. It is possible to develop the analysis using the four variables F/G, $1/G$, H and s, which are related by the equation

$$u d(F/G) + T\,ds = dH + pu\,d(1/G).$$

The results differ little from those in § 2, there being only two fresh processes involved. These are the cases where F/G and H or s are constant. For these cases $1/G$ and s or H, respectively, are stationary at the sonic point.

Another approach is offered by the selection of the four variables H, p, u and s for analogous treatment. The basic relation here is

$$\rho\,dH = dp + \rho T\,ds + G\,du.$$

No critical point like the sonic point occurs in this case, however. For instance, when H and s are fixed, p is stationary only when u and G vanish. Another case belonging to this family is that where s, p and hence the thermodynamic state are fixed. It corresponds to cases where the kinetic energy is converted reversibly into work by idealized impulse turbines or electromagnetic induction. Again the sonic point is not critical.

There are obviously many other similar, alternative selections of variables possible.

Interpretating the individual cases physically reveals an asymmetry in the way that heat and work influence the problem. In reversible cases, the external heat exchanged between two adjacent flow-sections is $T\,ds$ per unit mass flow, but the corresponding work quantity cannot be expressed in terms of any single perfect differential in general. Alternative, general expressions for dW, the external work exchanged between two adjacent flow-sections per unit mass flow in a reversible process, are

$$dW = T\,ds - dH = -(u\,du + dp/\rho) = (u\,dG - dF)/\rho = -dZ - s\,dT.$$

The difference between dW and the actual work exchanged in an irreversible case is the dissipation. In reversible cases without work exchange such as the two nozzle processes and the Rayleigh process, dW vanishes. This will be recognized as indicating that Euler's equation

$$u\,du + dp/\rho = 0$$

is applicable.

Gas dynamical analysis frequently makes use of the stagnation state corresponding to a given flow-section. This state, usually denoted by the suffix 0, is defined as that for which

$$u_0 = 0, \qquad h_0 = H, \qquad s_0 = s.$$

The stagnation temperature T_0 is of interest mainly for substances for which h is a function of temperature only, as for a perfect gas. For all normal fluids T_0 is larger than T, the 'static' temperature, since H is always greater than h, and

$$\left(\frac{\partial T}{\partial h}\right)_s = -\frac{T}{\rho c_p}\left(\frac{\partial \rho}{\partial T}\right)_p > 0$$

provided thermal contraction is excluded.

Variation of the stagnation pressure p_0 is given by the relation

$$dp_0 = \rho_0(dH - T_0\, ds).$$

p_0 is obviously constant in the isentropic nozzle process. In a Fanno process, H is constant and

$$dp_0 = -\rho_0 T_0\, ds.$$

Thus if the process is irreversible and adiabatic, p_0 must decrease.

In a Rayleigh process, $dH = T\, ds$ and

$$dp_0 = -\rho_0(T_0 - T)\, ds. \tag{15}$$

Thus the sonic point is the point of minimum p_0 for normal fluids without thermal contraction and for which $(\partial^2 p/\partial v^2)_s$ is positive.

In the process with s and F or G constant, p_0 behaves qualitatively like H, reaching a minimum at the sonic point for normal fluids. In the (F, H) process it is again minimum when $M = 1$ since s is then a maximum.

Thus, of the six F, G, H, s cases, p_0 is constant in one case and is minimal at the sonic point in all the others for normal fluids.

In the isothermal nozzle process, $dH = T\, ds$ and (15) again applies. Neither p_0 nor s has stationary points in this case, however.

Across a stationary shock, H is constant whereas s always increases. It follows that p_0 always decreases because $(\partial p_0/\partial s)_H = -\rho_0 T_0 < 0$.

5. Concluding remarks

One conclusion of the analysis is to confirm and generalize the result of Kline & Shapiro (1954) that the gas-dynamical behaviour of single-phase fluids in equilibrium is qualitatively similar to that of a perfect gas, provided that there is no thermal contraction and that $(\partial^2 p/\partial v^2)_s$ is positive. The additional demand that $(\partial^2 p/\partial v^2)_T$ be positive is made.

The speeds of adiabatic and Newtonian sound are seen to be significant since a flow-section where the velocity is sonic is capable of undergoing an infinitesimal acoustic-type change in which F and G together with either s and H (if $M = 1$) or T and Z (if $N = 1$) do not change. It is then apparent, for instance, why in a Rayleigh process with F and G constant, s or T is stationary at the two types of sonic point.

The tendency of nozzle, Rayleigh and Fanno processes to choke when the velocity becomes sonic is well known. The similar choking occurring in the (G, s), reversible, adiabatic work-exchange process is perhaps a new result. The minimum value of H which occurs at the sonic point means that a limit is placed on the work that may be extracted reversibly in a duct of constant cross-sectional area. The comparable process mentioned in § 4, in which the duct area varies in such a way that work extraction changes only the kinetic energy and not the thermodynamical state of the fluid, shows no choking tendency. The limit on the work extraction here is provided by the growth in duct area as the velocity falls.

References

Courant, R. & Friedrichs, K. O. 1948 *Supersonic Flow and Shock Waves*. New York : Interscience.

Kline, S. J. & Shapiro, A. H. 1954 Article in *Mémoires sur la Méchanique des Fluides*, p. 171. Publ. Sci. Tech. Minist. de l'Air, Paris.

Shapiro, A. H., & Hawthorne, W. R. 1947 *J. Appl. Mech.* **14**, 317.

CORRIGENDUM

"Wave formation in laminar flow down an inclined plane", by T. Brooke Benjamin (*J. Fluid Mech.* **2**, 1957, 554).

Page 560. In equation (3.11) the equals sign following the first term should be replaced by a minus sign.

Page 570. In equation (5.10) the numerical factor should be replaced by 0·448, and in equation (5.12) the numerical factor should be replaced by 0·00783. Equation (5.13) should read as

$$\mathscr{A} = \exp\{0{\cdot}108R^{7/3}\}.$$

REVIEWS

Elements of Gasdynamics, by H. W. LIEPMANN and A. ROSHKO. New York: John Wiley & Sons, 1957. 439 pp. $11.00 or 88*s*.

The term *gas dynamics*, which Liepmann and Roshko have chosen to combine into a single word, is now widely used to denote that area of fluid physics which deals with compressible flow and includes some of the more basic applications to aerodynamics. It is perhaps not more than a decade since the subject blossomed forth as a major category of aeronautical science, somewhat distinct from the more classical parts of fluid mechanics, and it is also a decade since the predecessor to the present book was published, namely Liepmann and Puckett's *Aerodynamics of a Compressible Fluid*. In 1947 and subsequent years, this work helped to fill an obvious need for an introductory gas dynamics book written in English. It gave an admirable treatment of the fundamentals and showed a wise choice of applications. Prior to 1947, coverage in the book literature was inadequate (with some exceptions such as Sauer's book *Theoretische Einführung in die Gasdynamik* (1943)), which is curious considering that the subject has roots extending well into the past century; for example, the work of St. Venant and Wantzel, Riemann, Mach and Rankine. Also, such investigations as Prandtl's schlieren measurements of waves in supersonic channel flow (1907) and Meyer's basic theoretical work on supersonic plane flows (1908) were four decades old at the end of World War II.

There are two principal reasons why the writing of a gas dynamics book represents a greater challenge now than ten years ago. Firstly, a number of authoritative books on the subject have already appeared during the past decade, which give a rather wide coverage and diversity of emphasis among component topics. The authors or editors, as the case may be, include Ferri, Courant and Friedrichs, Howarth, Oswatitsch, Shapiro, as well as Emmons, who edits the forthcoming gas dynamics volume of the Princeton series. Secondly, the discipline itself has been extended in scope. The subject matter has grown in volume and its conceptual boundaries have penetrated more deeply into the realm of particle physics, as energies and transit times have approached those characteristic of molecular processes. Thus, the problem of optimizing the choice of material for a book of reasonable size is more severe. According to the preface, it was the first of these reasons which led the authors to write a completely new book rather than revise the Liepmann–Puckett work. The second reason generated the decision to divide the material into two independent volumes of which this is the first, with the second yet to be written.

In this reviewer's opinion, the authors have, in fact, implemented effectively their aim of providing a working understanding of the essentials of high speed flow. The book combines an approach characteristic of a first class textbook with a careful choice of subject matter based on considerable classroom experience. As such, it should be appreciated particularly by

new students of gas dynamics. On the other hand, much of the contents should be largely familiar to those who already claim some competence in the field, and such persons will find that the book is well suited as a reference and review text.

The organization of material is largely parallel to that in Liepmann and Puckett. This is, if anything, another point in its favour. Part I of the older book has been replaced by the first six chapters of the present work and part II by the last eight chapters. The early chapters deal with one-dimensional flow where construction of the equations of momentum, continuity and energy is feasible in conjunction with simplified physical concepts. As is known, much ground can be covered before further generalization becomes necessary, and good advantage is taken of this opportunity here. A broader treatment of the basic equations takes place in two widely separated steps. The first of these occurs around the middle of the book and deals with the equations of frictionless flow. Some instructive features of the presentation at this point are the introduction and use of tensor notation, and an explicit comparison between the control surface or integral method of deducing the equations and the use of the Eulerian derivative. In connection with the tensor formulation, the reader may wonder whether the authors succumb to an aesthetic urge to use mathematical finery at the expense of physical concepts; he can be assured that this is not so, for Liepmann and Roshko are too much concerned with the clarity of the underlying physics.

The second step toward generalization occurs near the end of the book and deals with the formulation of the complete Navier–Stokes equations. Here, the tensor notation introduced earlier is put to work, and by means of a skilful presentation, the authors rapidly produce these equations. The treatment is somewhat more sophisticated here and, accordingly, the section in question is officially included among the more advanced ones which may be omitted at a first reading. This is, perhaps, consistent with the authors' inductive approach, at least in the sense that it progresses from one-dimensional gas dynamics to the introduction of the Navier–Stokes equations over a span of twelve chapters. It is possible, however, that the development of the basic physical theory would be strengthened by including a preliminary discussion of the Navier–Stokes equations at an earlier point. As it stands now, this material is somewhat removed from the main stream of the book. Even the bare outlines of a formulation from the basic stress–strain dynamics of a fluid element would provide an initial framework for subsequent special cases, such as the excursion into one-dimensional ideal gas flow. That this approach gives the reader a broad perspective of physical concepts at an early stage has already been shown by other authors such as Prandtl in his article "The Mechanics of Viscous Fluids", Volume III, Section G of *Aerodynamic Theory* edited by Durand (Berlin: Springer, 1935).

The many satisfying features of the book include two chapters dealing with the similarity rules of high-speed and transonic flow. The former presents a unified discussion which treats regimes from subsonic through to hypersonic. It is limited to small perturbation theory but, as the

authors point out, this is not especially restrictive from a practical point of view since modern aerodynamics is concerned mainly with thin wings. In the chapter on transonic flow, good use is made of the potential for plausibility arguments inherent in this branch of the subject. There is also a fruitful comparison between transonic flow over wedges and cones, a subject which has been of particular interest to the senior author in connection with his own experimental work in this area.

Turning to the matter of high speed flows with viscosity and conductivity, we recall that Liepmann and Puckett present an abbreviated treatment, too much so in the light of recent extended interest in the subject of boundary layers and other varieties of dissipative flows. Boundary layer theory is of engineering importance not only because it yields numerical results for friction drag and heat transfer but also, as the present authors emphasize, since it confirms that viscosity does not influence the pressure field in high Reynolds number flow past a slender body. In addition, the discipline harbours a variety of physical concepts whose explicit treatment should be of considerable pedagogical value, and nowhere is the interplay of dynamic behaviour and intrinsic physical properties in better evidence. The reviewer has in mind, for example, such matters as the variation of shearing stress distribution with temperature dependence of viscosity, interpretation of Prandtl number, its role in boundary layer energetics, and the examination of boundary-layer type flows as diffusion processes.

The treatment of non-ideal gas flows in the present book is, in fact, another one of its strong points. The boundary layer concept is developed in a way calculated to give the reader a proper physical insight, and newer material presented includes recent measurements of turbulent boundary layers at high Mach numbers, as well as a discussion of Couette flow of a dissociating gas.

The last mentioned topic reminds us that a growing variety of so-called ' real gas ' effects is now under investigation as a result of greater interest in high temperature gas dynamics. Their proper incorporation as part of the formal analytical foundation of the subject is not at all complete, as yet, but the authors manage to supply some clear thinking in their discussion of the problem. It seemed to the reviewer that their remarks will be particularly instructive to those who have tended to equate real *vs* ideal gases with particle *vs* continuum gas theories. Difficulties of this type arise because a particle theory is used to define the nature of various physical properties of the gas, such as those concerned with the transport of momentum and heat. It is possible of course to account for these two in particular on the basis of bulk coefficients which appear in the continuum equations. Also, the ' imperfections ' of dissociation, ionization and condensation can be treated by a continuum analysis. However, in the case of, say, viscous shear by itself, one can visualize a rather satisfactory macroscopic physical model, whereas proper physical insight as a prelude to correct continuum-type treatment of several other real gas phenomena does require an evaluation of the molecular behaviour of the gas. The intrinsic non-equilibrium character of the

effects in question does not make the analysis any easier. That the dynamics, and particularly the energetics of high temperature gas flow, does rest on this more complex foundation is a point which Liepmann and Roshko manage to transmit successfully to the reader. The same cannot be said for other current books in gas dynamics.

The authors stress the point, and correctly so, that the key to the relationship between the continuum formulation and that of the kinetic theory lies in the effect of fluctuations due to molecular structure on the ability of measuring instruments to obtain correct mean values. With this as the proper criterion, they suggest that it is possible to apply a continuum analysis even to rarefied gas flows in which the Knudsen number is appreciably larger than unity. This is done by measuring for a sufficiently long period of time and applying the ergodic hypothesis, which establishes an equivalence between time and space averages. (The approach is not new to the turbulence investigator who performs a statistical evaluation of hot-wire fluctuation data.) Beyond a certain point, however, the molecular fluctuations would grow so large that it is not practical to attempt the correct measurement of mean values. The kinetic theory treatment then becomes the proper one. The motivation on the part of some for stating unequivocally that the continuum theory breaks down for rarefied gas flow probably stems, in the authors' opinion, from attempting to use a solution of the Navier–Stokes equation, e.g. a high Reynolds number solution, which does not apply in the first place.

Each succeeding book in gas dynamics these days appears to include a correspondingly larger chapter devoted to a discussion of methods of physical measurement. This is entirely warranted as there can be little doubt that the developing nature of the science places ever-growing stress on the results of pertinent experiments. The discussion here is meant to centre around experiments of the wind-tunnel type. Except for omitting free flight techniques, this is not too restrictive, since shock tubes and other variations of the more conventional tunnel now require a wide variety of experimental techniques. There is probably a need for a completely new book in this field to supplement the 1954 volume of the Princeton series, *Physical Measurements in Gas Dynamics and Combustion*. An extended list of contents for such a work would, indeed, include several intriguing topics, such as recent experimental work in magneto-gasdynamics. The admittedly limited treatment by Liepmann and Roshko is, nevertheless, a substantial one marked by an excellent choice of material which is well presented. It represents a most suitable introduction to experimental problems for the student. This is hardly a surprise as both authors are first class experimentalists in their own right.

D. Bershader

INDEX

Alpher, R. A. and White, D. R. Flow in shock tubes with area change at the diaphragm section, 457.

Batchelor, G. K. Diffusion in free turbulent shear flows, 67.

Betchov, R. On the fine structure of turbulent flows, 205.

Binnie, A. M., Hookings, G. A. and Kamel, M. Y. M. The flow of swirling water through a convergent–divergent nozzle, 261.

Bloomer, N. T. Note on the position of ring singularities in an axisymmetric potential field, 217.

Chester, W. The effect of a magnetic field on Stokes flow in a conducting fluid, 304.

Chu, Boa-Teh and Kovásznay, Leslie S. G. Non-linear interactions in a viscous heat-conducting compressible gas, 494.

Clayden, W. A. *See* **Cox and Clayden.**

Comings, Edward W. *See* **Miller and Comings.**

Cowan, Robert D. Properties of the Hugoniot function, 531.

Cox, A. D. and Clayden, W. A. Cavitating flow about a wedge at incidence, 615.

Craggs, J. W. The supersonic motion of an aerofoil through a temperature front, 176.

Crane, L. J. The laminar and turbulent mixing of jets of compressible fluid. Part II. The mixing of two semi-infinite streams, 81.

Davies, P. O. A. L. The behaviour of a Pitot tube in transverse shear, 441.

Dhawan, S. and Narasimha, R. Some properties of boundary layer flow during the transition from laminar to turbulent motion, 418.

Dumas, R. J. *See* **Favre, Gaviglio and Dumas.**

Esch, Robin E. The instability of a shear layer between two parallel streams, 289.

Favre, A. J., Gaviglio, J. J. and Dumas, R. J. Further space-time correlations of velocity in a turbulent boundary layer, 344.

Feldman, Saul Some shock tube experiments on the chemical kinetics of air at high temperatures, 225.

Gaviglio, J. J. *See* **Favre, Gaviglio and Dumas.**

Griffith, Wayland C. and Kenny, Anne On fully-dispersed shock waves in carbon dioxide, 286.

Gundersen, Roy The flow of a compressible fluid with weak entropy changes, 553.

Hartunian, R. A. and Sears, W. R. On the instability of small gas bubbles moving uniformly in various liquids, 27.

Helliwell, J. B. Two-dimensional flow at high subsonic speeds past wedges in channels with parallel walls, 385.

Helliwell, J. B. and Mackie, A. G. Two-dimensional subsonic and sonic flow past thin bodies, 93.

Hookings, G. A. *See* **Binnie, Hookings and Kamel.**

Illingworth, C. R. The effects of a sound wave on the compressible boundary layer on a flat plate, 471.

Janssen, E. Flow past a flat plate at low Reynolds numbers, 329.

Jukes, J. D. The structure of a shock wave in a fully ionized gas, 275.

Kamel, M. Y. M. *See* **Binnie, Hookings and Kamel.**

Kenny, Anne *See* **Griffith and Kenny.**

Kovásznay, Leslie, S. G. *See* **Chu and Kovásznay.**

Lance, G. N. The effect of a vertical lapse rate of temperature on the spiral flow of a fluid in a heated rotating cylinder, 523.

Levine, Harold Skin friction on a strip of finite width moving parallel to its length, 145.

Liepmann, H. W. A simple derivation of Lighthill's heat transfer formula, 357.

Lighthill, M. J. The fundamental solution for small steady three-dimensional disturbances to a two-dimensional parallel shear flow, 113.

Mackie, A. G. *See* **Helliwell and Mackie.**

Meyer, R. F. The impact of a shock wave on a movable wall, 309.

Miles, John W. On the generation of surface waves by shear flows, 185.

Miller, David R. and Comings, Edward W. Static pressure distribution in the free turbulent jet, 1.

Narasimha, R. *See* **Dhawan and Narasimha.**

Powell, J. B. L. The diffraction of a rarefaction wave by a corner, 243.

Preston, J. H. The minimum Reynolds number for a turbulent boundary layer and the selection of a transition device, 373.

Proudman, J. On the series that represent tides and surges in an estuary, 411.

Rudinger, George The reflection of pressure waves of finite amplitude from an open end of a duct, 48.

Sakurai, Akira A note on Mott-Smith's solution of the Boltzmann equation for a shock wave, 255.

Sarma, L. V. K. Viswanadha Slow motion of a paraboloid of revolution in a rotating fluid, 404.

Sears, W. R. *See* **Hartunian and Sears.**

Shercliff, J. A. Some generalizations in steady one-dimensional gas dynamics, 645.

Stewartson, K. On almost rigid rotations, 17.

Townsend, A. A. Turbulent flow in a stably stratified atmosphere, 361.

Vaglio-Laurin, Roberto and Van Dyke, M. D. A discussion of higher-order approximations for the flow field about a slender elliptic cone, 638.

Van Dyke, M. D. A model of supersonic flow past blunt axisymmetric bodies, with application to Chester's solution, 515.

Van Dyke, M. D. *See* **Vaglio-Laurin and Van Dyke.**

Varley, E. An approximate boundary layer theory for semi-infinite cylinders of arbitrary cross-section, 601.

White, D. R. *See* **Alpher and White.**

Wood, W. W. The asymptotic expansions at large Reynolds numbers for steady motion between non-coaxial rotating cylinders, 159.

Wooding, R. A. An experiment on free thermal convection of water in saturated permeable material, 582.

REVIEWS

Rheology: Theory and Applications, Volume I, edited by F. R. Eirich, 110.

Combustion Processes (Volume II of High Speed Aerodynamics and Jet Propulsion), edited by B. Lewis, R. N., Pease and H. S. Taylor, 221.

Gas Dynamics, by Klaus Oswatitsch (English version by Gustav Kuerti), 324.

Wing Theory, by A. Robinson and J. A. Laurmann, 326.

Jets, Wakes and Cavities, by Garrett Birkhoff and E. H. Zarantonello, 437.

Viscous Flow Theory, II—Turbulent Flow, by Shih-I Pai, 546.

Magnetohydrodynamics, by T. G. Cowling, 550.

Elements of Gasdynamics, by H. W. Liepmann and A. Roshko, 658.

FLUID MECHANICS for ENGINEERS

By P. S. BARNA, M.E., A.F.R.Ae.S.
N.S.W. University of Technology

In this single volume adequate coverage is provided for students studying for a degree or diploma in Mechanical or Civil Engineering, and parts will be found equally useful for Higher National Certificate Courses.

Emphasis is upon the broad representation of the fundamentals and the subjects covered include fluid statics, fluid motion, wing theory, centrifugal pumps, and hydraulic turbines. A large number of examples with complete solutions are given; these have been carefully selected to illustrate the preceding theory. *Price* 57*s.* 6*d.*

"*This very modern text-book can be recommended to students and engineers.*"—*CIVIL ENGINEERING.*

REGIME BEHAVIOUR of CANALS and RIVERS

By Professor T. BLENCH, B.Sc., M.A.S.C.E.
University of Alberta

The aim of this book is to give the practising engineer the means to solve, with practical quantitative accuracy, problems that arise in dealing with canals and rivers that form their boundaries from sediment, so will not submit to arbitrary interference.

The development is logical, in terms of formulas of dynamically satisfactory form that have been discovered by observing the natural self-adjustment of canals that were designed arbitrarily but allowed to adjust to natural dimensions eventually. Major practical problems are illustrated by worked examples. *Price* 30*s.*

"*. . . should appeal alike to the student and the practising engineer.*"—*ENGINEERING.*

Descriptive literature available, post free from—

BUTTERWORTHS SCIENTIFIC PUBLICATIONS

88, Kingsway, London, W.C.2.

Journal of Fluid Mechanics

for notes of advertisement rates please apply to:—

The Advertisement Department,
Cambridge University Press,

Bentley House,
200 Euston Road,
London, N.W.1.

Engineering Fluid Mechanics

by

DR. C. JAEGER
The English Electric Company Limited

An attempt has been made in this book to cover the methods of analysis and calculation required for the design of water-power schemes. The selection of the material has been based on many years' experience of this type of work. First published in German and also translated into French. **60s.** net

17 STANHOPE ST., GLASGOW, C.4

BLACKIE & SON

FULL PARTICULARS OF THE

JOURNALS

PUBLISHED BY THE

CAMBRIDGE UNIVERSITY PRESS

MAY BE HAD FROM

THE MANAGER, CAMBRIDGE UNIVERSITY PRESS
BENTLEY HOUSE, 200 EUSTON ROAD
LONDON, N.W.1

Cambridge Monographs on Mechanics & Applied Mathematics

Edited by G. K. BATCHELOR & H. BONDI

A series of monographs, presenting in permanent form some recent advances in mechanics and in applied mathematics generally. The scope of the series can best be described by saying that the books in it treat various topics in classical physics, usually from a mathematical standpoint.

The Theory of Homogeneous Turbulence
By G. K. BATCHELOR
30*s. net*

Geometrical Mechanics and de Broglie Waves
By J. L. SYNGE
30*s. net*

Linearized Theory of Steady High-Speed Flow
By G. N. WARD
35*s. net*

Static and Dynamic Electron Optics
By P. A. STURROCK
35*s. net*

The Theory of Hydrodynamic Stability
By C. C. LIN
27*s.* 6*d. net*

Surveys in Mechanics
Edited by G. K. BATCHELOR & R. M. DAVIES
50*s. net*

The Structure of Turbulent Shear Flow
By A. A. TOWNSEND
40*s. net*

Fourier Analysis and Generalised Functions
By M. J. LIGHTHILL
17*s.* 6*d. net*

CAMBRIDGE UNIVERSITY PRESS

JOURNAL OF FLUID MECHANICS

Volume 3, Part 6 March 1958

CONTENTS

The flow of a compressible fluid with weak entropy changes
by ROY GUNDERSEN 553

An experiment on free thermal convection of water in saturated permeable material
by R. A. WOODING 582

An approximate boundary layer theory for semi-infinite cylinders of arbitrary cross-section
by E. VARLEY 601

Cavitating flow about a wedge at incidence
by A. D. COX and W. A. CLAYDEN 615

A discussion of higher-order approximations for the flow field about a slender elliptic cone
by ROBERTO VAGLIO-LAURIN and M. D. VAN DYKE 638

Some generalizations in steady one-dimensional gas dynamics
by J. A. SHERCLIFF 645

Reviews 658

Index to Volume 3 662

Printed in Great Britain by Taylor & Francis Ltd.

9075